

EFFICIENCY IMPROVEMENTS OPTIONS FOR COAL FIRED POWER PLANTS

by

Sriram Ramanujam

A thesis submitted to the faculty of  
The University of North Carolina at Charlotte  
In partial fulfilment of the requirements  
for the degree of Master of Science in  
Mechanical Engineering

Charlotte

2020

Approved by:

---

Dr. Nenad Sarunac

---

Dr. Harish Cherukuri

---

Dr. Russell Keanini



## ABSTRACT

## SRIRAM RAMANUJAM Efficiency Improvement Options for Coal Fired Power Plants. (Under the direction of DR. NENAD SARUNAC)

Efficiency improvement of the existing coal-fired power plants has been recognized as a path of no regret. The Affordable Clean Energy (ACE) rule issued on August 21, 2018, requires 2.1% to 4.5% reduction in net plant heat rate and 1.5% improvement in net unit efficiency from each coal-fired power plants in the U.S. [2].

The main objective of this study is identification of cost-effective commercially-ready options, newly developed technologies, and concepts nearing commercial application for improving efficiency for existing coal-fired power plants. The further objective is analysis of performance improvement options, and quantification of achievable performance improvements.

To accomplish the objective, system modeling and design analysis were performed by employing EBSILON Professional software (EPV-11). More specifically, the thesis goals include:

- Comprehensive review and analysis of potential heat rate improvement.
- Identification of practical cost-effective options for efficiency improvement and reduction of environmental compliance cost.
- Quantification of efficiency improvement and cost for each of the selected performance improvement options.
- Development and application of methodology and analysis tools for determining effects of identified performance improvement techniques.

- Determination of cumulative performance improvements that could be achieved at two selected power plant designs (supercritical) firing high-rank and low-rank coals.

## ACKNOWLEDGEMENTS

I would like to thank my advisor Dr. Nenad Sarunac for his immense support and guidance throughout the spell of this research which broadened my horizon in the field of Power engineering. And I am also indebted to my friends and parents for providing me with the required motivation & moral support in the process of completing my research.

## TABLE OF CONTENTS

LIST OF TABLES .....	viii
LIST OF FIGURES .....	ix
CHAPTER 1: INTRODUCTION .....	1
1.1 Overview .....	1
1.2 Background and Motivation.....	4
1.3 Performance Parameters.....	9
1.3.1 Turbine Cycle Heat Rate .....	9
1.3.2 Gross Power, Net Power and Auxiliary power output .....	10
1.3.3 Net Unit Heat Rate .....	11
1.3.4 Net Unit Efficiency .....	12
1.3.5 Unit Cycle Efficiency.....	13
1.3.6 Fuel Heat Input.....	13
1.4 Heat Rate and Efficiency Relation .....	14
1.4 EBSILON Professional Modeling Code .....	16
CHAPTER 2: USE OF LOW-TEMPERATURE HEAT FOR FEED WATER HEATING AND COMBUSTION AIR PREHEAT.....	23
2.1 Overview .....	23
2.2 Ebsilon Professional Performance analysis Modelling.....	23
2.3 Flue gas coolers and Heat Exchangers .....	35
CHAPTER 3: PARTIAL AND FULL ARC STEAM ADMISSION TO TURBINE .....	42
3.1 Overview .....	42
3.2 Basis of Calculations performed in Ebsilon Professional Code.....	50
3.2.1 Minimum Part Load consideration and Losses in a Steam Turbine: .....	55
3.2.1.1 Anticipate Increased HP-IP Rotor Vibration: .....	56
3.2.1.2 Nozzle and Valve Erosion Rates:.....	56
3.2.1.3 Expect the Possibility of More Water Droplet Erosion: .....	58
3.2.2 Total Isentropic Efficiency versus Static Isentropic Efficiency.....	60
3.3 Illustration of Performance Evaluation using Ebsilon Professional Code .....	61
3.3.1 Ebsilon Professional Code Settings to model arc admission for Steam Turbines	65
3.3.2 Performance Evaluation using Ebsilon Professional Code at different load operation.....	66

3.3.2 Alstom Power (Rugby, UK) Steam Turbine Full Arc Vs Partial Arc admission.	71
CHAPTER 4: IMPROVEMENTS OF STEAM TURBINE INTER STAGE SEALS .....	73
4.1 Overview .....	73
4.2 Calculation of Leakage Flow .....	77
4.3 Analysis of the Proposed Improved Labyrinth Seal.....	81
4.4 Effect of steam leakage on turbine performance.....	87
4.5 Improved Seal Configurations .....	93
4.2.1 Retractable® Seals .....	94
4.2.2 Abradable Coating Seals .....	95
4.2.3 Brush Seals.....	96
4.2.4 Guardian Seal.....	97
CHAPTER 5: FLUE GAS INJECTION INTO COOLING TOWER .....	99
5.1 Overview .....	99
5.2 Natural Draft Cooling Towers without Flue Gas Injection.....	100
5.3 Natural Draft Wet Cooling Tower with Flue Gas Injection.....	102
5.4 Performance Evaluation of a Natural Draft Wet Cooling Tower with flue gas injection.....	105
5.4.1 Merkel's Equation (Wet Cooling Zone).....	106
5.4.2 Dry Zone (Heat Exchanger) .....	116
5.4.3 Stack/Tower Height and Air flow .....	117
5.4.4 Cooling Tower Losses.....	118
5.5 Illustration of Performance Evaluation using Epsilon Professional Code .....	118
CHAPTER 6: CUMMULATIVE PERFORMANCE IMPROVEMENT .....	124
6.1 Overview .....	124
6.2 Calculation basis for key performance parameters .....	124
6.3 Illustration of Performance Evaluation using Epsilon Professional Code .....	127
CHAPTER 7: SUMMARY AND CONCLUSIONS.....	136
7.1 Flue Gas Cooler.....	137
7.2 Improvements to the Steam Turbine Cycle.....	138
7.3 Improvements to the Heat Rejection System .....	139
REFERENCES .....	142

## LIST OF TABLES

TABLE 1.1: Reference Plant Operating Parameters .....	3
TABLE 1.2: Reference Plant Performance Parameters .....	3
TABLE 2.1: Coal Composition, Ultimate Analysis and HHV [7] .....	25
TABLE 2.2: Performance parameters for Bituminous Coal fired plant .....	30
TABLE 2.3: Performance parameters for Washed Illinois Coal fired plant.....	30
TABLE 2.4: Performance parameters for PRB Coal fired plant .....	30
TABLE 2.5: Performance parameters for Lignite Coal fired plant .....	31
TABLE 2.6: Results- Increase in Power Output with Respect to Reference.....	31
TABLE 2.7: Results – Improvement in Net Unit Heat Rate with Respect to Reference .	31
TABLE 2.8: Results – Increase in Net Unit Efficiency with Respect to Reference.....	32
TABLE 3.1: Efficiency at different loads and admissions of the steam turbine .....	70
TABLE 3.2: Performance comparison of Power plants with Partial and Full Arc admission .....	70
TABLE 4.1: Comparison of computational and Experimental Results [21] .....	82
TABLE 4.2: Baseline Vertical and Improved Labyrinth Seal Leakage Flows [21, A-1 to 4] .....	86
TABLE 5.1: Reference plant operating parameters.....	119
TABLE 5.2: Performance comparison between power plants with and without flue gas injection into cooling tower. ....	120
TABLE 6.1: Performance comparison between Power plants with and without Flue gas Injection into Cooling Tower.....	132

## LIST OF FIGURES

FIGURE 1.1: Net Power Generation (in MW) in US from Coal Fired Power Plants in 2017.....	5
FIGURE 1.2: Number of US Coal Fired Power Plants in 2017 (Source: US Energy Information Administration).....	5
FIGURE 1.3: US electricity generation from Various Energy Sources in 2017 .....	7
FIGURE 1.4: US electricity generation from Various Energy Sources from 1950-2017 ..	7
FIGURE 1.5: In 2017 Top Five Coal Producing Sates in US (Source: EIA).....	8
FIGURE 1.6: Unit Efficiency vs. Heat Rate [3] .....	14
FIGURE 1.7: Installed Package Rotary Air preheaters on a power plant site [35] .....	19
FIGURE 1.8: Bisector Rotary Regenerative Air preheater [34].....	19
FIGURE 1.9: Trisector Rotary Regenerative Air preheater [34].....	20
FIGURE 1.10: Heat Transfer Process in a Rotary Regenerative Air preheater (Temperature profile not pertaining to this study) [34] .....	20
FIGURE 1.11: Parts of a Regenerative Air preheater [34].....	21
FIGURE 2.1: Reference Power Plant Configuration (Fuel used is Bituminous Coal) [3] 25	
FIGURE 2.2: Power Plant with FGC for Air Preheating – Configuration A [3].....	26
FIGURE 2.3: Power Plant with FGC for FW Heating and SAH for Air Preheating – configuration B [3].....	28
FIGURE 2.4: Power Plant with FGC’s for Feed Water Heating and Air Preheating [3].	29
FIGURE 2.5: Increase in Power Output as a Function of Configuration and Coal Type.	33
FIGURE 2.6: Improvement in Net Unit Heat Rate as a Function of Configuration and Coal Type.....	33
FIGURE 2.7: Increase in Net Unit Efficiency as a Function of Configuration and Coal Type .....	34
FIGURE 2.8: General Design of the BBS Flue Gas Cooler [3] .....	36
FIGURE 2.9: Installation of FGC module [3] .....	36
FIGURE 2.10: Acid Condensation within the FGC [3].....	37
FIGURE 2.11: Condensation of Hydrochloric Acid [3].....	37
FIGURE 2.12: Side View of the FGC at Schwarze Pumpe Retrofitted with Corrosion-Resistant Alloy Tubes, October 2008 [3] .....	38
FIGURE 2.13: GAGAVO Flue Gas Cooler by Flucorex [3].....	40
FIGURE 2.14: Modular Design of GAGAVO Heat Exchanger with PTFE Tubes. Internal Surface are Lined by PFA Fluoroplastic Sheets [3] .....	40

FIGURE 3.1: Main Steam line to a Turbine [44] .....	42
FIGURE 3.2: Steam Chest with Control Valves [44].....	43
FIGURE 3.3: Side-mounted Steam Chest with a Stop Valve & Control Valves [44].....	44
FIGURE 3.4: Hydraulic Control Scheme [44] .....	45
FIGURE 3.5: Main Steam line to turbine [44] .....	46
FIGURE 3.6: Two control valves in partially open position in an over-head mounted steam chest [44] .....	47
FIGURE 3.7: Distortion and cracking due to single arc admission [44] .....	48
FIGURE 3.8: Side mounted steam chest with four control valves [44] .....	48
FIGURE 3.9: Full arc admission with throttling of stop valves [44] .....	49
FIGURE 3.11: Enthalpy-entropy diagram for multi-stage expansion [45, 49] .....	50
FIGURE 3.10: Enthalpy (h) - Entropy (s) diagram of an expansion stage (Efficiency values mentioned in the figure are for illustration only) [1].....	55
FIGURE 3.11: Nozzle Block Solid Particle Erosion ( <i>Courtesy: TG Advisers Inc.</i> ) [52, 53] .....	57
FIGURE 3.12: Vanes Solid Particle Erosion ( <i>Courtesy: TG Advisers Inc.</i> ) [52, 53].....	57
FIGURE 3.13: Droplet formation at salt solution zone [52, 53] .....	58
FIGURE 3.14: Wilson line dicing the wet and dry expansion region [54].....	59
FIGURE 3.15: Total and static properties in the enthalpy-Entropy diagram [1].....	61
FIGURE 3.16: Sketches showing two ways of throttling. Left-hand picture: Throttling by pressure reduction valve. Right-hand picture: Throttling by a control stage, i.e. partial admission [56].....	62
FIGURE 3.17: H-s diagram for partial arc admission throttling three control valve in governing stage [1]. .....	63
FIGURE 3.18: Ebsilon code Efficiency Characteristics of HP Turbine Section [57] .....	64
FIGURE 3.19: Basis of modelling governing stage of the steam turbine in Ebsilon code [1].....	66
FIGURE 3.20: Ebsilon power plant model with 100% load with Turbine Full arc admission .....	68
FIGURE 3.21: Variation of heat rate with load for Full arc admission Vs Partial arc steam admission in a steam turbine [55] .....	71
FIGURE 4.1: Schematic Representation of a Generic Stepped Labyrinth Seal, Depicting Two Cycles of a Seal [21].....	76
FIGURE 4.2: Schematic Representation of a Generic Straight-Through Labyrinth Seal, Depicting Two Cycles of a Seal [21].....	77

FIGURE 4.3: Labyrinth Factor according to Equation 4.2 using Martin's Formulation (K=1) [1] .....	80
FIGURE 4.4: Comparisons of Computational and Experimental Results [21] .....	82
FIGURE 4.5: Baseline Stepped Labyrinth Vertical Seal Geometry used for Modeling Showing cross-section and teeth's (see Figure 4.1) [21] .....	83
FIGURE 4.6: Variation of Predicted Total Pressure across the multistage baseline Seal Assembly, flow through the seal being from right to left [21] .....	84
FIGURE 4.7: Baseline Vertical seal with Bent Knives, Resulting in increased clearance [21].....	86
FIGURE 4.8: Improved Labyrinth Seal - C-Shaped Flat-Edged Knives, One Tall and Three Short Knives (C Flat + CCC) [21].....	86
FIGURE 4.9: Steam Turbine Gland Sealing System with Baseline Labyrinth Seal .....	88
FIGURE 4.10: Steam Turbine Gland Sealing System with Improved Labyrinth Seal ....	89
FIGURE 4.11: Improvement in net plant heat rate and efficiency firing Bituminous Coal .....	91
FIGURE 4.12: Retractable Seal Segment and Coil Spring.....	95
FIGURE 4.13: Typical Abradable Seal Arrangement [13] .....	96
FIGURE 4.14: Brush Seal Arrangement .....	97
FIGURE 4.15: Guardian® Seal Geometry .....	98
FIGURE 5.1: Schematic representation of a wet natural draft cooling tower .....	101
FIGURE 5.2: Working scheme of a power plant with cleaned flue gas injection [42] ..	104
FIGURE 5.3: Flue gas stack inside a natural draft wet cooling tower [42].....	104
FIGURE 5.4: Epsilon Professional code different zones inside a cooling tower [1] .....	106
FIGURE 5.5: Water Drop with Interfacial Film [27] .....	109
FIGURE 5.6: Cooling Tower Characteristics [27, 31] .....	113
FIGURE 5.7: Power plant without flue gas injection into cooling tower.....	120
FIGURE 5.8: Power Plant with Flue gas Injection into Cooling Tower .....	121
FIGURE 5.9: Cooling Tower diagram – Wet zone (Merkel) .....	122
FIGURE 6.1: Reference power plant with 100 mbar condenser operating pressure.....	128
FIGURE 6.2: Power plant equipped with cooling tower flue gas injection .....	129
FIGURE 6.3: Power plant equipped with FGC for waste heat recovery from flue gas .	131
FIGURE 6.4: Power plant equipped with FGC for waste heat recovery from flue gas and flue gas injection into CT.....	132
FIGURE 6.5: Analysis of Cumulative Performance Improvement Technique .....	133

## CHAPTER 1: INTRODUCTION

### 1.1. Overview

This study focuses on the efficiency and heat rate improvement options for existing coal fired power plants that could be achieved by implementing commercially available and cost-effective solutions.

Some of the investigated options involve application of advanced technologies, such as the heat recovery and utilization from flue gas option. The amount of heat in the flue gas is simply too large to be discharged into the atmosphere. Recovered heat can be used for air preheating and feed water heating. A flue gas cooler (FGC) is enabling technology, commercially available from several vendors, for recovering heat from the flue gas. The cost ranges from \$0.06 to \$0.13 per Btu [3, 4] of recovered heat, depending on the choice of corrosion-resistant materials.

Improvements to the steam turbine cycle involve application of better seals, improvement and conversion of partial to full arc admission, and use of more efficient 3D blading. Although the cost of turbine upgrades could be in the \$30 million range [3] (depending on the turbine size and extent of the upgrade), these improvements not only improve efficiency, but also increase unit capacity. This capacity increase represents fuel-free or “green” megawatts, because no additional fuel is used.

Although improvements to the heat rejection system can provide performance improvements similar in magnitude to the turbine cycle improvements, these can be, in most cases, achieved by improving the performance of a cooling tower by injection of the exhaust flue gas above the fill inside the cooling tower (CT) to increase buoyancy and, thus

air flow through the tower. Also, a more efficient fill and streamlining of the air flow through the tower may be used.

Thermodynamic analysis of commercially available heat rate improvement options, technologies nearing commercialization stage, and newly developed technologies and concepts for efficiency improvement of existing coal-fired power plants, firing coal was conducted. An analysis methodology and analytical first principles models for modeling of power plant performance and performance of its components were developed to evaluate various technology options and determine their effect on power plant efficiency and heat rate.

To accomplish these objectives, EBSILON® Professional code and a spreadsheet-based first principles analysis based on conservation of mass and energy and equilibrium thermodynamics was used. The analysis also included combustion calculations and heat transfer analysis. Model results and predictions were, wherever possible, compared and verified against test or plant operating data, or results from the literature.

A Reference Plant used for benchmarking (i.e., as a Base Case) is a 1970 vintage 650 MW supercritical power plant firing bituminous, sub-bituminous and lignite coals, equipped with the air pollution control system capable of satisfying current emission limits for PM, NO<sub>x</sub>, SO<sub>x</sub>, and Hg. Performance of the reference plant employing an open cooling system (no CT) will be utilized to illustrate the efficiency improvement options considered in this study. The plant is equipped with a Steam Air Preheater (SAH) using steam extraction (~92 MBTU/hr) from the turbine for heating combustion air.

Table 1.1: Reference Plant Operating Parameters

Plant Design Capacity	650 MW
HP Pressure	253 bar
HP Temperature	538°C
HRH Temperature	538°C
IP Pressure	46 bar
IP Temperature	419°C
LP Pressure	11.38 bar
LP Temperature	343°C
Condenser Operating Pressure	0.3 bar

Table 1.2: Reference Plant Performance Parameters

Gross Heat Rate ( $HR_g$ )	7186 MBTU/hr
Cycle Efficiency	47.48%
Net Efficiency	43.82%
Net Heat Rate ( $HR_{net}$ )	7787 MBTU/hr
Auxiliary Power Consumption	7.72%
Condenser Heat Duty	2335 MBTU/hr
Boiler Efficiency	88.86%

## 1.2. Background and Motivation

USA's fossil fuels play a significant role in the global and domestic energy economy as they provide easily accessible, reliable, dispatchable and low-cost energy. Coal is the second-largest energy source for U.S. electricity generation. In 2017, about 30% of the total electricity generation in the U.S (about 1,206 Billion kWh) was generated by coal-fired power plants. Nearly all coal-fired power plants use steam turbines. A few coal-fired power plants convert coal to a gas for use in a gas turbine to generate electricity. In 2017 approximately 51% of the US operating fossil fuel fleet was coal-based having an average operating net efficiency of 32.60%. A significant part of that capacity is over 35 years old having average net efficiency of 30% or lower (EIA Form 860 & 923) and requires modernization.

In 2017 US produced ~1,205,835,000 MWh from coal fired power plants. As of 2017, there are about 565 Coal fired power plants actively operating and producing power in the US. The state of Texas produces close to 135,000,000 MWh (see Figure 1) of electricity from coal fired plant with 23 Power Plants (see Figure 2) actively operating. The other prominent coal-based power producing states are Missouri, Illinois, Indiana, West Virginia, Pennsylvania, Ohio, and Kentucky. Pennsylvania has 34 Coal fired power plants as of 2017, which is the most in the US. Figures 1.1 & 1.2 picture the amount of coal-based net power generation and number of coal fired-power plants in the USA in 2017.

Net generation : coal : all sectors 2017

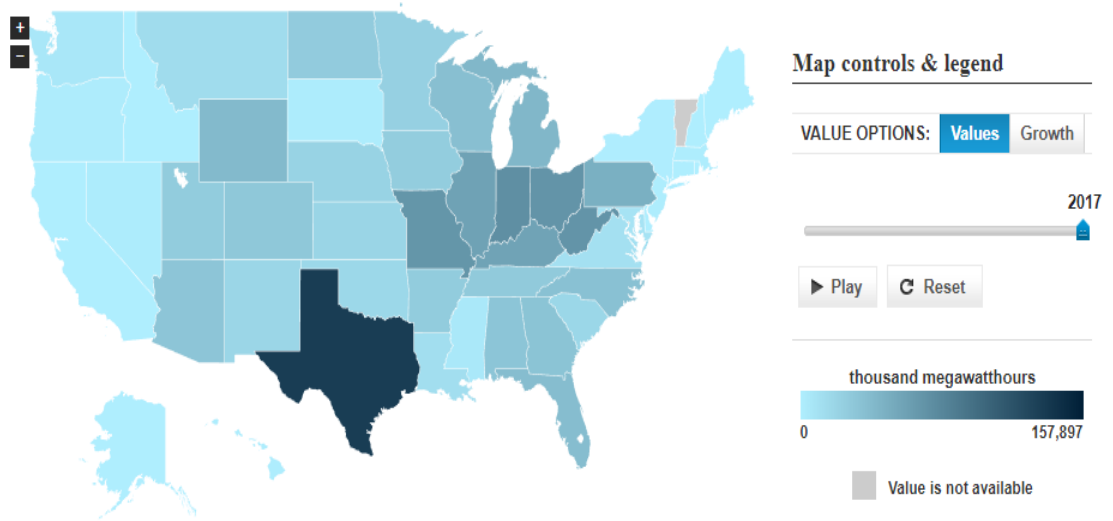


Figure 1.1: Net Power Generation (in MW) in US from Coal Fired Power Plants in 2017  
 (Source: US Energy Information Administration)

Number of plants for coal, United States, all sectors

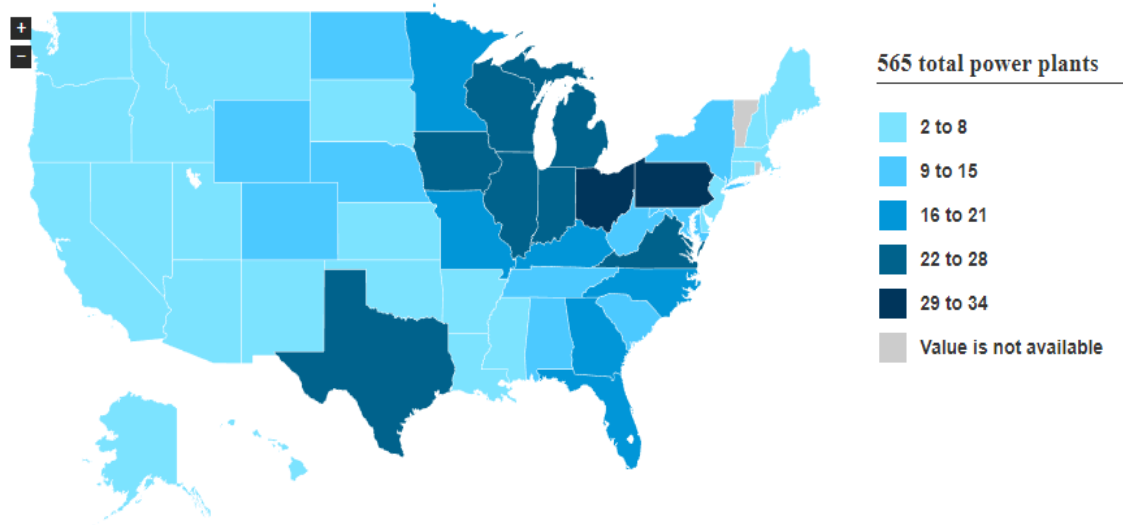


Figure 1.2: Number of US Coal Fired Power Plants in 2017  
 (Source: US Energy Information Administration)

Although new, more efficient power-generating technologies are nearing commercialization, significant market penetration will take some time. Estimates concerning market penetration of new technologies range from 2030 to 2050 and beyond. Improving efficiency of existing power plants, and newly build generation (approximately 140,000 MW by 2030) is the first logical, inexpensive, and necessary step. Also, efficiency of a coal-fired power plant has a large effect on annual fuel use and emissions, i.e., on sustainability, as well as on generation capacity.

The efficiency improvement of existing power plants is of great importance for the U.S. mining industry in Utah, Wyoming, Nevada and other western states producing sub-bituminous coals (generally known as Powder River Basin, PRB, coals) used almost exclusively for power generation, also at least 90% of the coal mined in Illinois (approximately 32.5 million short tons annually) is used by the electric utility industry for power generation, Virginia, Kentucky and other states.

The three major categories of energy sources for electricity generation are fossil fuels (coal, natural gas, and petroleum), nuclear energy, and renewable energy sources. Most electricity is generated with steam turbines using fossil fuels, nuclear, biomass, geothermal and Concentrated Solar Power (CSP).

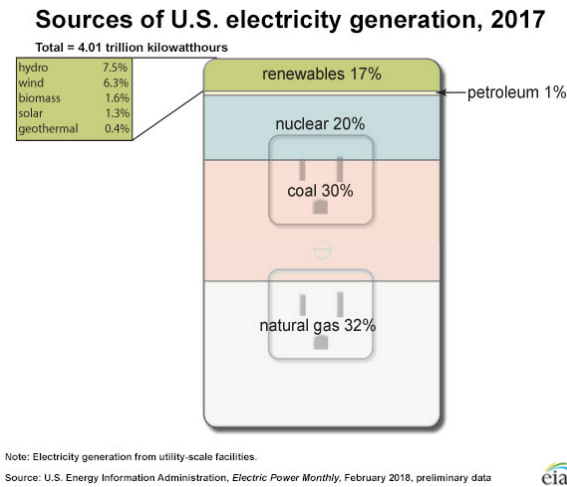


Figure 1.3: US electricity generation from Various Energy Sources in 2017

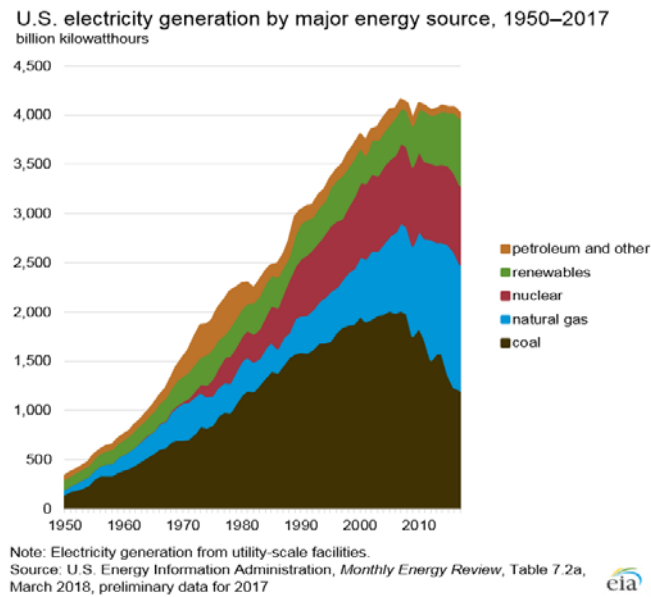


Figure 1.4: US electricity generation from Various Energy Sources from 1950-2017

As of December 31, 2015, estimates of total world proved recoverable reserves of coal were about 1,136 billion short tons, (or 1.1 trillion short tons). Five countries have about 74% of the world's coal reserves. The top five countries and their share of world proved coal reserves:

- United States—22%
- Russia—16%
- Australia—14%
- China—13%
- India—9%

In 2017, about 775 million short tons of coal were produced in 24 U.S. states. Five states produced a total of about 538 million short tons, or about 71% of total U.S. coal production. The five largest coal-producing states are given in Figure 1.5.

## Top five coal producing states, 2017

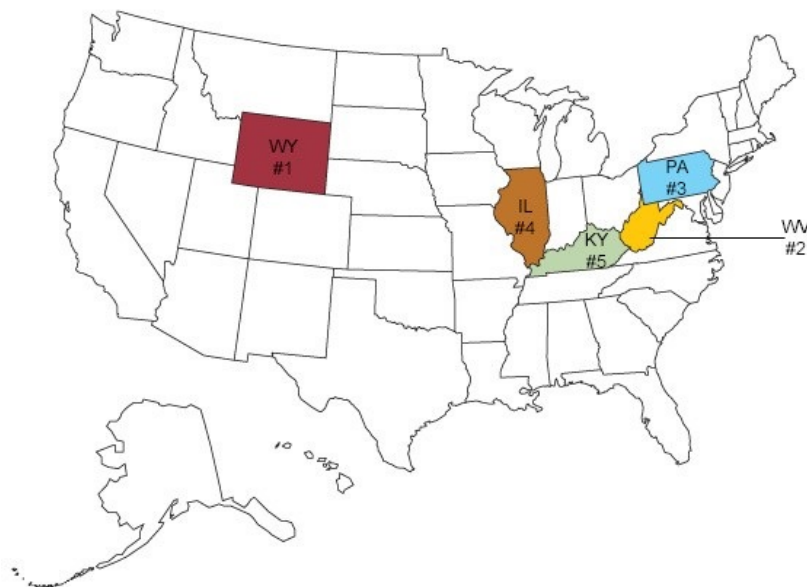


Figure 1.5: In 2017 Top Five Coal Producing States in US (Source: EIA)

Their production in million short tons and share of total U.S. coal production in 2017:

- Wyoming—316.5—41%
- West Virginia—92.8—12%

- Pennsylvania—49.1—6%
- Illinois—48.2—6%
- Kentucky—41.8—5%

The efficiency improvement of existing power plants is of great importance for the Illinois coal mining industry because at least 90% of the coal mined in Illinois (approximately 32.5 million short tons annually) [3] is used by the electric utility industry for power generation.

The major operating cost of a coal-fired power plant is fuel purchase. Given the higher heating value of coal (HHV), the flow rate of coal required to generate desired gross power output is directly proportional to net generation efficiency. The net efficiency is, therefore, a very important factor affecting plant economics.

### 1.3 Performance Parameters

To evaluate plant performance for the various performance improvement options analyzed in this study, the following parameters were calculated and compared with the base (reference) plant performance parameters. Each of these performance parameters plays a vital role in quantifying the magnitude of the performance improvement for each performance improvement options. A detailed explanation of each of these parameters is presented in this chapter, as well as the relationship between these parameters and overall plant performance.

#### 1.3.1 Turbine Cycle Heat Rate

Steam turbine heat rate is the parameter commonly used to define the overall thermal performance of the steam turbine and feed water cycle. Turbine cycle heat rate is

defined as the amount of heat input provided by the boiler to the turbine for generating one unit of electricity.

$$HR_{cycle} = \frac{[Q_1 \cdot (H_1 - h_2) + Q_2 \cdot (H_3 - H_2)]}{P_G} \quad (1.1)$$

Where,

$HR_{cycle}$  - Turbine Cycle Heat Rate, Btu/kWh

$Q_1$  - Main steam flow, lb/hr

$H_1$  - Main steam enthalpy, Btu/lb

$h_2$  - Feed water enthalpy, Btu/lb

$Q_2$  - Hot reheat steam flow, lb/hr

$H_3$  - Hot reheat enthalpy, Btu/lb

$H_2$  - Cold reheat enthalpy, Btu/lb

$P_G$  - gross power output, MW

### 1.3.2 Gross Power, Net Power and Auxiliary power output

Gross power generated or gross power output ( $P_G$ ) is the total amount of electricity produced by the power plant at the generator terminals over a specified amount of time.

$$\text{Gross Power Output } (P_G) = \text{Net power output } (P_{net}) + \text{Auxiliary power use } (P_{SS}) \quad (1.2)$$

Over all plant auxiliary power consumption or the station own use is from the following operating components,

1. Induced draft Fan (ID)
2. Forced draft Fan (FD)
3. Condensate Extraction Pump (CEP)
4. Main Boiler Feed Water Pump (BFP)

## 5. Feed Water Recirculation Pump (RCP)

Net Power is the power sold to the grid. It is calculated by subtracting auxiliary power from the gross power.

$$\text{Net power output } (P_{net}) = \text{Gross Power Output } (P_G) - \text{Auxiliary power use } (P_{ss}) \quad (1.3)$$

### 1.3.3 Net Unit Heat Rate

The net unit heat rate ( $HR_{net}$ ) is defined as the ratio of fuel energy input to that of the net electric output generated by the plant. Net unit Heat rate is an inverse of net unit efficiency (multiplied by the unit conversion factor of 3,412 for engineering set of units or by 3600 for SI units).

$$HR_{net} = \frac{Q_{fuel}}{P_{net}} = \frac{(M_{coal} \cdot HHV)}{(P_G - P_{ss})} \quad (1.4)$$

The boiler type in base plant configuration is once through Benson boiler using pulverized coal combustion PCC technology. Heat losses considered in calculating efficiency of the boiler are due to radiation sensible loss with flue gas leaving the boiler, and unburnt (unburned) residue, such as unreacted carbon. Radiation losses are calculated according to EN 12952 by using AMBE chart. Boiler efficiency is defined the ratio of total heat input to the working fluid (steam and water) involved in the power generation to that of heat input from the fuel consumed for power generation.

$$\eta_B = \frac{P_G \cdot HR_{cycle}}{Q_{fuel}} = \frac{Q_T}{(M_{coal} \cdot HHV)} \quad (1.5)$$

The definition of net unit heat rate, expressed in terms of boiler efficiency ( $\eta_B$ ), turbine cycle heat rate ( $HR_{cycle}$ ), station service (auxiliary power) use ( $P_{ss}$ ) and gross power output ( $P_G$ ) is shown in Equation 1.6, This equation provides a roadmap to heat rate

improvement options. The net unit heat rate can be improved by improving boiler efficiency, improving turbine cycle heat rate and reducing auxiliary power use.

$$HR_{net} = \frac{HR_{cycle}}{\eta_B \cdot \left(1 - \frac{P_{ss}}{P_G}\right)} \quad (1.6)$$

Where,

$Q_T$  – Total Heat input, MBtu/hr

$Q_{fuel}$  - Heat input with fuel, MBtu/hr

$P_{net}$  - Net unit power output, MW

$M_{coal}$  - Flow rate of coal fired to generate gross power output, lb/hr

$P_G$  - Gross power output, MW

HHV - Coal higher heating value, Btu/lb

$P_{ss}$  - Auxiliary power consumed (station service power), MW

$\eta_B$  – Boiler Efficiency, %

#### 1.3.4 Net Unit Efficiency

Net thermal efficiency or net efficiency ( $\eta_{net}$ ), is defined as the electric energy output as a fraction (or percentage) of the fuel energy input. Net unit efficiency is an inverse of Net unit Heat rate (multiplied by the unit conversion factor of 3,412 for the engineering set of units).

$$\eta_{net} = \frac{P_{net}}{Q_{fuel}} = \frac{3412}{HR_{net}} \quad (1.7)$$

Where,

$Q_{fuel}$  - heat input with fuel, MBtu/hr

$P_{net}$  - net unit power output, MW

$HR_{net}$  – Net Unit Heat Rate, MBtu/kWh

### 1.3.5 Unit Cycle Efficiency

Cycle efficiency or Unit cycle efficiency ( $\eta_{cycle}$ ), is defined as the gross electric energy output as a fraction (or percentage) of the fuel energy input. Cycle efficiency is an inverse of Unit cycle Heat rate (multiplied by the unit conversion factor of 3,412 for the engineering set of units).

$$\eta_{cycle} = \frac{P_G}{Q_{fuel}} = \frac{3412}{HR_{cycle}} \quad (1.8)$$

Where,

$Q_{fuel}$  - heat input with fuel, MBtu/hr

$P_G$  - Gross unit power output, MW

$HR_{cycle}$  – Unit Cycle Heat Rate, MBtu/kWh

### 1.3.6 Fuel Heat Input

Total Heat Input ( $Q_T$ ), Fuel Heat Input ( $Q_{coal}$ ) and Mass or quantity of coal fired ( $M_{coal}$ )

$$Q_T = P_G \cdot HHV_{fuel} \quad (2.3)$$

$$Q_{fuel} = \left( \frac{Q_T}{\eta_{boiler}} \right) \quad (2.4)$$

$$M_{coal} = \left( \frac{Q_{coal}}{HR_{cycle}} \right) \quad (2.5)$$

#### 1.4 Heat Rate and Efficiency Relation

A relationship between the net unit efficiency ( $\eta_{\text{net}}$ ) and net unit heat rate ( $\text{HR}_{\text{net}}$ ) is presented in Figure 6. References are often made in the literature to changes in efficiency by the percentage point (%-points), which should be distinguished from relative changes in heat rate given as percentage. For example (see Figure 1.6), a change of 1%-point in efficiency (for example from 36 to 37%) represents a relative change in net unit heat rate of 2.7%.

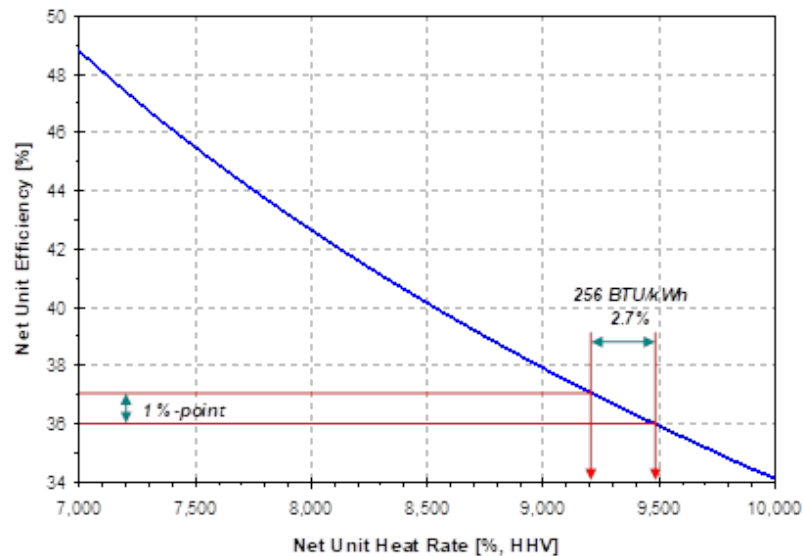


Figure 1.6: Unit Efficiency vs. Heat Rate [3]

The Higher Heating Value (HHV) of a fuel source is determined by the adiabatic bomb calorimeter where products of combustion are cooled back to the initial (pre-combustion) temperature, and thus includes the latent heat of condensation ( $h_{fg}$ ) vapor produced from fuel moisture. The HHV thus includes the latent heat of vaporization of water (condensation of vapor) in the combustion products. HHV assumes

all the water component is in the liquid state at the end of combustion and that heat delivered at temperatures below 150 °C (302 °F) can be put to use.

The Lower Heating Value (LHV) of a fuel source is determined by subtracting the heat of vaporization  $h_{fg}$  of the water from the higher heating value. This treats any H<sub>2</sub>O formed as a vapor. The energy required to vaporize the water (moisture) in fuel is, therefore not released as heat. LHV calculations assume that the water component of a combustion process is in a vapor state at the end of combustion, as opposed to the higher heating value (HHV), which assumes that all the water in a combustion process is in a liquid state after a combustion process. The LHV assumes that the latent heat of vaporization of water in the fuel and the reaction products is not recovered, which is a more realistic assumption compared to HHV.

Both efficiency and heat rate can be expressed on the HHV- or LHV-basis. In the U.S., HHV is used for coal-fired power plants, while in Europe, efficiency calculations are based on LHV. The difference in efficiency between HHV and LHV for a bituminous coal is about 2%-points (5% relative), while for the high-moisture sub-bituminous coals and lignite's, the difference is about 3-4%-points (8 to 10% relative), depending on the coal composition and moisture content. For gaseous fuels, LHV is used both in US and in Europe. Due to the difference in performance parameters calculated by using HHV and LHV, and in order to avoid confusion by comparing the two, performance parameters need to be properly labeled, such as Btu/kWh on HHV-basis, or efficiency in % on LHV-basis.

#### 1.4 EBSILON Professional Modeling Code

The detailed thermodynamic models of the Reference Plant and proposed performance improvement options were developed using EBSILON® Professional code.

EBSILON Professional Version 11 (EPV-11) used in this work, is a commercial software developed by STEAG Energy Services company. The EPV-11 code performs mass and energy balance for modeling, design and optimization of power plants and power generation systems based on the Rankine, Brayton, combined, IGCC (Integrated Gasification Combined Cycle), and IGFC (Integrated Gasification Fuel Cell), and hybrid power cycles. It is also used for the modeling, design, and optimization of power generation systems. The code is used by major European universities and power companies for research, design, and optimization purposes. Thermo-physical properties of the working fluids used in the analysis are determined by REFPROP [5] developed by NIST. The main EPV-11 features include are the following:

- The code has an embedded scripting language that gives user access to input, output, and calculation capabilities and to combine these with the user-written codes.
- Powerful calculation module and robust solution algorithm.
- Extensive component library.
- Material properties library for fuels and working fluids.
- Intelligent error analysis and online user help.

The REFPROP library, used to obtain the thermo-physical properties of the working fluids, is integrated with EPV-11 for accurate simulation of thermodynamic power cycles [5, 6].

### 1.5 Analysis Methodology and Modeling

To accomplish study objectives, the Ebsilon professional model based on conservation of mass and energy and equilibrium thermodynamics was developed for the Reference Plant. The analysis also includes combustion (stoichiometric) calculations, heat transfer analysis, analysis of heat exchanger performance and determination of the capacitance ( $UA$  product, where  $U$  is the overall heat transfer coefficient and  $A$  is the total heat transfer area) and determination of the fan and pump power. Ebsilon Professional modelling code was used in this work because it offers flexibility and freedom in modeling, complete understanding of employed analytical models and modeling assumptions, and also allows building models of unconventional system configurations. Model results and predictions were, wherever possible, compared and verified against test or plant operating data, or results from the literature.

The Ebsilon Professional model of a regenerative Rankine steam turbine cycle was employed for modeling of heat recovery from the flue gas and its use for feedwater heating and air preheating (advanced air preheating), and evaluation of tradeoffs between different options. Although, modeling of the steam turbine cycle can also be conducted by using commercial codes such as PEPSE and Aspen Plus, Gate Cycle etc. Ebsilon Professional code modeling allows ultimate flexibility and realism when analyzing unconventional system configurations. The code performs calculations by avoiding violations of the 2<sup>nd</sup> Law of Thermodynamic, which is not the case with all commercially available modeling

tools. The model results were verified against the design and performance test data and results from the literature. Model of the entire power plant was developed to facilitate analysis of a regenerative steam turbine cycle and modeling of heat recovery (sensible and latent heat) from the flue gas. The results obtained from the heat recovery models were verified against design data received from manufacturer of flue gas coolers (Geurts Heilig Group) [3].

The Epsilon Professional code models performs combustion analysis, mass and energy balance, and heat transfer analysis to determine heat input with fuel, net unit heat rate, boiler efficiency, and flow rates of air and flue gas at a number of state points throughout the power plant.

Both the bi-sector and tri-sector APH configurations can be modeled. Bisector design provides one air stream and one gas stream per air heater (Figure. 1.8). The tri-sector design provides two air streams and one gas stream per air heater (Figure. 1.9). The trisector air heater incorporates both the primary and secondary air (PA and SA) within one housing. The bi-sector and tri-sector terminology is typically associated with the Fredrik Ljungstrom design (Rotating-plate regenerative air preheater – RAPH). Figure 1.7 shows a newly installed air preheater (APH) by Howden (OEM) [35] with its corresponding duct work at a power plant site.



Figure 1.7: Installed Package Rotary Air preheaters on a power plant site [35]

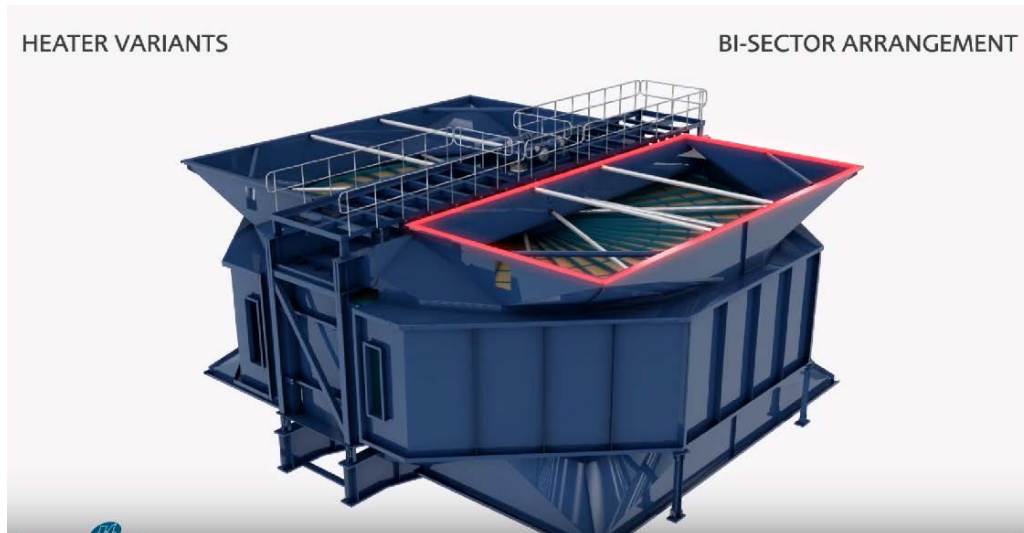


Figure 1.8: Bisector Rotary Regenerative Air preheater [34]

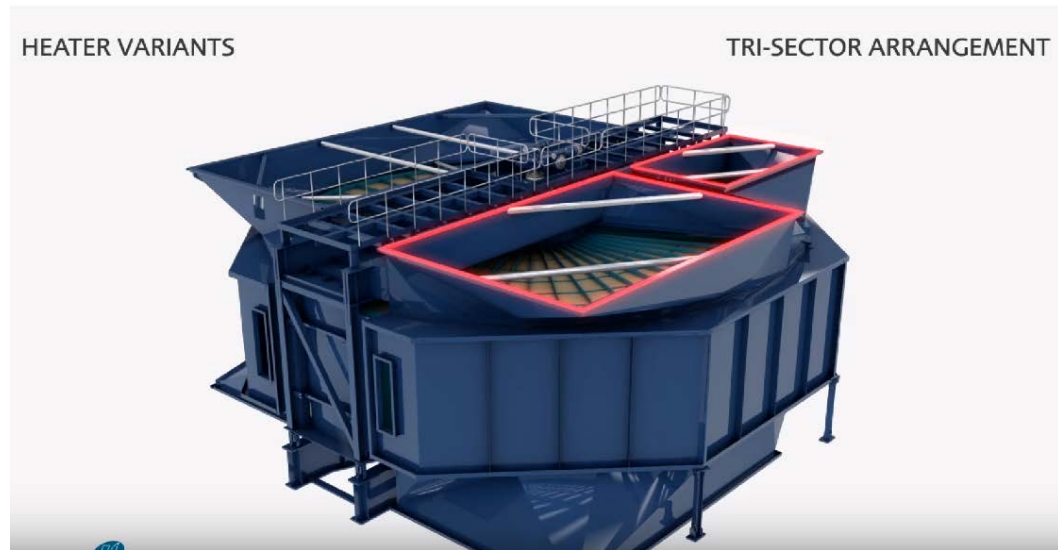


Figure 1.9: Trisector Rotary Regenerative Air preheater [34]

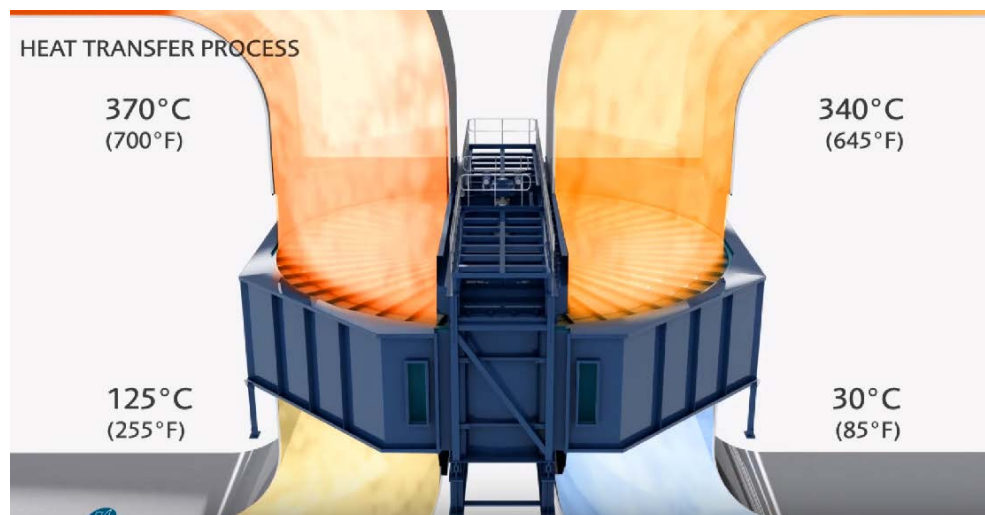


Figure 1.10: Heat Transfer Process in a Rotary Regenerative Air preheater (Temperature profile not pertaining to this study) [34]

The rotating-plate design (RAPH) consists of a central rotating-plate element installed within a casing that is divided into two (bi-sector type) or three (tri-sector type) sectors containing seals around the element. The seals allow the element to rotate through all the sectors, but keep gas leakage between sectors to a minimum while providing

separate gas air and flue gas paths through each sector (Refer Figure 1.11). The rotor itself is the medium of heat transfer in this system, and is usually composed of some form of steel and/or ceramic structure. It rotates slowly (around 1-2 RPM) to allow optimum heat transfer first from the hot exhaust gases to the plate element, then as it rotates, from the plate element to the cooler air in the other sectors (Figure 1.10).

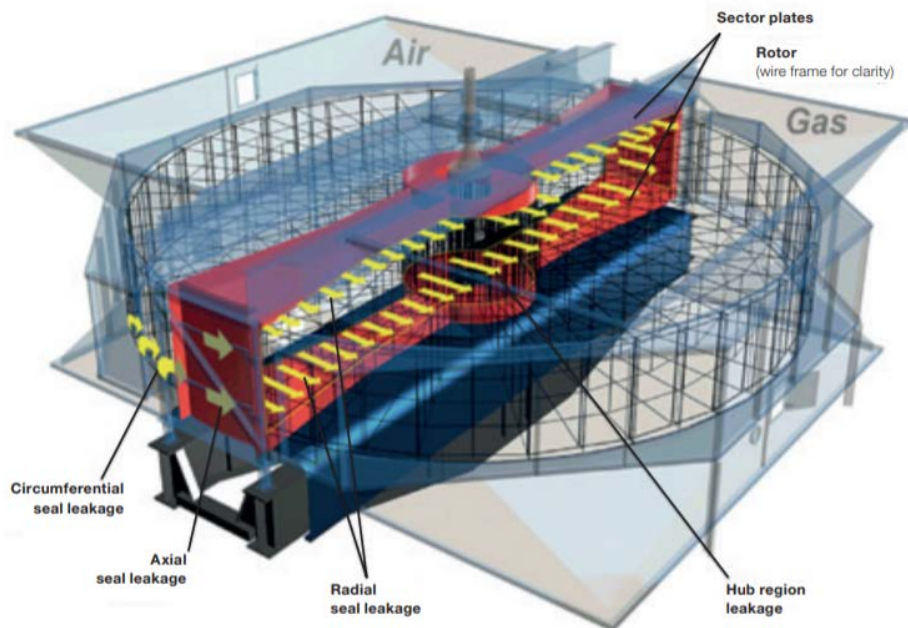


Figure 1.11: Parts of a Regenerative Air preheater [34]

Epsilon professional code employs mass and energy balance and heat transfer analysis to determine thermal performance of the APH, and temperatures of heat transfer surfaces, combustion air, and flue gas throughout the heat transfer matrix. The EPV-11 code was used for prediction of the effects of plant and APH operating conditions on thermal performance of the APH and, temperature of the heat transfer matrix, which is

needed to assess condensation of sulfuric acid on the APH heat transfer surfaces operating below the acid dew point.

## CHAPTER 2: USE OF LOW-TEMPERATURE HEAT FOR FEED WATER HEATING AND COMBUSTION AIR PREHEAT

### 2.1 Overview

Configurations for using recovery of low-temperature heat from the flue gas analyzed in this work include configurations for feedwater (FW) heating, combustion air preheating and combination of both. The low-temperature heat is recovered from the flue gas using the flue gas cooler (FGC) located upstream of the induced draft (ID) fan and Flue Gas Desulfurization (FGD) equipment (also known as the SO<sub>2</sub> scrubber). A configuration was developed for the post-combustion CO<sub>2</sub> capture retrofit or for a new construction, where the flue gas is cooled to the 129°F to 139°F range. This configuration includes FGC upstream of the ID fan. Performance benefits achieved by using recovered low-temperature heat instead of steam extracted from a steam turbine were determined for the analyzed heat recovery options. All the analyzed configurations used in this study are from a previous study conducted by Dr. Nenad Sarunac [3].

### 2.2 Epsilon Professional Performance analysis Modelling

To determine benefits of using heat recovered from the flue gas for the FW heating, and combustion air preheating, analyses were performed for the reference (baseline) plant configuration presented in Figure 2.1 for three coal types: washed Illinois, PRB, and lignite. The composition and calorific value (HHV) of each coal are specified in Table 2.1. The baseline configuration is a conventional coal-fired power plant employing a boiler, steam turbine cycle with seven stages of regenerative heating of the condensate/feedwater. The condensed steam leaving the condensate pump downstream of the steam condenser is referred to as the condensate up to the main boiler feed pump where its pressure is increased

significantly above the main steam pressure to overcome pressure losses in the boiler. Downstream from the main boiler feed pump, the high-pressure condensate is referred to as feedwater (FW).

Temperature of the condensate leaving the main steam condenser in the Reference Plant is, in this example, 28.52°C (84.34°F). It has to be noted that the condenser outlet temperature is highly site-specific and depends on the temperature of the cooling water into the condenser, condenser size, design, cooling load and state of maintenance (tube cleanliness and air in-leakage, for example). Temperature of the cooling water is also subject to seasonal variations and location of the plant. For the plants equipped with a cooling tower (CT), performance of the cooling tower, being affected by the ambient conditions (temperature and humidity of cooling air, or its wet bulb temperature) process conditions (maldistribution of the cooling air and water, liquid-to-gas (L/G) ratio), and state of maintenance (cleanliness of fill surfaces and the amount of missing or damaged fill) introduces another set of variables, which are discussed in Chapter 5. Combustion air is preheated in a steam air heater (SAH) using steam extracted from the steam turbine cycle to keep temperature of the heat transfer surface in the APH above the acid dewpoint temperature, except in the APH cold end (CE).

Table 2.1: Coal Composition, Ultimate Analysis and HHV [7]

Coal type	Bituminous	Washed Illinois	Powder River Basin (PRB)	Lignite
Coal Classification	High-volatile B	High-volatile C	Subbituminous C	Lignite
Coal Location	Kentucky Muhlenburg	Illinois Sangamon	Wyoming Campbell	North Dakota McLean
<i>Total Moisture</i>	8.5	14.4	26.6	36.8
Ash (% Volume)	10.8	9.6	9.6	5.9
Sulphur (% Volume)	2.8	3.8	0.6	0.9
Hydrogen (% Volume)	5.4	5.8	6.5	6.9
Carbon (% Volume)	65.1	59.7	50	40.6
Nitrogen (% Volume)	1.3	1.0	0.9	0.6
Oxygen (% Volume)	14.6	20.1	36.2	54.1
Calorific value (Btu per Pound)	11,680	10,810	8,630	7,000

The heat transfer surfaces in the APH CE are considered and designed as sacrificial surfaces. The results for all three coals are summarized in Tables 2.2 to 2.4 and Figures 2.5 to Figure 2.7.

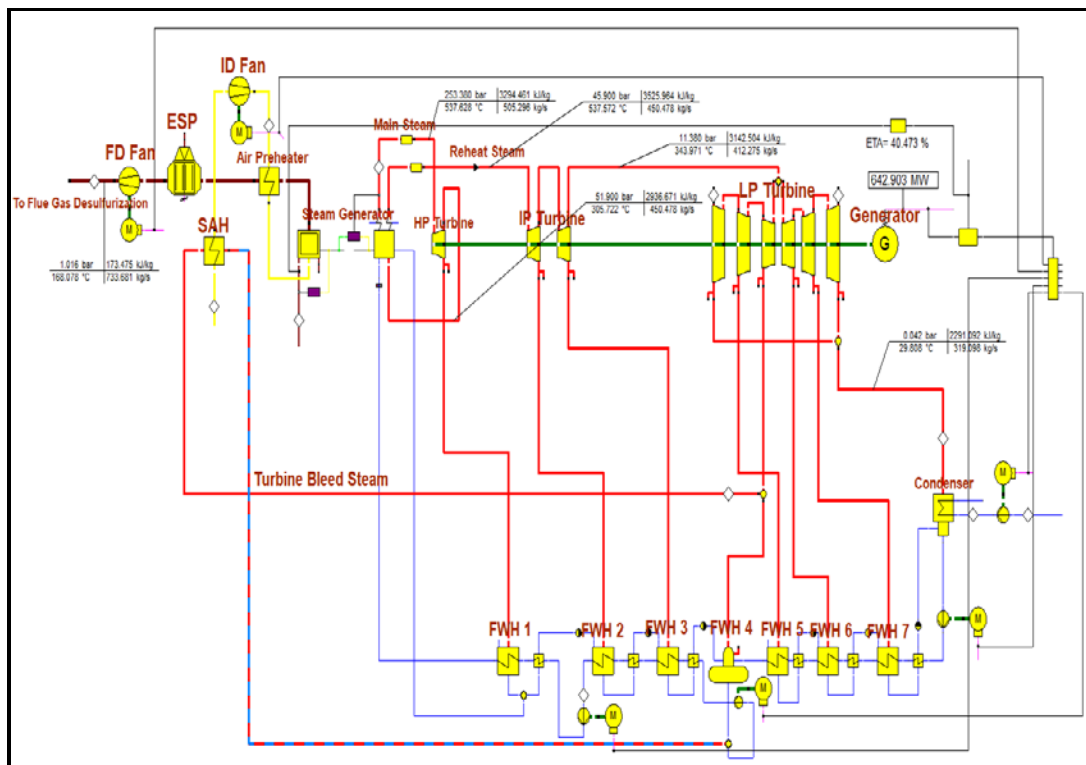


Figure 2.1: Reference Power Plant Configuration (Fuel used is Bituminous Coal) [3]

The first investigated configuration (Configuration A) for using low-temperature heat from the flue gas, involving an FGC upstream of the FGD, is presented in Figure 2.2. Instead of using steam extracted from the steam turbine cycle for the combustion air preheat, combustion air is preheated by the heat recovered from the flue gas stream. This increases steam flow through the low pressure (LP) turbine with resulting increase in the steam turbine power output. The increase in the turbine power output results in an improvement in turbine cycle heat rate, and ultimately in net unit heat rate. Also, since steam extraction for the SAH is eliminated the heat rejected by the condenser, and the condensate flow increase. In the analyzed case the amounts of heat supplied by the extraction steam and recovered from the flue gas were matched  $\sim 97$  MJ/hr ( $\sim 92$  MBtu/hr) to achieve the same level of combustion air preheat. Also, the feed water temperature  $261.1^{\circ}\text{C}$  ( $502^{\circ}\text{F}$ ) entering the boiler was kept constant for all analyzed cases.

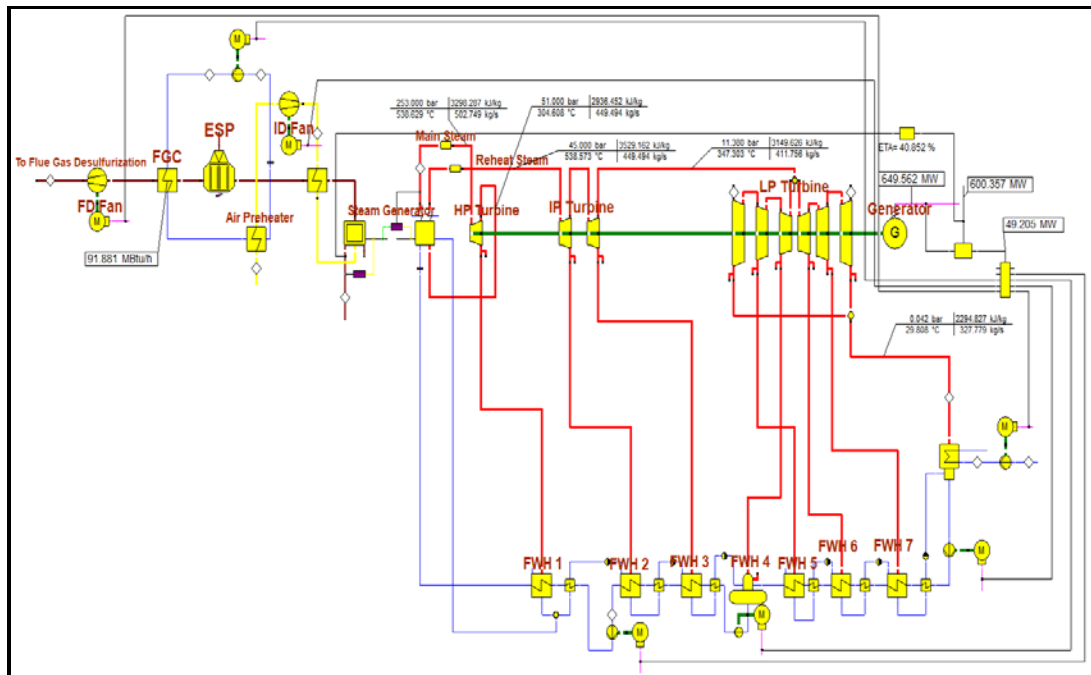


Figure 2.2: Power Plant with FGC for Air Preheating – Configuration A [3]

The second analyzed configuration (Configuration B), for using low-temperature heat from the flue gas involves the FGC upstream of the FGD (see Figure 2.3). As the Figure shows, 100% of the condensate flow leaving the main steam condenser flows through the FGC where it is heated  $\sim 264$  MJ/hr ( $\sim 250$  Mbtu/hr). The heated condensate is circulated back to the steam turbine cycle, eliminating low-pressure (LP) feed water heaters (FWH's) 6 and 7. This arrangement eliminates LP steam extractions and the steam that would normally be used in the FWH6 and FWH7 is expanded in the LP turbine. The result is an increase in the steam turbine power output, increase in steam flow to the condenser and main condensate flow, and increase in heat rejected by the main steam condenser. The increase in turbine power output results in an improvement in turbine cycle and net unit heat rates. In this example, the flue gas is cooled to a temperature of  $115^{\circ}\text{C}$  ( $239^{\circ}\text{F}$ ). Combustion air is preheated by the steam extracted from the steam turbine cycle  $\sim 97$  MJ/hr ( $\sim 92$  Mbtu/hr).

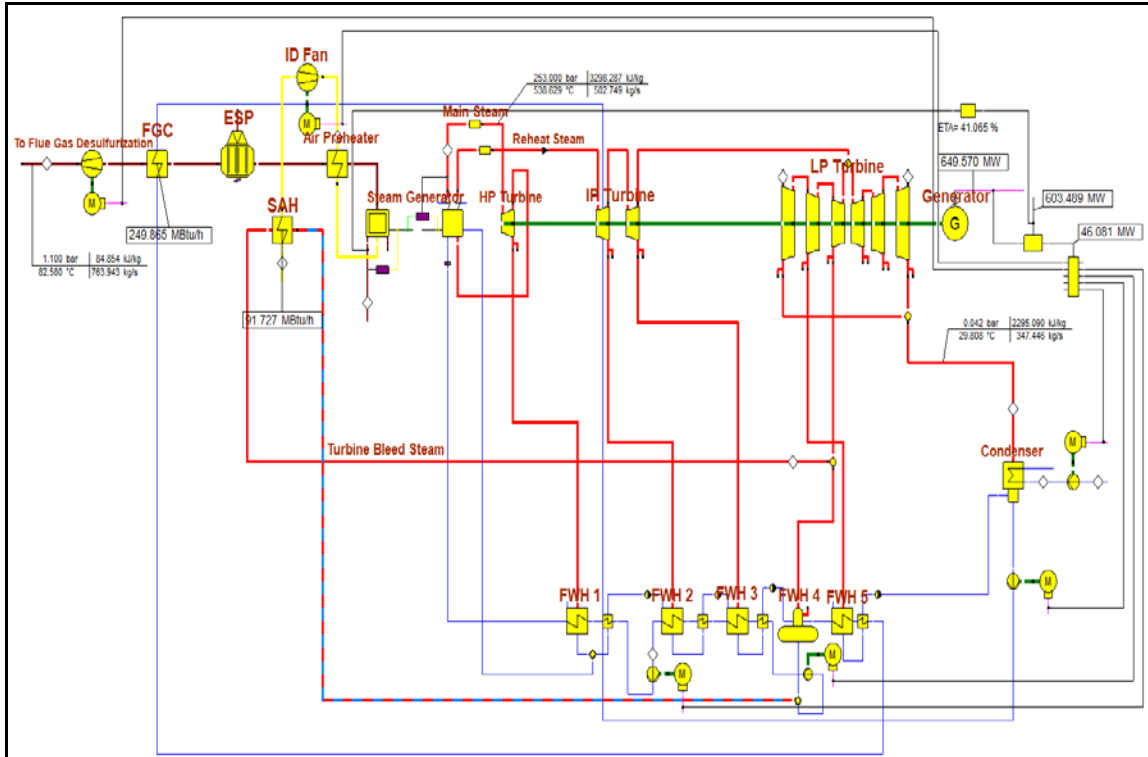


Figure 2.3: Power Plant with FGC for FW Heating and SAH for Air Preheating – configuration B [3]

The third Configuration (Configuration C) represents combination of the above-mentioned configurations A & B, where a portion of heat recovered from the flue gas is used for FW heating  $\sim 167$  MJ/hr ( $\sim 158$  Mbtu/hr), while the remaining heat is used for the combustion air preheat  $\sim 97$  MJ/hr ( $\sim 92$  Mbtu/hr). Schematic of Configuration C is presented in Figure 2.4. For clarity, the FGC is divided into two parts where FGC 1 is used for the FW heating, and FGC 2 is used for combustion air preheat.

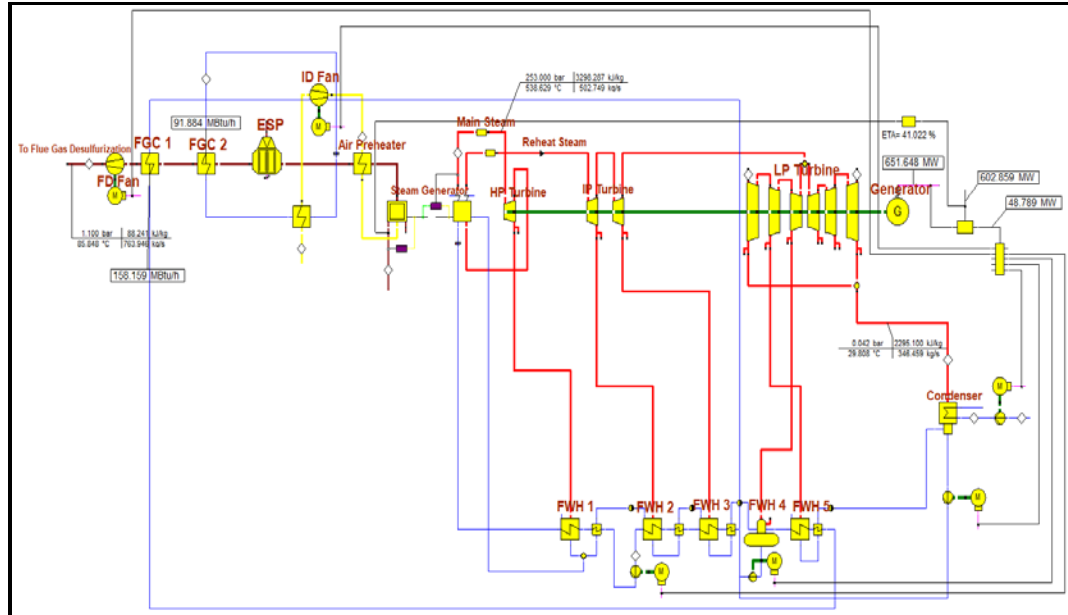


Figure 2.4: Power Plant with FGC's for Feed Water Heating and Air Preheating [3]

Table 2.2 to 2.5 shows various performance parameters of different configurations firing Bituminous, Washed Illinois, PRB and Lignite coals as described in this Chapter. The performance parameters such as Gross Power output ( $P_G$ ), Net Power Output ( $P_{net}$ ), Unit Cycle Heat rate ( $HR_{cycle}$ ), Unit Net Heat rate ( $HR_{net}$ ), Unit cycle Efficiency ( $\eta_{cycle}$ ) and Net cycle efficiency ( $\eta_{net}$ ) are calculated using the Equations 1.1 to 1.7 stated in Chapter 1. Heat Rejected in the condenser ( $Q_{condenser}$ ), is calculated using equation 2.1.

$$Q_{condenser} = (P_G \cdot HR_{cycle} \cdot (1 - \eta_{cycle})) - Q_{sah} \quad (2.1)$$

$Q_{sah}$  is the heat input from turbine steam extraction utilized by steam air preheater. Equation 2.1 is applicable to configurations which employs SAH to preheat the combustion air using steam from steam turbine bleed extraction.

Table 2.2: Performance parameters for Bituminous Coal fired plant

<b>Description (Configuration)</b>	<b>P<sub>G</sub></b>	<b>HR<sub>cycle</sub></b>	<b>P<sub>SS</sub></b>	<b>P<sub>net</sub></b>	<b>HR<sub>net</sub></b>	<b>Q<sub>condenser</sub></b>	<b>η<sub>net</sub></b>
	MW	Btu/kWh	MW	MW	Btu/kWh	MBtu/kWh	%
Design with SAH (Reference plant)	642.90	7,186	49.60	593.30	7,787	2,335	43.82
FGC for air heating (A)	649.56	7,113	49.21	600.36	7,695	2,404	44.34
SAH + FGC for FW heating (B)	649.07	7,118	46.31	602.76	7,688	2,314	44.52
FGC for air and FW heating (C)	651.65	7,090	48.78	602.87	7,664	2,397	44.52

Table 2.3: Performance parameters for Washed Illinois Coal fired plant

<b>Description (Configuration)</b>	<b>P<sub>G</sub></b>	<b>HR<sub>cycle</sub></b>	<b>P<sub>SS</sub></b>	<b>P<sub>net</sub></b>	<b>HR<sub>net</sub></b>	<b>Q<sub>condenser</sub></b>	<b>η<sub>net</sub></b>
	MW	Btu/kWh	MW	MW	Btu/kWh	MBtu/kWh	%
Design with SAH (Reference)	642.90	7,186	51.10	591.81	7,807	2,335	43.71
FGC for air heating (A)	649.56	7,113	50.44	599.12	7,720	2,404	44.22
SAH + FGC for FW heating (B)	649.46	7,114	47.40	602.06	7,715	2,312	44.30
FGC for air and FW heating (C)	652.24	7,083	49.86	602.38	7,695	2,395	44.35

Table 2.4: Performance parameters for PRB Coal fired plant

<b>Description (Configuration)</b>	<b>P<sub>G</sub></b>	<b>HR<sub>cycle</sub></b>	<b>P<sub>SS</sub></b>	<b>P<sub>net</sub></b>	<b>HR<sub>net</sub></b>	<b>Q<sub>condenser</sub></b>	<b>η<sub>net</sub></b>
	MW	Btu/kWh	MW	MW	Btu/kWh	MBtu/kWh	%
Design with SAH (Reference)	642.90	7,186	53.28	589.62	7,836	2,335	43.55
FGC for air heating (A)	649.56	7,113	54.10	595.46	7,759	2,404	44.05
SAH + FGC for FW heating (B)	650.65	7,101	50.63	600.02	7,730	2,308	44.31
FGC for air and FW heating (C)	652.66	7,079	53.85	598.81	7,715	2,393	44.22

Table 2.5: Performance parameters for Lignite Coal fired plant

<b>Description (Configuration)</b>	<b>P<sub>G</sub></b>	<b>HR<sub>cycle</sub></b>	<b>P<sub>SS</sub></b>	<b>P<sub>net</sub></b>	<b>HR<sub>net</sub></b>	<b>Q<sub>condenser</sub></b>	<b>η<sub>net</sub></b>
	MW	Btu/kWh	MW	MW	Btu/kWh	MBtu/kWh	%
Design with SAH (Reference)	642.90	7,186	55.81	587.09	7,869	2,335	43.36
FGC for air heating (A)	649.56	7,113	58.22	591.34	7,790	2,404	43.85
SAH + FGC for FW heating (B)	651.99	7,086	54.39	597.60	7,730	2,304	44.18
FGC for air and FW heating (C)	654.71	7,057	57.47	597.24	7,710	2,386	44.12

Tables 2.6 to 2.8 provides percentage of increase in Net power output, Net unit efficiency and Net unit Heat rate with respect to the reference plant configuration with SAH for different configurations firing all four types of coal (Bituminous, Washed Illinois, PRB and Lignite) analyzed in this study.

Table 2.6: Results- Increase in Power Output with Respect to Reference

<b>Increase in Power Output [%]</b>					
<b>Configuration Description</b>	<b>Configuration</b>	<b>Bituminous</b>	<b>Washed Illinois</b>	<b>PRB</b>	<b>Lignite</b>
FGC for air heating	A	1.04	1.04	1.04	1.04
SAH + FGC for FW heating	B	0.96	1.02	1.21	1.41
FGC for air and FW heating	C	1.36	1.45	1.52	1.84

Table 2.7: Results – Improvement in Net Unit Heat Rate with Respect to Reference

<b>Improvement in Net Unit Heat Rate [%-relative]</b>					
<b>Configuration Description</b>	<b>Configuration</b>	<b>Bituminous</b>	<b>Washed Illinois</b>	<b>PRB</b>	<b>Lignite</b>
FGC for air heating	A	1.17	1.11	0.98	1.01
SAH + FGC for FW heating	B	1.27	1.17	1.35	1.77
FGC for air and FW heating	C	1.58	1.43	1.53	2.03

Table 2.8: Results – Increase in Net Unit Efficiency with Respect to Reference

<b>Increase in Net Unit Efficiency [%-point]</b>					
<b>Configuration Description</b>	<b>Configuration</b>	<b>Bituminous</b>	<b>Washed Illinois</b>	<b>PRB</b>	<b>Lignite</b>
FGC for air heating	A	1.19	1.18	1.16	1.13
SAH + FGC for FW heating	B	1.59	1.36	1.76	1.90
FGC for air and FW heating	C	1.61	1.47	1.56	1.76

Performance improvements for Configurations A to C and four analyzed coal types (bituminous, lignite, PRB, and Illinois<sup>1</sup>) are presented in Figures 2.5 to 2.7. Improvement in power output for Configuration A is virtually insensitive to the type of coal used. For all three configurations magnitude of performance improvement is a function of the coal type and increases with the increase in coal moisture content and is highest for lignite's. Higher moisture content in coal results in higher content of water vapor (diatomic gas) in the flue gas. Since diatomic gases have substantially higher specific heat content compared to monoatomic gases, heat content (thermal capacity) of flue gas increases as fuel moisture content increases. Thus more waste heat is available for recovery and beneficial use for coals containing higher amounts of moisture. The results reported in [8, 9, and 10] are compared to the results found in this study and found to be of similar magnitude.

The results presented in [8] for a subcritical unit and higher temperature of the condensate leaving the condenser (40.7°C vs 30°C; 105.3°F vs. 85.9°F) for low- and mid-moisture fuels show approximately 0.2% lower improvement in net unit heat rate compared to Figure 2.6.

---

<sup>1</sup> Illinois coals are washed to reduce sulfur content. Associated reduction in mercury content is a co-benefit.

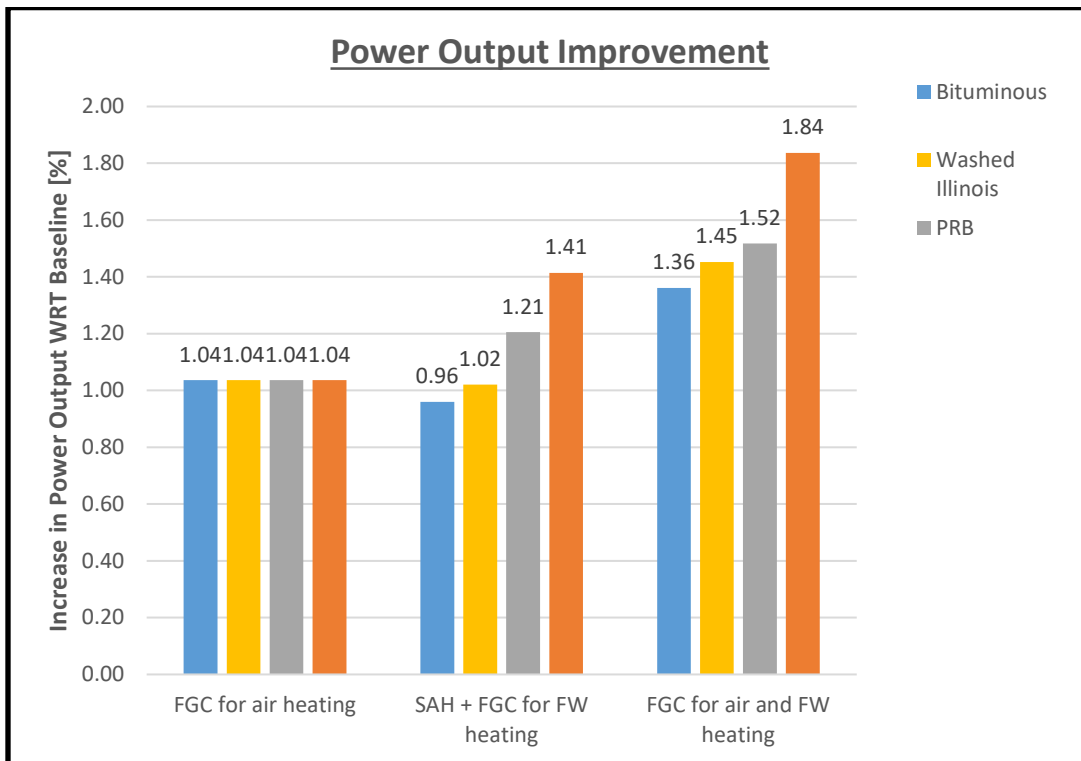


Figure 2.5: Increase in Power Output as a Function of Configuration and Coal Type

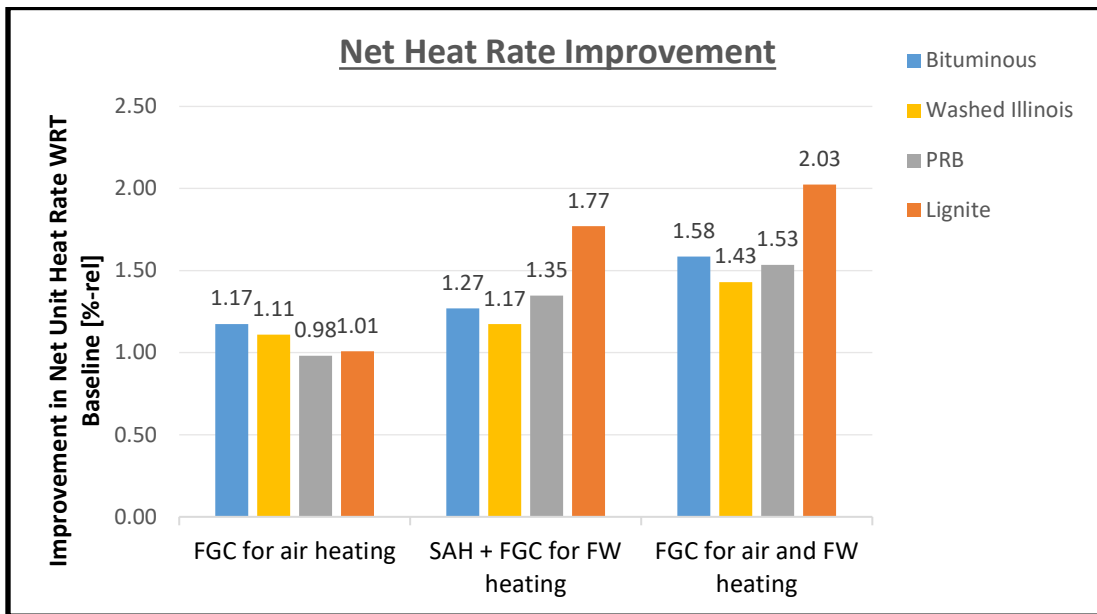


Figure 2.6: Improvement in Net Unit Heat Rate as a Function of Configuration and Coal Type

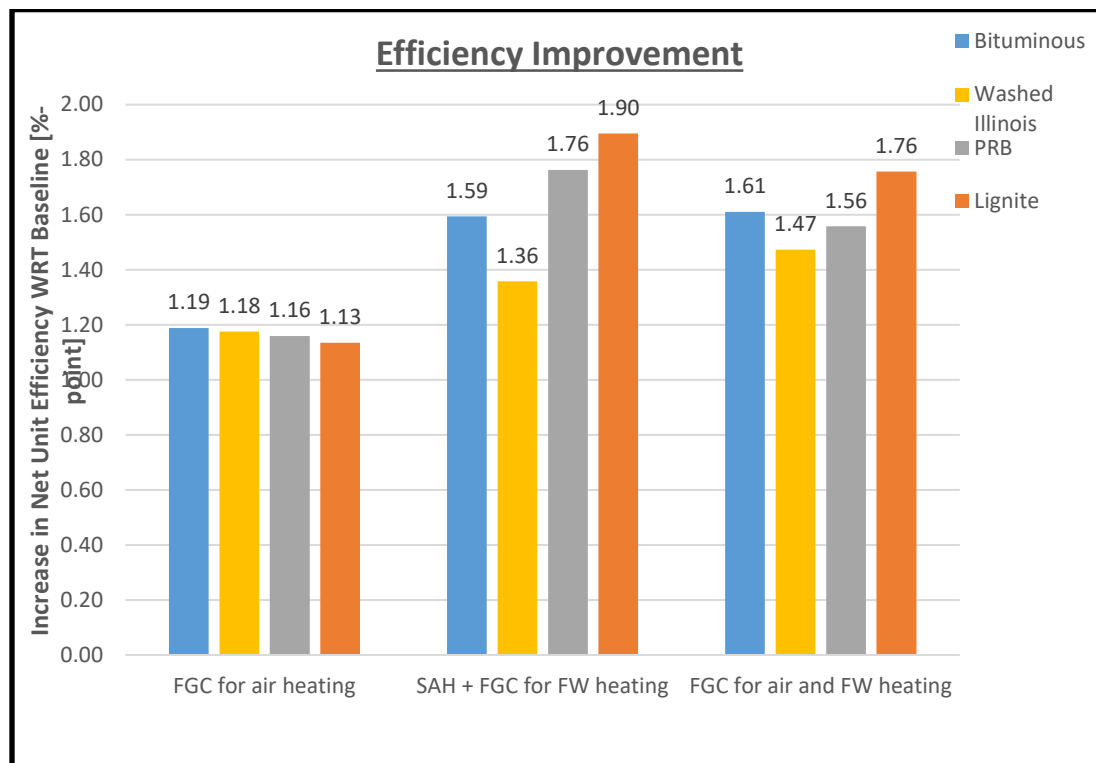


Figure 2.7: Increase in Net Unit Efficiency as a Function of Configuration and Coal Type

In summary, performance improvements achievable by using heat recovered from the flue gas for FW heating and combustion air preheat can be significant and should be considered as measures for improving performance and reducing emissions of existing and newly constructed power plants. For the existing power plants where it is difficult or impossible to raise steam parameters to improve performance of the steam turbine cycle, the use of heat recovered from the flue gas offers an attractive alternative. Optimization of system configuration, such as temperature of the preheat air leaving the APH, and FW bypass (fraction of the FW flow bypassing low-pressure FWHs -100% bypass was used in this work) and efficiently utilizing optimum amount of waste heat for both air preheating

and FW heating is needed for highest performance improvement, or highest return on investment (ROI).

The FGCs operates below the acid dew point and FGC heat transfer surfaces have to be constructed of corrosion-resistant materials. The FGCs is discussed in more detail in Chapter 2.3 and the information about the FGC's are referenced from a previous study conducted by Dr. Nenad Sarunac in his ICCI project report [3].

The use of low-temperature heat, recovered from the flue gas originated from Europe, where this technology has been used to improve performance of coal-fired power plants and industrial plants for more than 15 years. Utility companies such as RWE Power, Vattenfall and others utilize the low-temperature heat from flue gas for feed water (FW) heating and preheating of combustion air. Several different configurations with different commercial names, such as PoweriseR, were developed and successfully used at power plants such as: Schwarze Pumpe, Mehrum, Niederaussem, Lippendorf, and Werndorf in Germany, Voitsberg in Austria, and other locations, including industrial plants, and waste-to-energy plants, such as Vestforbraending in Denmark, where recovered low temperature heat is used for district heating.

### 2.3 Flue gas coolers and Heat Exchangers

A flue gas cooler is an important piece of equipment enabling recovery of heat from the flue gas. Since a significant section of the FGC operates below the acid dewpoint temperature, heat transfer surface need to be constructed from the corrosion-resistant materials, such as corrosion-resistant alloys, carbon steel coated by corrosion-resistant coatings, high-temperature corrosion-resistant plastic tubing, or borosilicate glass.

The Babcock Borsig Services GmbH (BBS), from Oberhausen, Germany has a long experience with the low-temperature heat recovery from the flue gas. The low temperature heat recovery technology PoweriseR, originally developed by BDT Engineering (Balke-Durr Energietechnik, GmbH), has been used since 1985 at utility- and industry owned power plant to improve efficiency and reduce emissions.

The heat exchanger is built of smooth fluoroplastic Teflon (G-FlonR) tubes arranged in a U-tube configuration, Figures 2.8, 2.9 and 2.10. A G-Flon foil lining protects the FGC casing against condensing acid. G-Flon features high resistance to corrosion and reasonable heat conduction transfer characteristics.

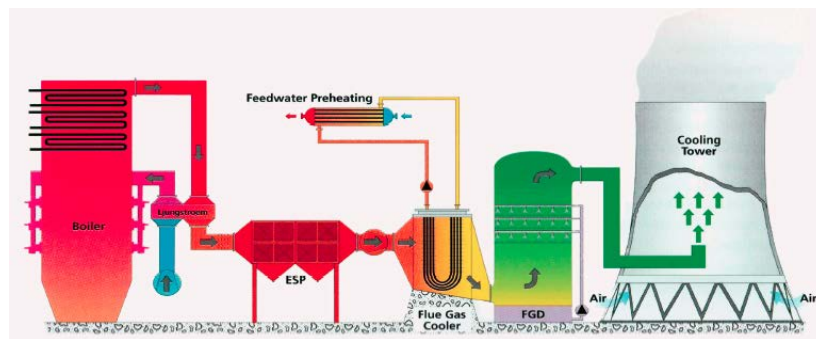


Figure 2.8: General Design of the BBS Flue Gas Cooler [3]



Figure 2.9: Installation of FGC module [3]

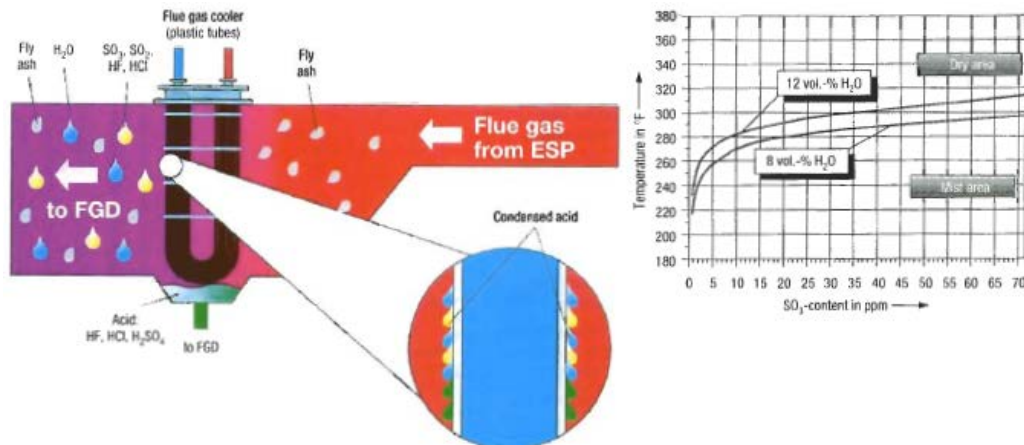


Figure 2.10: Acid Condensation within the FGC [3]

Sulfuric acid condenses on surfaces of the heat transfer tubes and the FGC skin, forming a thin layer of diluted sulfuric acid which attracts fly ash and forms deposits. The deposits, forming on vertical heat transfer tubes, are cleaned (washed) by using an integrated proprietary water washing system. Wash water and condensed acid are discharged into the FGD. Some acid forms mist in the flue gas stream, Figure 2.10. Other acids from the flue gas, such as HCl and HF condense as well, either on heat transfer surface or as a mist. Condensation rates of hydrochloric acid, measured in [36], are presented in Figure 2.11.

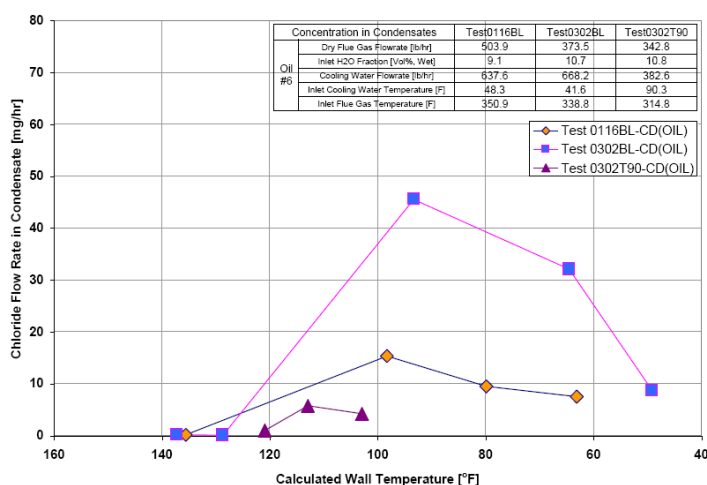


Figure 2.11: Condensation of Hydrochloric Acid [3]

Recent design changes to the non-metallic design at some power generation sites, such as Schwarze Pumpe, involve application of corrosion-resistant alloys in FGC areas subject to severe acid attack and fouling. This material change has enabled better cleaning of the heat transfer tubes. Plastic tubes in the original heat exchanger design appeared to be flexing in the flue gas stream, making it difficult to remove accumulated deposits by the water-wash system. As a result, pressure drop across the FGC has increased. Retrofit with corrosion-resistant alloy tubes has solved the cleaning problem. The retrofitted FGC at Schwarze Pumpe is presented in Figure 2.12.



Figure 2.12: Side View of the FGC at Schwarze Pumpe Retrofitted with Corrosion-Resistant Alloy Tubes, October 2008 [3]

Use of corrosion-resistant plastic or alloy tubes increases cost of an FGC. As a rule of the thumb, the cost of an FGC operating below acid dewpoint is about ten times higher compared to the finned tube design employing carbon steels. The cost of the BBS heat exchanger is approximately \$0.13 per Btu/hr of recovered heat, installed.

The Flucorex AG, located in Switzerland, is another manufacturer of the corrosion-resistant heat exchangers. The company has been commissioned to supply FGCs for lignite-fired power plants at Neurath and Boxberg, Germany. The heat transfer tubes are made of nickel base alloy (DIN 2.4605/UNS N06059, trade name "Alloy 59"), corrosion-resistant fluoroplastic, or mild steel tubes double lined with an enamel/glass + PFA. The casing is lined with 1.5 mm PFA fluoroplastic sheets. Alloy 59 is suitable for cooling gas with a low concentration of HCl and HF ( $\sim 20 \text{ mg/m}^3$ ).

The cost of the gas-to-water heat exchanger (WAGAVO) made of Alloy 59 is approximately \$0.095 per Btu/hr of recovered heat (price as of 2007, [3]). A WAGAVO heat exchanger made of enamel glass lined mild steel is approximately \$0.063 per Btu/hr of recovered heat (price as of 2007, [3]). This price does not include piping, valves, pumps, tanks, and any other components of the closed water loop. The materials are used in a flue gas-to-water heat exchanger design.

The gas-to-gas heat exchanger (GAGAVO) with in-line placed plastic tubes in cross flow arrangement is specifically designed for flue gas reheat, Figure 2.13. Raw flue gas flows inside the tubes from top to bottom, while the clean gas exiting the FGD flows around the tubes. All parts in contact to flue gas are corrosion resistant and made of PTFE,

PFA, or nickel base alloy, Figure 2.14. The GAGAVO price is approximately \$0.1 per Btu/hr of recovered heat.

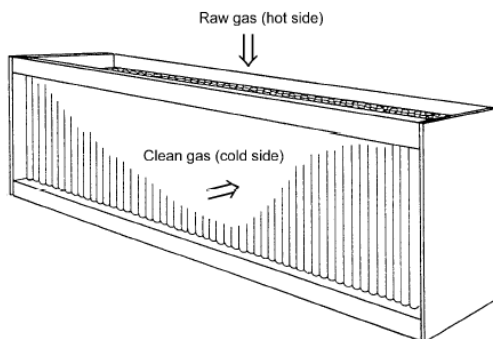


Figure 2.13: GAGAVO Flue Gas Cooler by Flucorex [3]



Figure 2.14: Modular Design of GAGAVO Heat Exchanger with PTFE Tubes. Internal Surface are Lined by PFA Fluoroplastic Sheets [3]

Depending on the plant operating conditions a water washing system may be installed at the top of the GAGAVO casing. Water washing of the inner surface of the plastic tubes removes any deposits that may form due to the dust load and acid content of

the untreated gas. The cleaning system is designed for each particular application and comprises of a stationary or retractable water washing lance with several nozzle groups.

The washing cycle is programmable to meet plant-specific conditions

## CHAPTER 3: PARTIAL AND FULL ARC STEAM ADMISSION TO TURBINE

### 3.1 Overview

For steam turbine operation and control we will begin by looking at the means of controlling turbine speed (in case turbine generator is not synchronized to the grid) or turbine output. When a generator driven by a steam turbine is synchronized to the grid, grid frequency determines the speed. For a 60 Hz system, synchronous speed for a two-pole generator is 3,600 RPM. The principle of turbine control is relatively simple, if turbine output needs to be increased, the mass flow rate of steam through the turbine has to be increased. Conversely in order to decrease power output the amount of steam admitted to the turbine needs to be decreased. Steam flow is controlled by adjusting the turbine admission valves or control valves as they are often called. In the arrangement shown in Figure 3.1 there is one control valve which depending on its setting admits more or less steam to flow into the turbine from the steam chest. When the turbine stop valve is fully open, the steam chest is charged with steam directly from the boiler.

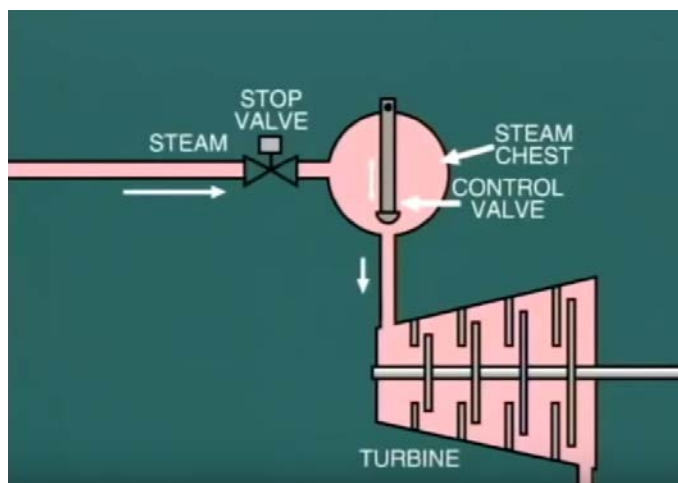


Figure 3.1: Main Steam line to a Turbine [44]

In most steam turbines multiple control valves are used as shown in Figure 3.2. In this arrangement the steam chest is located above the high-pressure section of the turbine shell. Eight control valves shown in Figure 3.2 are opened in sequence according to the position of the cross-arm which is adjusted by the hydraulic control system. These control valves are set in such that only one valve at a time is throttling steam (for example highlighted valve in Figure 3.2), while the others are either fully open or closed depending on the actual load. This valve manipulation scheme results in reduced throttling losses compared to one large control valve which throttles the entire steam flow.

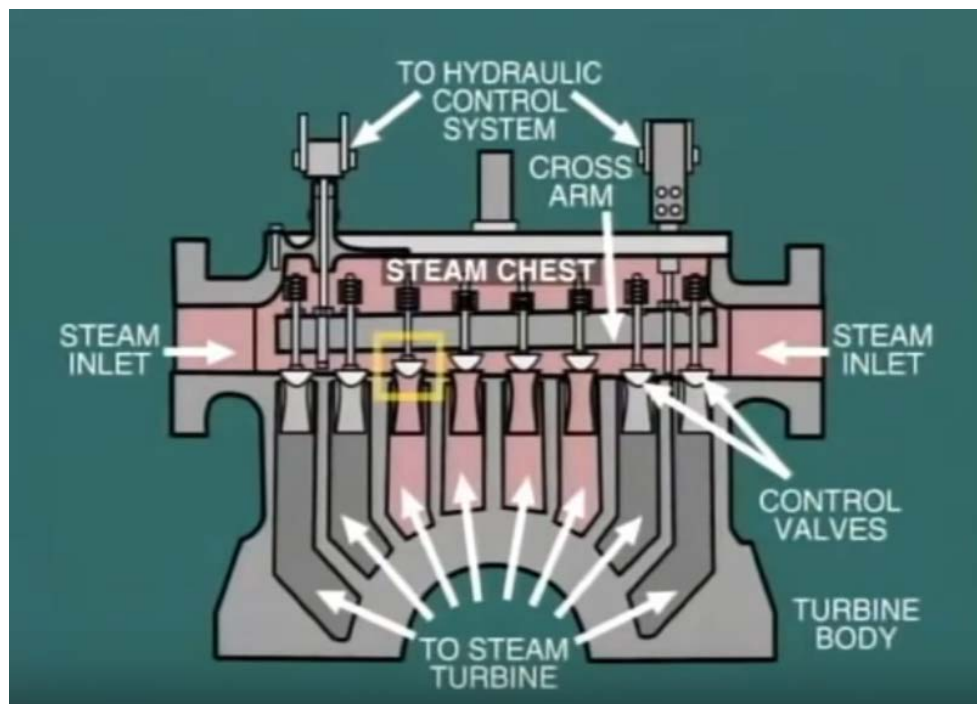


Figure 3.2: Steam Chest with Control Valves [44]

In large machines (larger than 100 megawatts) it is more common to have two steam chests; one located above and one below the shell centerline or on either side of the turbine. In most arrangements of this type a stop valve is fitted at the entrance to each steam

chest (Figure 3.3). During normal operation the stop valve remains in the wide-open position, while the control valves are modulated to adjust steam flow. The actual opening of the control valves is determined by the position of the operating lever which is adjusted by the power cylinder of the hydraulic control gear. The schematic in Figure 3.4 shows us a simplified version of a hydraulic control scheme. In this arrangement a mechanical governor is used to regulate speed until turbine is synchronized to the grid.

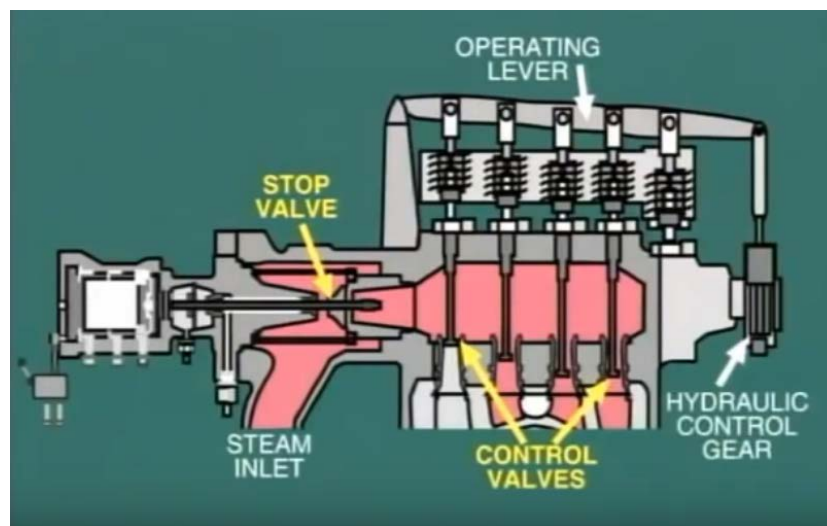


Figure 3.3: Side-mounted Steam Chest with a Stop Valve & Control Valves [44]

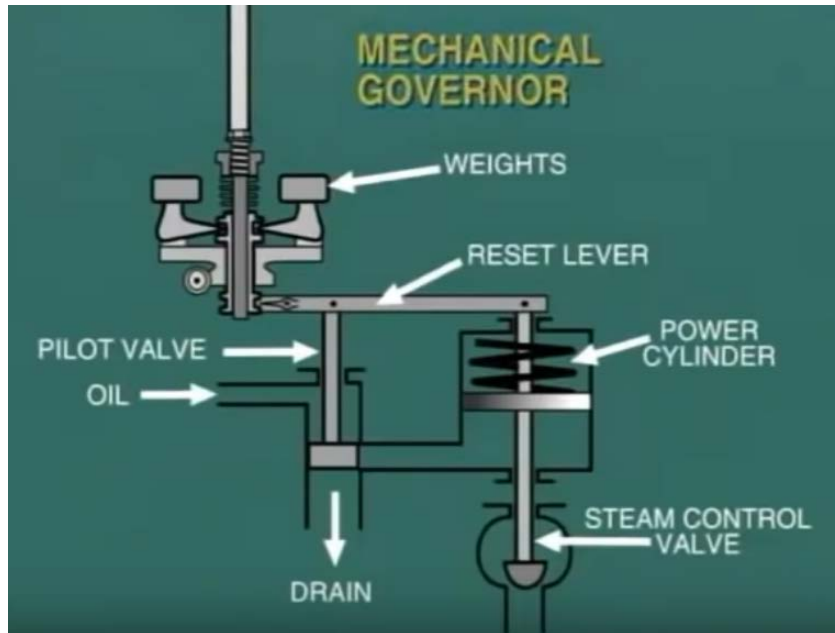


Figure 3.4: Hydraulic Control Scheme [44]

The start-up operation for a steam turbine begins with making sure pipe line leading to the turbine stop valve is charged with a super-heated steam from the boiler. The stop valve drains are open sufficiently to allow any condensed steam to be discharged from the pipe work. This is important since ingestion of the condensate might result in a catastrophic damage to the turbine. Once the main steam line is charged to the full boiler pressure the steam chest is charged by opening the turbine stop valve (Figure 3.5). The stop valve drains retained fully open during this maneuver. Eventually, when the steam chest is fully charged the stop valve will be opened wide and the stop valve drains will be throttled.

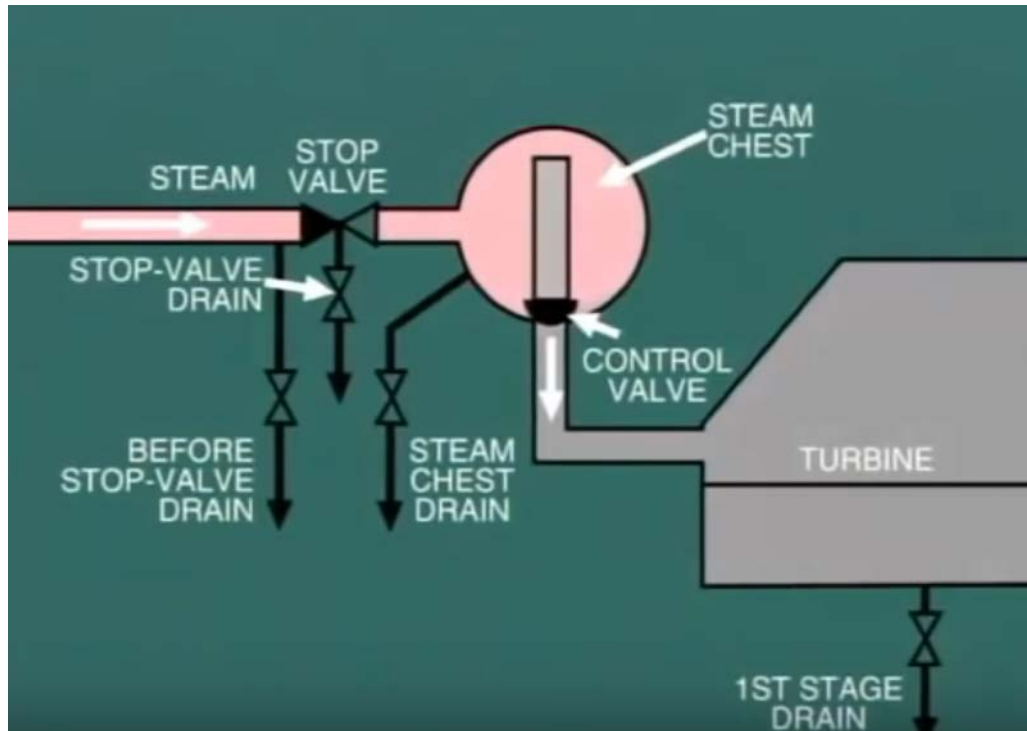


Figure 3.5: Main Steam line to turbine [44]

One of the methods of admitting steam to the turbine and running it up to speed is to operate the control valves by manual operation of the hydraulic control system. In bringing the turbine up to speed relatively little steam is required and it is likely that only one or at the most two of the control valves will be open or partially open to control the rate of speed increase (Figure 3.6). Throttling is undesirable since it has a negative effect on turbine performance.

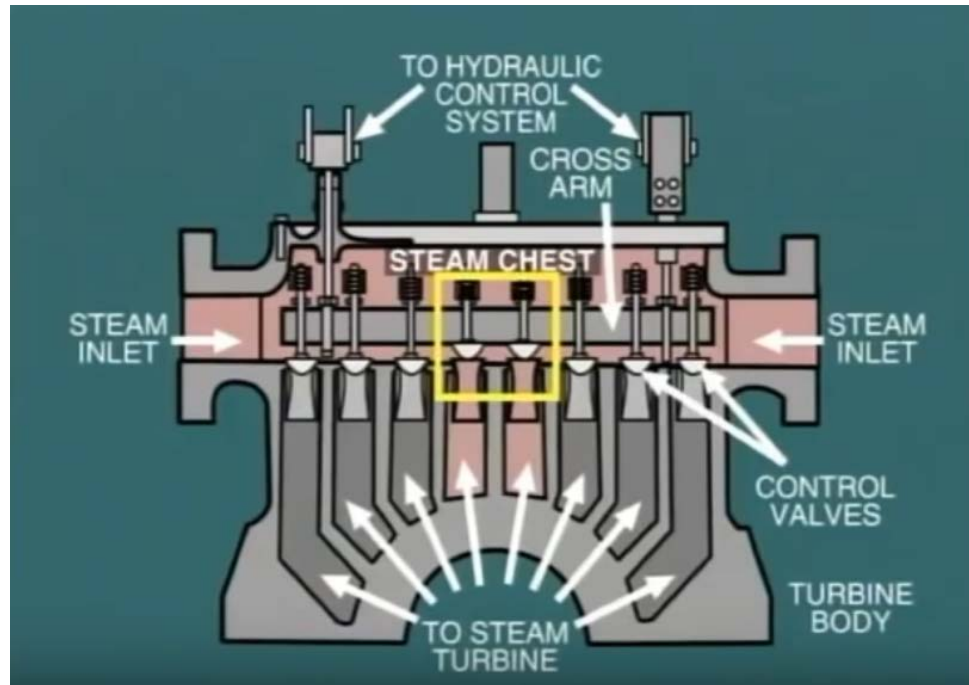


Figure 3.6: Two control valves in partially open position in an over-head mounted steam chest [44]

In the overhead steam chest shown in Figure 3.6 each of the eight control valves is supplying steam to a small arc of the admission nozzles (first stator), consequently with only one or two valves open there would be a tendency for uneven heating of the turbine block (Figure 3.7). This could also lead to differential distortion and eventual cracking of the metal. In addition, steam admission to the turbine is very non-uniform resulting in large aerodynamic losses and non-uniform vane and blade loading. The side mounted steam chests have the same problem, in this arrangement (Figure 3.8) each of the four control valves supplies its arc of steam to the admission nozzles resulting in heat distortion. This method of control is known as the **partial arc admission**.

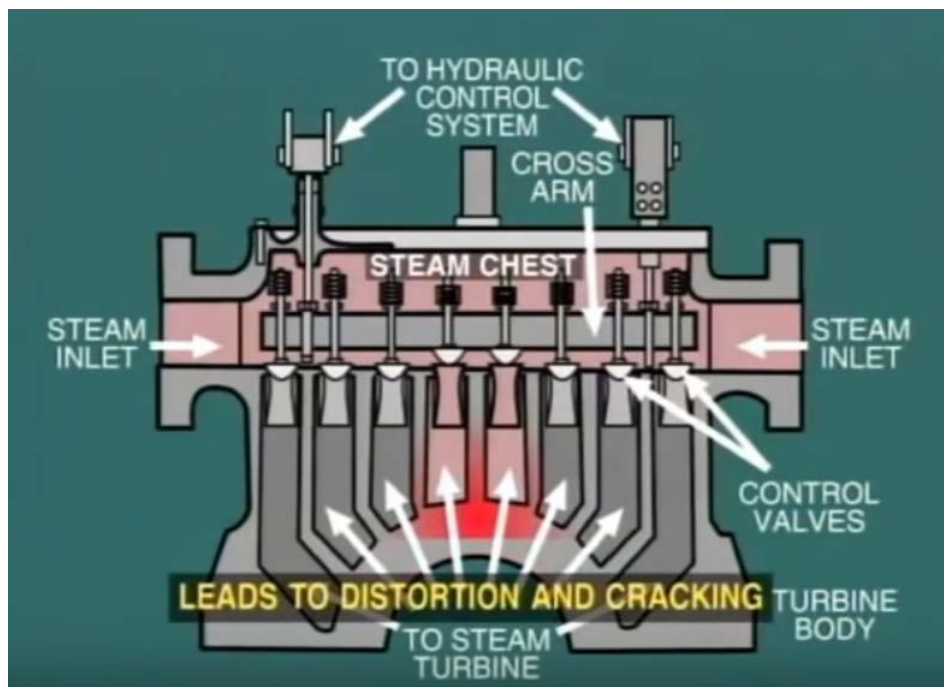


Figure 3.7: Distortion and cracking due to single arc admission [44]

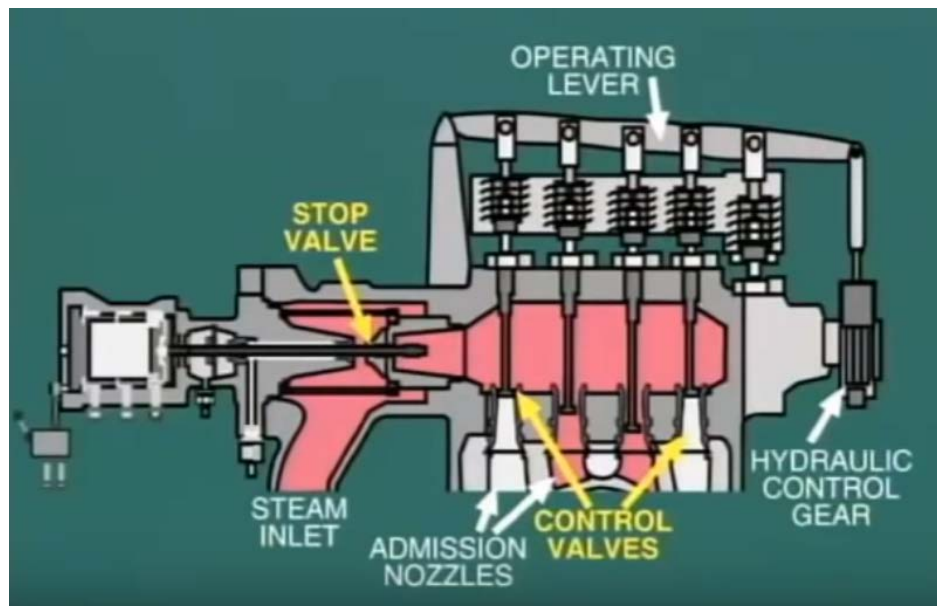


Figure 3.8: Side mounted steam chest with four control valves [44]

When the turbine is on load more of the valves are opened thus providing more even heating of the nozzle block. In large turbines non-uniform heating caused by partial arc admission is particularly pronounced, and turbine startup is usually performed in a different manner that is by the **full arc admission**. In this case the stop valve is closed after heating the steam chest and all control valves are fully opened providing access to the complete 360 degrees, or full arc, of admission nozzles. Steam flow to the turbine is controlled by throttling the stop valve (Figure 3.9). This may be carried out by manual operation on a hand wheel from the turbine deck or remotely from the control room. With this arrangement the turbine governor takes control by throttling the control valves as the turbine speed approaches its normal operating level before synchronization.

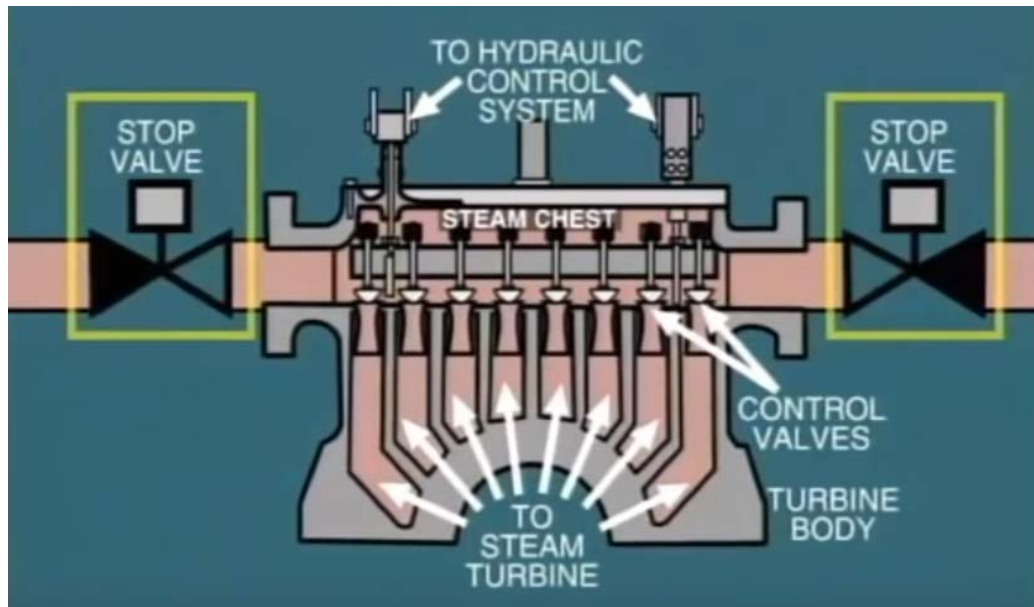


Figure 3.9: Full arc admission with throttling of stop valves [44]

### 3.2 Basis of Calculations performed in Epsilon Professional Code

The thermodynamic effect on the turbine efficiency is best understood by explaining the expansion process through the turbine with number of stages. We have considered 4 stages between states 1 and 5 as shown in Figure.3.11 with total expansion being divided into four stages with same stage efficiency and pressure ratio. Pressure ratio is expressed as stated in equation 3.1,

$$\frac{P_1}{P_2} = \frac{P_2}{P_3} = \frac{P_3}{P_4} = \frac{P_4}{P_5} \quad (3.1)$$

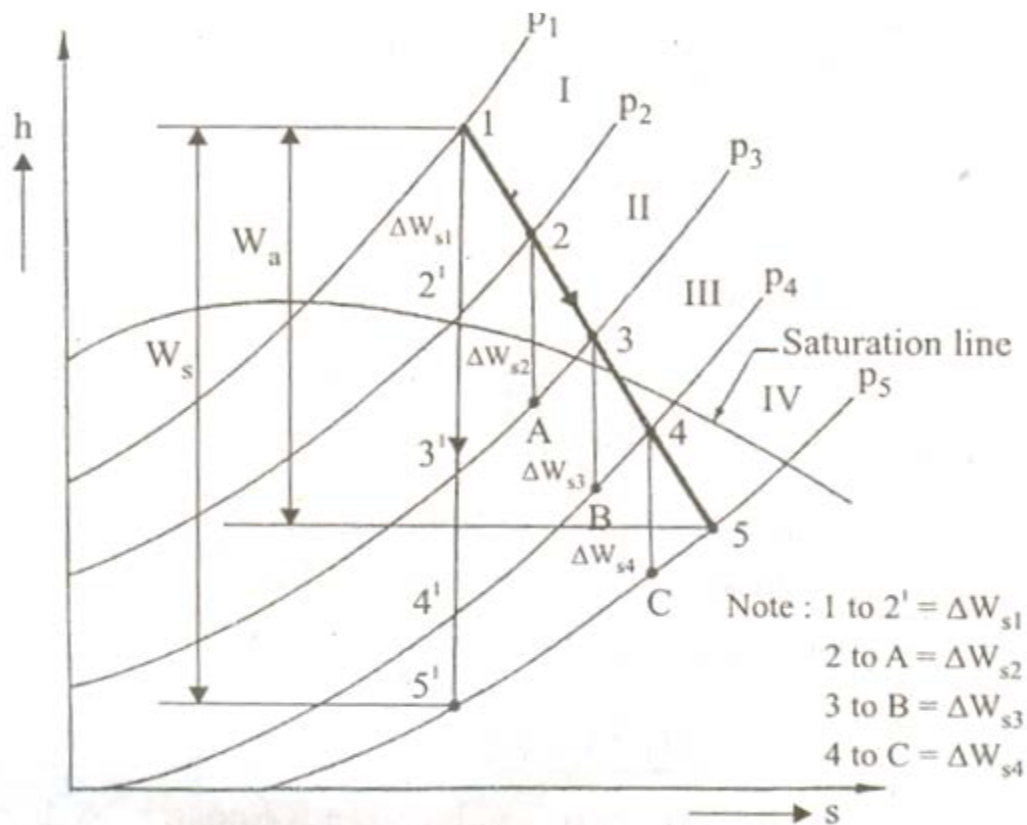


Figure 3.10: Enthalpy-entropy diagram for multi-stage expansion [45, 49]

Let  $\eta_o$  is the overall efficiency of expansion and is defined as the ratio of actual work done per kg of steam to the isentropic work done per kg of steam between 1 and 5 [48].

$$\eta_o = \frac{W_a}{W_s} \quad (3.2)$$

$$\eta_o = \frac{h_1 - h_5}{h_1 - h'_5} \quad (3.3)$$

The actual work done per kg of steam  $W_a$  is,

$$W_a = \eta_o \cdot W_s \quad (3.4)$$

Isentropic or ideal values in each stage are  $\Delta W_{s1}, \Delta W_{s2}, \Delta W_{s3}, \Delta W_{s4}$ . Therefore, the total value of the actual work done in these stages is,

$$W_a = \Sigma (1 - 2) + (2 - 3) + (3 - 4) + (4 - 5) \quad (3.8)$$

Also, stage efficiency for each stage is given by,

$$\eta_s = \frac{\text{Actual work done per kg of steam}}{\text{Isentropic work done in stage}} = \frac{W_{a1}}{W_{s1}} \quad (3.9)$$

For Stage 1,

$$\eta_{s1} = \frac{W_{a1}}{W_{s1}} = \frac{h_1 - h_2}{h_1 - h'_2} = \frac{W_{a1}}{\Delta W_{s1}} \quad (3.10)$$

Or

$$W_{a1} = \eta_{s1} \cdot \Delta W_{s1} \quad (3.11)$$

$$\Delta W_a = \Sigma \Delta W_a = \Sigma [\eta_{s1} \cdot \Delta W_{s1} + \eta_{s2} \cdot \Delta W_{s2} + \eta_{s3} \cdot \Delta W_{s3} + \eta_{s4} \cdot \Delta W_{s4}] \quad (3.12)$$

For same stage efficiency in each stage;  $\eta_{s1} = \eta_{s2} = \eta_{s3} = \eta_{s4}$

$$W_a = \eta_s \cdot \Sigma [\Delta W_{s1} + \Delta W_{s2} + \Delta W_{s3} + \Delta W_{s4}] = \eta_s \cdot \Sigma \Delta W_s \quad (3.13)$$

From Equations 3.7 and 3.13,

$$\eta_s \cdot W_o = \eta_s \cdot \Sigma \Delta W_s \quad (3.14)$$

$$\eta_o = \eta_s \cdot \frac{\sum \Delta W_s}{W_s} \quad (3.15)$$

The slope of constant pressure lines on h-s plane is given by,

$$\left(\frac{\partial h}{\partial s}\right)_p = T \quad (3.16)$$

This shows that the constant pressure lines must diverge towards the right. Therefore,

$$\frac{\sum \Delta W_s}{W_s} > 1 \quad (3.17)$$

For expansion process. It is obvious that the enthalpy increases when we move towards right along the constant pressure line. Hence, the summation of  $\Delta W_{s1}$  is more than the total isentropic enthalpy drop  $W_s$

The ratio of summation of isentropic enthalpy drop for individual stage to the total isentropic enthalpy drop is called Reheat factor. Thus,

$$RF = \frac{\sum [\Delta W_{s1} + \Delta W_{s2} + \Delta W_{s3} + \Delta W_{s4}]}{W_s} \quad (3.18)$$

$$RF = \frac{\sum [(1 - 2') + (2 - a') + (3 - b') + (4 - c')]}{(1 - 5)} \quad (3.19)$$

$$RF = \frac{\sum \Delta W_s}{W_s} \quad (3.20)$$

Therefore, the overall efficiency of the expansion process

$$\eta_o = \eta_{stage} \cdot RF \quad (3.21)$$

$$RF = \frac{\sum \Delta W_s}{W_s} > 1 \quad (3.22)$$

The overall efficiency of the turbine  $\eta_o$  is greater than stage efficiencies  $\eta_s$ ,

$$\eta_o > \eta_s \text{ for turbines} \quad (3.23)$$

The calculation of the steam turbine performance has two main objectives:

- The determination of the flow characteristics which describe the correlation of throughput and inlet pressure.
- The power output which is determined as shaft power by means of an efficiency model.

The flow characteristic (inlet pressure as function of mass flow) is determined according to **Stodola's law**. Which means that the flow coefficient at the inlet is defined by a constant for all operating modes.

$$Const = \frac{m_1}{\sqrt{\frac{p_1}{v_1}}} \quad (3.24)$$

With  $m_1$  = Inlet flow,  $P_1$  = Inlet pressure and  $V_1$  = Inlet specific volume. For off-design calculations the inlet pressure is calculated based on induced mass flow and specific volume:

$$\left(\frac{M_1}{MN_1}\right)^2 = \frac{P_1^2 - P_2^2}{PN_1^2 - PN_2^2} \cdot \frac{PN_1}{P_1} \cdot \frac{VN_1}{V_1} \quad (3.25)$$

With  $MN_1$ ,  $PN_1$ ,  $PN_2$  and  $VN_1$  as nominal conditions at the design;  $M_1$ ,  $P_1$ ,  $P_2$  and  $V_1$  as conditions at off-design. An isentropic efficiency model is used to calculate the enthalpy drop during the expansion.

The mechanical energy output at the shaft is evaluated as follows:

$$P = (m_1 \cdot (h_1 - h_2)) \cdot \eta_{mech} - Q_{LossM} \quad (3.26)$$

Energy output can be calculated utilizing isentropic efficiency as below,

$$P = (m_1 \cdot (h_1 - h_{2is}) \cdot \eta_{is}) \cdot \eta_{mech} - Q_{LossM} \quad (3.27)$$

Where,

$m_1$  = Inlet flow, lb/hr (kg/hr)

$h_1$  and  $h_2$  = Inlet and Outlet Enthalpy, Btu/lb (kJ/kg)

$\eta_{is}$  = Isentropic Efficiency, %

$Q_{lossM}$  = Mechanical losses, Btu/hr (kJ/hr)

$\eta_{mech}$  = Mechanical Efficiency, %

Ebsilon profession code takes OEM data to evaluate these losses based on the geometric of the turbine employed, pressure ratio and number of turbine stages of expansion. In practice the flow of steam through nozzle is not isentropic, but accompanied with losses which decrease the kinetic energy of steam coming out of the nozzle. The decrease in kinetic energy is due to the following reasons,

- Viscous forces between steam particles
- Heat loss from steam before entering the nozzle
- Deflection of flow in the nozzle
- Boundary layer development in the nozzle
- Turbulence in the nozzle

The friction in the nozzle which reduces available enthalpy drop and hence actual velocity leaving the nozzle is less than that obtained with is-entropic expansion Figure 3.10 shows a how Ebsilon professional considers various isentropic efficiency based on the exit conditions (pressure) from a Mollier chart. For design condition (100% load operation) the isentropic efficiency of 87% (OEM data) [13, 8] is used in this study with the parameter

ETAİN in the Ebsilon code. The off-design mode (60% - 90% load conditions) estimates the off-design efficiency relative to the nominal efficiency by means of correction curves derived various OEM data (characteristic lines) [1], which correlate the change of efficiency with the ratio of mass flow rate, or the ratio of volumetric flow rate, or the of change expansion pressure ratio.

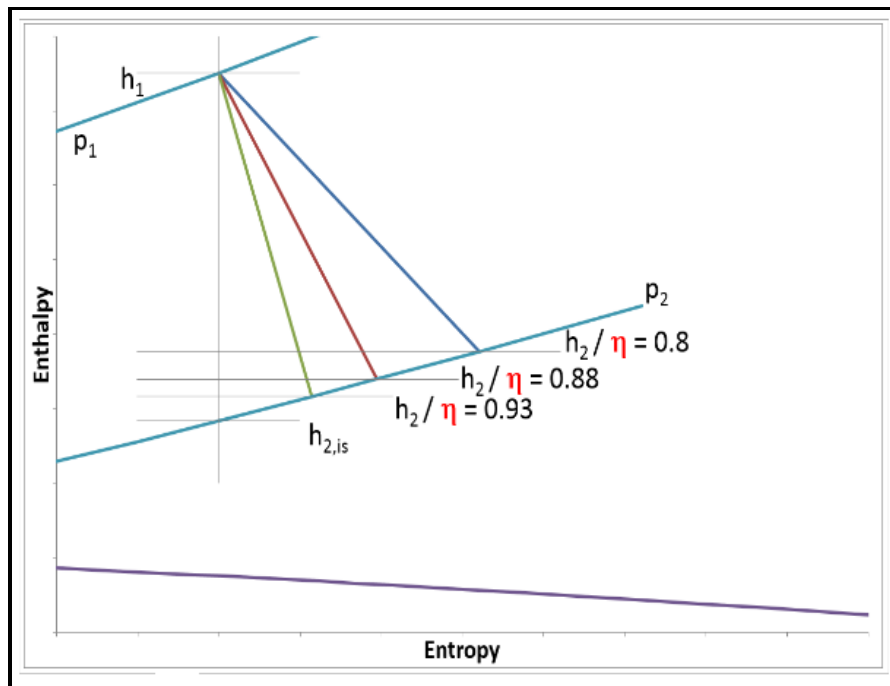


Figure 3.11: Enthalpy (h) - Entropy (s) diagram of an expansion stage (Efficiency values mentioned in the figure are for illustration only) [1]

### 3.2.1 Minimum Part Load consideration and Losses in a Steam Turbine:

Reducing the minimum load at which a steam turbine can reliably operate is one way to increase revenue for marginal base-loaded units during periods of low electrical demand. For this reason, it is not unusual to see merchant plants operating at "super minimum" load levels that are well below the typical 25% rated full-load limits. However,

such units are operating well outside the original equipment manufacturer (OEM) design basis, and owners may experience undesirable damage to their turbines for a number of reasons. That's why it is important for owners to understand the trade-offs and risks that come with such operation. The following is an overview of the main steam turbine issues that must be considered before deciding to operate a steam turbine generator below OEM minimum load limits.

#### 3.2.1.1 Anticipate Increased HP-IP Rotor Vibration:

Units with partial arc admission, where the lower arc valves open first, are more susceptible to increased vibration at reduced minimum loads. This is due to unbalanced upward steam pressure forces that tend to lift the rotor and partially unload the high-pressure/intermediate-pressure (HP-IP) bearings.

Older units employing plain journal bearings may experience oil whip and related vibration at reduced bearing loads. If proper supervisory instrumentation exists, a load test can determine if this is a concern. The operator can perform a load test and perform bearing adjustments at the next outage to determine if minimum load can be reliably reduced. Proper bearing clearances and preloads may be enough to eliminate this concern. If adjustments to the bearings alone do not address oil whip concerns, the operator has an option to change the admission sequence such that the cover valves open first and convert to full arc admission, which will be explored in detailed in this chapter.

#### 3.2.1.2 Nozzle and Valve Erosion Rates:

At super minimum loads, particles exfoliating from the boiler are throttled at much higher velocities through the inlet valves. As a result, the rate of erosion is accelerated on the first

few stages of stationary and rotating vanes, especially on units with partial arc admission (Figures 3.11 and 3.12). Increased throttling also results in additional thermodynamic losses that affect heat rate. Treating the vanes with an erosion-resistant coating can mitigate nozzle block wear.



Figure 3.12: Nozzle Block Solid Particle Erosion (*Courtesy: TG Advisers Inc.*) [52, 53]

Nozzle block erosion, Minute solid material that is thrown off from the boiler is accelerated through the steam turbine nozzle valves and can increase erosion. The nozzle valves accelerate the steam much as a garden hose nozzle accelerates the velocity of water. This increased velocity increases the erosion on the valves and nozzle block [52].



Figure 3.13: Vanes Solid Particle Erosion (*Courtesy: TG Advisers Inc.*) [52, 53]

The HP nozzle block vanes may also experience increased particle erosion but can, under most circumstances, be weld-repaired and returned to service [53].

### 3.2.1.3 Expect the Possibility of More Water Droplet Erosion:

Boiler temperature drop at lower loads typically occurs in both reheat and main steam conditions. Lower steam temperatures will increase moisture levels and move the saturation line further upstream (near the Wilson line) of the last stages of the low-pressure (LP) turbine. At the Wilson line, the state where the first liquid droplets appear, chlorides become concentrated and stress corrosion concerns are elevated (Figure 3.13).

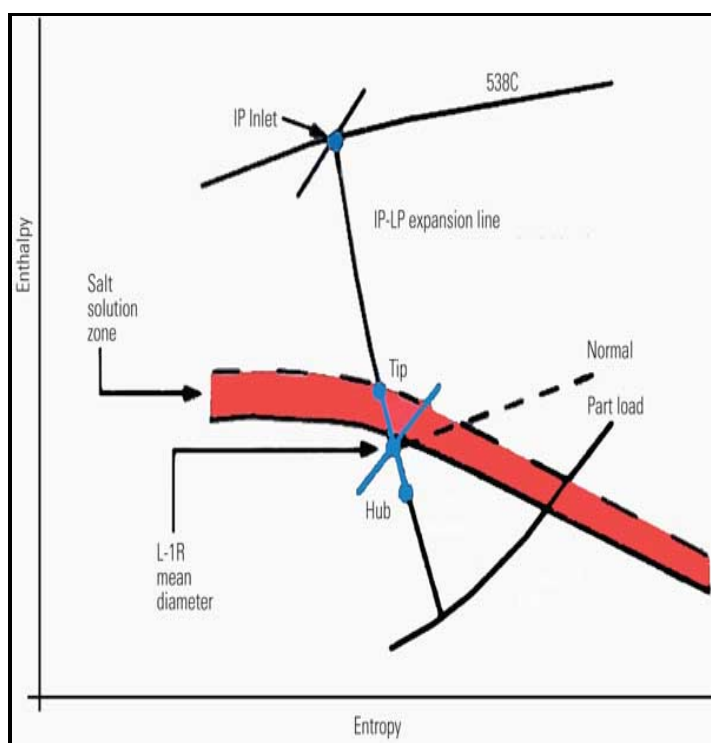


Figure 3.14: Droplet formation at salt solution zone [52, 53]  
(Source: TG Advisers Inc.)

LP salt solution line - The Wilson line is often the zone of first condensation in the LP steam turbine, where steam moisture is typically about 3% to 4%. Concentrated chloride

solutions are often present. The salt solution zone is bordered by the saturation line (dashed line) on top and the Wilson line (the solid line) below the red area, refer figure 3.13 [53]

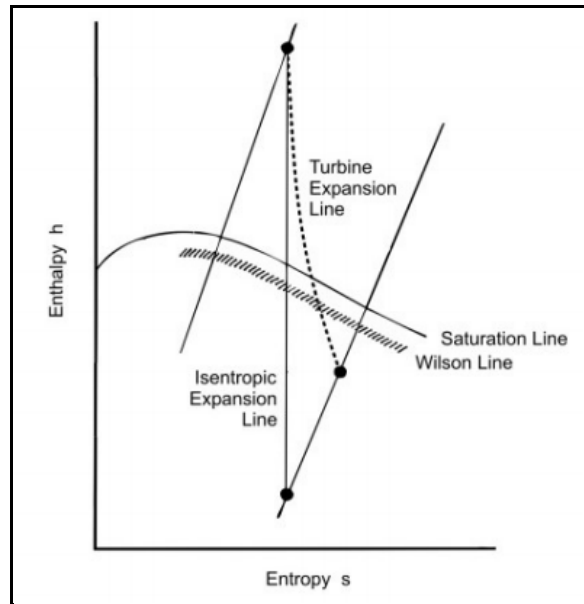


Figure 3.15: Wilson line dicing the wet and dry expansion region [54]

At some point condensation suddenly takes place and the fluid is once again in thermal equilibrium and subject to the laws of a saturated mixture. The points at which this condensation occurs vary depending upon conditions and are scattered in a band somewhat below the saturation line as shown in Figure 3.14. This band is known as the Wilson Line. This expansion results in steam at the later stages with a moisture content of 25%. A high moisture content is intolerable as it results in blade erosion and stage efficiency losses. The undesirability of blade erosion was discussed earlier in this chapter. As steam is expanded through the turbine it starts to condense in the wet region along the 'Wilson line' which corresponds to a wetness factor of 3-4% (see Fig 3.14). Above the Wilson line, the steam behaves as dry steam; below the line, wetness becomes apparent in the turbine expansion.

Water droplets entrained in the steam flow only accelerate to a small proportion of the dry steam velocity as they pass through the fixed blades.

The wetness in the HP turbine can be a little higher than that for the LP turbine as the blades are shorter and the tip velocities are considerably less.

Considering all the factors started in sections from 3.2.1.1 to 3.2.1.3 of this chapter and literature review [3, 54 & 52] the reference plant considered in this study has an optimum load trade-off balance established based on operation regime is 60%. Further a LP exhaust steam was found to have dryness fraction less than 0.87 [13, 53, 54, 57], which is not acceptable as per OEM standards and caused phase transition issues with set pinch and approach point downstream of the turbine [13].

### 3.2.2 Total Isentropic Efficiency versus Static Isentropic Efficiency

It is important to note that working fluid property calls are conducted without any reference to the flow velocity of the process streams, consequently all stream properties are based upon the total or stagnation enthalpies. The underlying convention all the steam turbine calculations are performed based on total enthalpies.

The energy balance of turbomachinery can only be closed precisely and physically correct on basis of the total enthalpy values, unless exact knowledge of the flow velocities and inlet and exit swirls exists. Total and static enthalpies of a process stream correlate as follows [46, 47]:

$$h_{tot} = h_{stat} + \frac{C^2}{2} \quad (3.28)$$

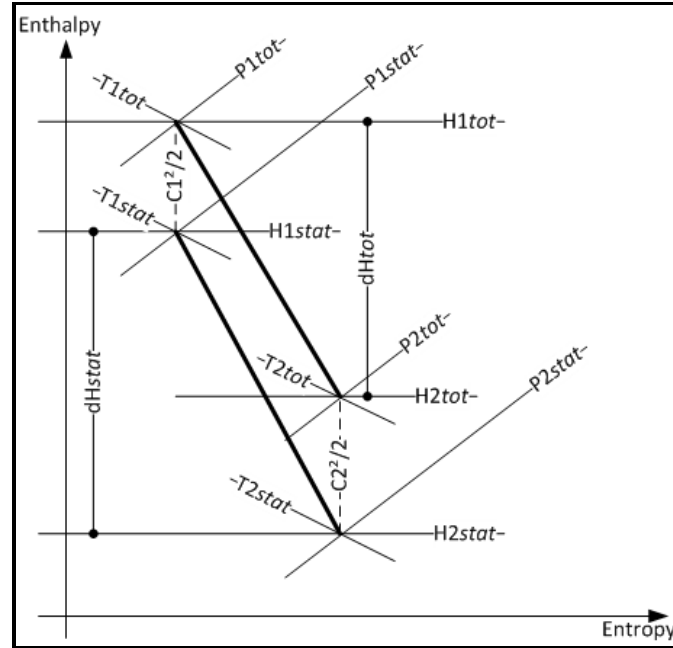


Figure 3.16: Total and static properties in the enthalpy-Entropy diagram [1]

Figure 3.11 shows the corresponding expansion line in the enthalpy-entropy diagram, exactly relating static and total properties by the portion of kinetic energy. Isentropic efficiencies are built consistently using either static or total properties.

### 3.3 Illustration of Performance Evaluation using Epsilon Professional Code

The thermodynamics used in Epsilon professional code for modelling partial admission can be explained by a comparison to simple throttling valve, as illustrated in Figure 3.16, where it is noted that the average entropy of the steam into the subsequent stage is lower for the control stage than for a simple throttling valve due to the maintained large pressure ratio across the open admission arcs [56]. It must be stressed that the simplified explanation illustrated in Figure 3.16 is valid, efficiency-wise, if the additional losses caused by partial admission (explained further on) are less detrimental than the loss

in connection to throttling the entire mass flow. In practice, the final choice is a tradeoff between these considerations.

Figure 3.16 depicts the arrangement and throttling conditions for partial arc admission. As described earlier to achieve the partial arc admission, the control valves in the governing stage need to be throttled and open fully depending on the load condition of the turbine. In this study modeling has been done for both 100% load condition, where all the control valve was throttled, and a part load condition 60% load where only few of the control valve groups were throttled to achieve the required mass flow through the turbine [1, 56].

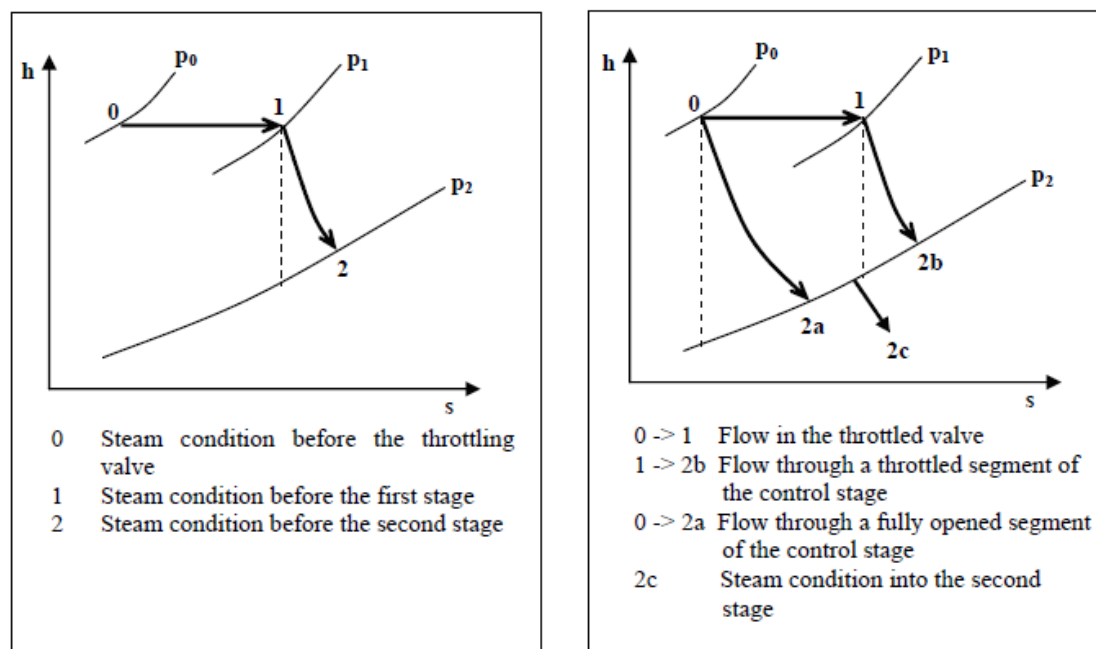


Figure 3.17: Sketches showing two ways of throttling. Left-hand picture: Throttling by pressure reduction valve. Right-hand picture: Throttling by a control stage, i.e. partial admission [56]

Where,

$P_0$  – Inlet pressure (238 bar), bar/psi

P1 – Throttling pressure, (throttled control valve downstream), bar/psi

P2 – Valve Wide Open (VWO) Pressure, bar/psi

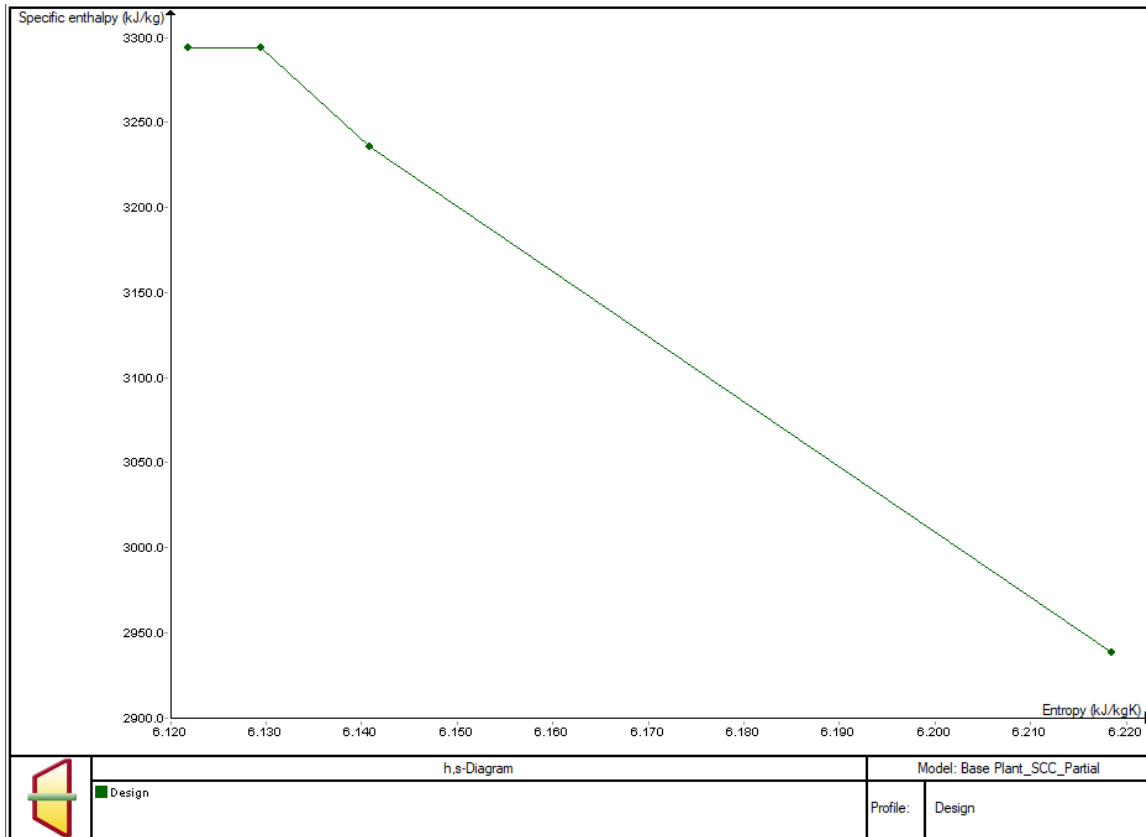


Figure 3.18: H-s diagram for partial arc admission throttling three control valve in governing stage [1].

Various studies on steam turbine characteristics have proved that the turbine efficiency characteristics must be understood to compare test results to design or to previous test results. Figure 3.18 illustrates the efficiency characteristics of an HP turbine section in a considered sub-critical plant model [1, 57]. An HP turbine achieves its best efficiency with all control valves wide open (VWO) and, as the control valves are closed (or throttled), the efficiency decreases. The parameters usually used to represent valve position are a percent

of valve wide-open flow (at rated throttle pressure and temperature) or a pressure ratio, such as first stage pressure divided by throttle pressure. The upper curve represents a partial arc or partial admission unit with the first stage nozzles divided into four separate nozzle arcs, each being supplied with steam from its own control valve. The lower curve represents full arc or single admission with all control valves connected into a common chamber ahead of the first stage nozzles. Both curves demonstrate the significant effect of valve position on HP efficiency and the need for testing at valve positions, which can be set repeatedly and held constant for the test.

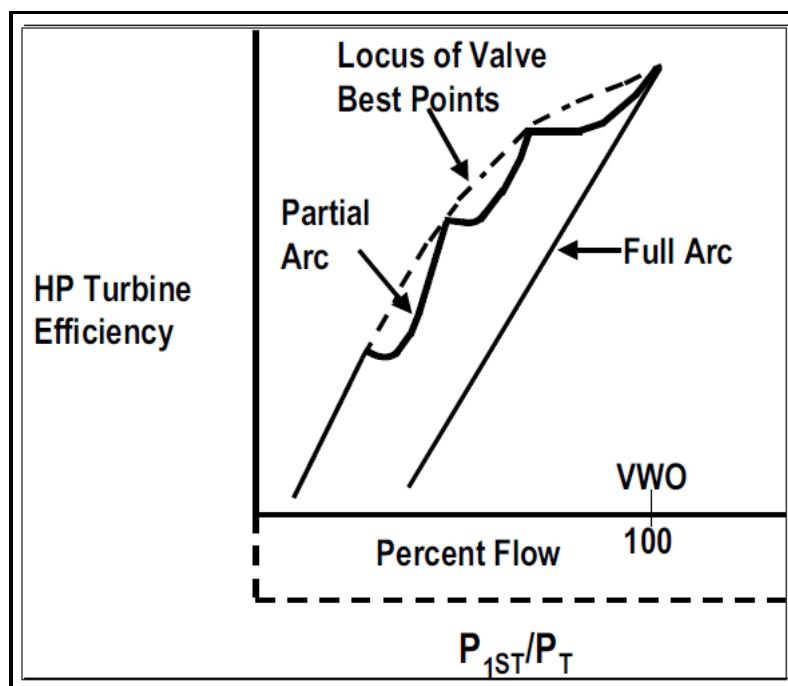


Figure 3.19: Ebsilon code Efficiency Characteristics of HP Turbine Section [57]

### 3.3.1 Ebsilon Professional Code Settings to model arc admission for Steam Turbines

As shown in figure 3.16 and figure 3.17, Ebsilon Professional Version 14 does not have a feature to plot the valve positions vs % flow in its steam chest region or the governing stage to graphically represent full arc and partial arc admission. However, appropriate h-s diagram to depict the admission process is provide to better understand throttling process. To model full arc steam admission condition in Ebsilon professional code, suitable FGS setting must be chosen. The suitable off label in the code to achieve this condition is FGSOD=4, Which is the valves wide open condition in the governing stage of the turbine. As described in detail earlier in this chapter, a full arc condition is a condition were all the control valves in the governing stage are either 100% wide open or 100% closed to achieve the full arc mode operation. In this study some or all six (6) governing stage control valves were either in VWO (Valve Wide Open) or valve completely closed position to achieve both 100% design load and part load (60% in this study) operation of the steam turbine under full arc admission.

Besides the internal expansion efficiency, the inlet and outlet structures also affect the apparent (effective, overall) total efficiency, and therefore the turbine is divided into several sub-sections:

- Inlet
- Governing stage
- Bowl
- Turbine section
- Outlet

The entry section of the turbine is defined with appropriate selection made in label FGS in Ebsilon code. FGS=2 as shown in Figure 3.18 represents governing stage of the turbine with multiple control valves (this study had 6 control valves or arcs) in addition to the main steam stop valve.

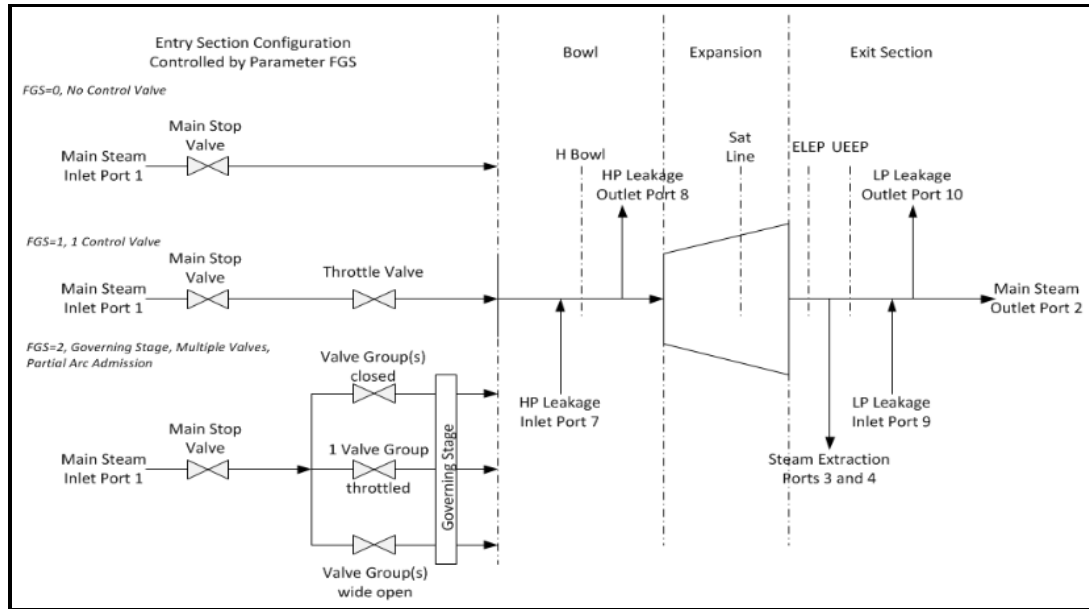


Figure 3.20: Basis of modelling governing stage of the steam turbine in Ebsilon code [1]

### 3.3.2 Performance Evaluation using Ebsilon Professional Code at different load operation

A steam turbine including the governing stage was modeled to determine its performance under the full (100%) and partial (60%) load conditions using the full and partial arc admission. A steam turbine operating at subcritical steam conditions corresponding to the Reference Plant was selected firing Bituminous coal with 8.5% moisture content with a High Heating Calorific Value of 11,680 BTU/lb. Although numerical results presented in this chapter are strictly valid for the selected turbine, the predicted trends are general.

There are no features in Ebsilon professional code to map different valve positions when they are operated/throttled to switch between full arc and partial arc positions and study the performance of the steam turbine. However the performance of these two operation in both full load and partial was studied and the performance parameters were compared.

**After a detailed analysis of the power cycle performance taking into consideration the Wilson line criteria (>3 to 4% LP exhaust wetness) at different loads ranging from 25% [54-57] (minimum load recommended by Alstom and GE OEM's) to 59.7%, it was observed that there were numerous heat exchanger two-phase scenarios encountered and the Ebsilon code failed to simulate the plant configuration with the boundary conditions. Even though the turbine machinery seems to be operating well and exhaust flow parameters or the downstream equipment do not support the lower part load operation.**

Hence forth it was concluded for this study 60% load is the most optimum and reliable part load condition. Operating at this load, the overall plant performance and performance of the steam turbine downstream equipment's (condensers, heat exchangers, etc) are found to be operating efficiently.

Figure 3.20 shows a sub-critical steam turbine cycle under full load operation with full arc admission. The operating parameters are the same as the one described in Chapter 1 of this thesis, with inlet pressure ahead of the control valves is 253.38 bar at 537.62 °C. If the pressure drop across the valves is taken as 2% of the inlet pressure (253 bar), the pressure immediately downstream of the valves at the inlet to the first stage of the HP steam

path is 248.312 bar. The isentropic internal efficiency of the HP steam path is **87%**. The overall efficiency of the HP expansion including the inlet valves is then **86.57%**. Refer Table 3.1

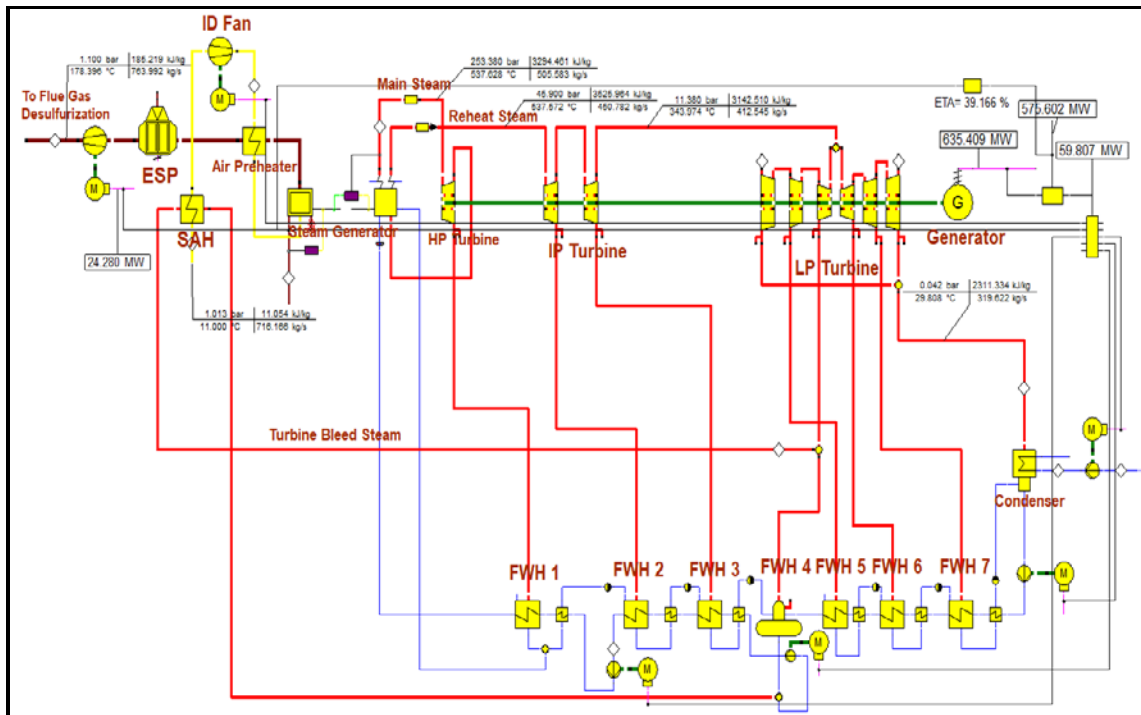


Figure 3.21: Epsilon power plant model with 100% load with Turbine Full arc admission

As shown in Figure 3.16 & Figure 3.17, inlet arranged for full arc admission with all four control valves wide open (VWO) condition and is operating at 60% load. Throttling and hence losses across the inlet valves have now significantly increased. Load is roughly proportional to steam flow. The condenser pressure is fixed and so for 60% flow, all steam conditions back up through the turbine train and the HP turbine inlet stage must scale in proportion. The effect of temperature is relatively small and so the HP exhaust pressure drops to approximately 30.132 bar and HP inlet stage pressure becomes approximately  $248.312 \times 0.6 = \sim 146$  bar.

The internal efficiency of the HP steam path is essentially insensitive to volumetric flow and it remains almost the same at **86.9%**. But the HP efficiency including valves has now become lower to **84.29%** owing to the large valve throttling losses.

When the turbine is configured for partial arc admission as shown in figure 3.16 and Figure 3.18. The 60% load point typically corresponds to operation with three arcs (control valves) closed on a six-arc admission machine with arcs of equal area. The valve losses associated with the three open arcs will now increase to more than 2% (~4%) because now 50% of the valve system is carrying 60% of the full load flow. Where,  $P_1 = 243.24$  bar.

The steam conditions from HP inlet stage through the turbine train to the condenser must be the same for 60% load, so the HP exhaust pressure must have almost same value as full arc admission, **which is 29.86 bar**.

At partial arc admission, the internal efficiency of the HP steam path has been lowered to **82.74%** to reflect these increased losses. However, despite this lower internal efficiency, the overall efficiency of the HP cylinder including valves **85.11%** which is higher than that of the equivalent full arc admission.

In conclusion, at part load conditions, despite the lower internal efficiency of the HP steam path, partial arc admission offers better performance than the equivalent cylinder with full arc admission. If you compare the Net power output from both the admission which can be seen from Table 3.2, it is evident that at part load conditions (60% load) a partial arc admission provides **2.7 MW** more than a full arc admission turbine.

Table 3.1: Efficiency at different loads and admissions of the steam turbine

Description	Total Isentropic Efficiency
	%
Full Arc at 100% Load	86.57
Partial Arc at 100% Load	84.29
Full Arc at 60% Load	82.97
Partial Arc at 60% Load	85.11

Table 3.2: Performance comparison of Power plants with Partial and Full Arc admission

Description	$P_G$	$HR_{cycle}$	$h_{cycle}$	$P_{net}$	$HR_{net}$	$h_{net}$
	MW	Btu/kWh	%	MW	Btu/kWh	%
Full Arc at 100% Load	635.40	7,270.97	46.93	575.60	8,026.36	42.51
Partial Arc at 100% Load	634.87	7280.13	46.87	575.06	8,037.31	42.45
Full Arc at 60% Load	358.03	7,742.50	44.07	324.29	8,548.05	39.92
Partial Arc at 60% Load	360.73	7584.48	44.99	327.05	8365.54	40.79

At full load, the turbine with partial arc has a slightly worse heat rate (7,280.13 Btu) than the full arc turbine (7,270.97 Btu), because of the higher HP inlet stage losses. Initially, as the valve controlling the first arc is closed, the heat rate of the partial arc and full arc machines degrade at a similar rate. However, on the partial arc machine, the throttling losses reduce as the first valve progresses towards full closure. Below 60% load the partial arc machine will throttle constantly on 2 valves and so the heat rate will degrade accordingly.

This shows that for units with load profiles that require significant periods of operation at part loads, partial arc admission can offer a significant performance advantage over units featuring full arc admission. Table 3.2 shows that at full load, full arc admission has a heat rate advantage of 0.125% over partial arc. However, as load reduces the position is quickly reversed and at 60% load, partial arc has the heat rate advantage by 2.04%. Also, from Table 3.1, its evident that in full load operation a full arc turbine provides close to

0.53MW increase in Net power compared to a partial arc machine due to the heat rate advantage.

### 3.3.2 Alstom Power (Rugby, UK) Steam Turbine Full Arc Vs Partial Arc admission

As shown in Figure 3.21, this Alstom partial arc admission machine [55] is configured for 2+1+1 steam admission (i.e. the valves controlling the steam flow to two of the four inlet arcs can be closed in series). At full load, the turbine with partial arc has a slightly worse heat rate than the full arc turbine, because of the higher HP stage 1 losses.

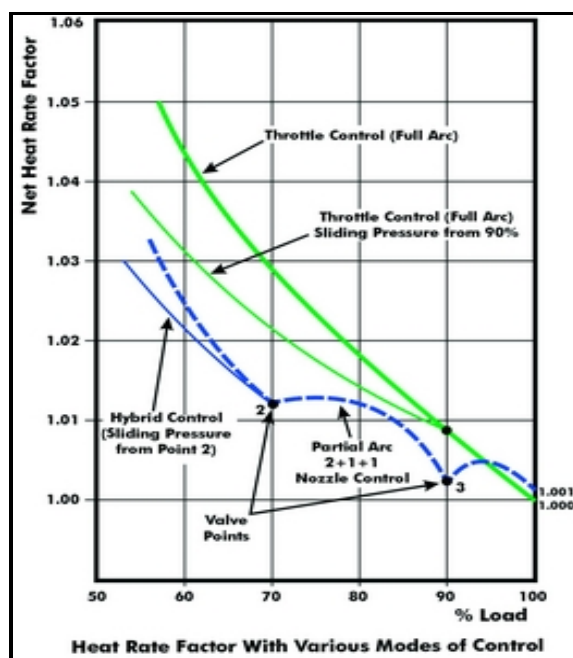


Figure 3.22: Variation of heat rate with load for Full arc admission Vs Partial arc steam admission in a steam turbine [55]

Initially, as the valve controlling the first arc is closed, the heat rate of the partial arc and full arc machines degrade at a similar rate. However, on the partial arc machine, the throttling losses reduce as the first valve progresses towards full closure, with the effect that for this example, by about 94% load the heat rates for both admission types are equal.

Below 94% load, the partial arc admission machine has the better performance. At 90% load the first arc is fully closed and so HP valve throttling losses are eliminated, and the partial arc performance is more than 0.5% better on heat rate than the full arc performance. The cycle then repeats as the second arc is closed as shown in Figure 3.20. Below 70% load the partial arc machine will throttle constantly on 2 valves and so the heat rate will degrade accordingly as illustrated in Figure 3.20.

This example shows that for units with load profiles that require significant periods of operation at part loads, partial arc admission can offer a significant performance advantage over units featuring full arc admission. Figure 3.20 shows that at full load, full arc admission has a heat rate advantage of 0.1% over partial arc. However, as load reduces the position is quickly reversed and at 0% load, for example, partial arc has the heat rate advantage by 1.7%. The effect on fuel consumption can be illustrated as follows:

**24 hours operation at 100% load.**

Full Arc Admission (FAA) better than Partial Arc Admission (PAA) by:

$$(24 \times 100 \times 0.1) / (24 \times 100) = 0.1\%$$

**24 hours at 70% load.**

PAA better than FAA by:

$$(24 \times 70 \times 1.7) / (24 \times 70) = 1.7\%$$

**6 hrs. at 100% load + 6 hrs. at 90% load + 12 hrs. at 70% load.**

PAA better than FAA by:

$$(6 \times 100 \times 0.1) + (6 \times 90 \times 0.7) + (12 \times 70 \times 1.7) = 0.88\%.$$

## CHAPTER 4: IMPROVEMENTS OF STEAM TURBINE INTER STAGE SEALS

### 4.1 Overview

The efficiency of modern steam turbines is dependent on a number of factors, including steam leakage, which negatively affects performance of the steam turbine and the entire steam turbine cycle. Minimizing leakage of steam that bypasses stationary vanes and rotating blade elements and passes through the shaft end packing is critical in modern machines operating at high inlet main steam pressure. Maintaining low leakage rates requires improved seal (packing) designs. One traditional type of interstage packing uses labyrinth seals—a non-contacting type of seal that is designed to produce a significant pressure drop in the leakage steam and, therefore, reduce leakage flow since the flow is proportional to the square root of pressure drop. These seals have been in use for decades in a variety of turbo-machinery applications [14–17].

The problem of leakage between the different pressure zones, or stages, directly affects the amount of steam flow performing useful work and thus the amount of power delivered by the turbine. An attractive feature of the labyrinth seals is that they do not contact the rotating shaft. This has a direct impact on the integrity of the rotor and also drastically decreases the cost of regular replacement and maintenance compared to other contacting seals, such as brush seals.

When considering a seal design, the specific operation of the steam turbine needs to be considered. Each application requires an evaluation to determine the best solution. There are four factors that need to be taken into consideration [11]:

- Installation – Replacing the OEM labyrinth seal with improved seal designs will impact axial clearance. Modifications should have a careful engineering review to avoid leakage issues problems due to seal clearance and alignment during installation.
- Cost – Replacement seals, other than a replacement straight tooth design, have high manufacturing costs. The increased cost for the replacement seal needs to be evaluated against the expected improved performance and efficiency that might be expected from the steam turbine with the new seal.
- Durability – Brush seals, which are flexible, provide the best wear resistance. Other replacement seals are rigid designs with knife-edge fins for sealing. These types of seals are prone to damage from rubbing during load transients and other unsteady modes of operation causing differential expansion of turbine rotor and casing.
- Performance – One often overlooked area in a steam turbine performance is improvements in seal design. On a 500 MW steam turbine, replacing straight seals with brush seals in the HP and IP sections can result in an approximate performance gain of about 3.7 MW as compared to a 0.8 MW to 1.3 MW performance gain with dimpled seals and slant tip seals respectively [Appendix II, 3].

Advantages derived from the lower maintenance and replacement costs in the long run have led to renewed efforts in enhancing the performance of a labyrinth seal. The key design factor restricting leakage is the large total pressure drop produced by flow passing

through multiple labyrinth seals. If not damaged, multiple labyrinth seals are capable of reducing pressure of the leakage stream to a level close to the exhaust pressure, thus significantly reducing the leakage flow.

The leakage flow through a labyrinth seal can be considered as a flow through a series of orifice restrictions. Figure 4.1 depicts a schematic representation of a labyrinth seal with vertical knives and steps, including the definition of key parameters. In general, losses caused by individual restrictions and obstacles combine to produce a net energy loss to the system. As the fluid passes through the restriction (acting as an orifice), it undergoes an increase in velocity and a corresponding decrease in pressure with increased turbulence, flow separation and secondary flows due to the sharp knife tip. At some point after the orifice, the fluid adjusts to the pressure condition in the next chamber. During this process, some of the kinetic energy of the fluid is recovered as a pressure rise and some losses due flow separation and secondary flow are mainly converted to heat by viscous dissipation. The remaining total pressure of the fluid provides the pressure difference that forces the fluid to enter the next stage of the seal. Ideally, the kinetic energy of the fluid resulting from the previous stage of throttling will be dissipated before the fluid enters the next stage [24, 25]. In this manner, by the time the fluid has traveled through all of the stages of the seal, its total pressure difference is greatly reduced, leading to the negligible leakage flow through the seal.

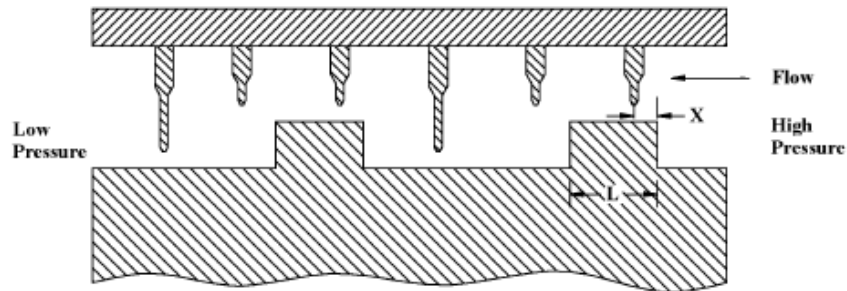


Figure 4.1: Schematic Representation of a Generic Stepped Labyrinth Seal, Depicting Two Cycles of a Seal [21]

In a labyrinth seal, the flow locally often changes direction and speeds up and slows down as it negotiates a path through the seal. Total pressure is lost continuously through the seal, but there may be local rises in static pressure due to area changes, local stagnation points, and sudden expansions as the fluid flows into a chamber of the seal.

Based on a review of the open literature, there appears to be a deficiency in available information detailing the behavior of stepped labyrinth seals with constant rotor diameter (see Figure 4.1). Better success has been obtained analyzing and predicting the leakage of the straight-through labyrinth seals (see Figure 4.2) due to the relative simplicity of the internal flow and the wide availability of experimental results [33–35] compared to the stepped labyrinth seal presented in Figure 4.1. This study addresses flow physics of the stepped labyrinth seal flow physics and relates it to the seal design through modeling. Leakage flow through the seal may be theoretically quantified in terms of various flow and design parameters.

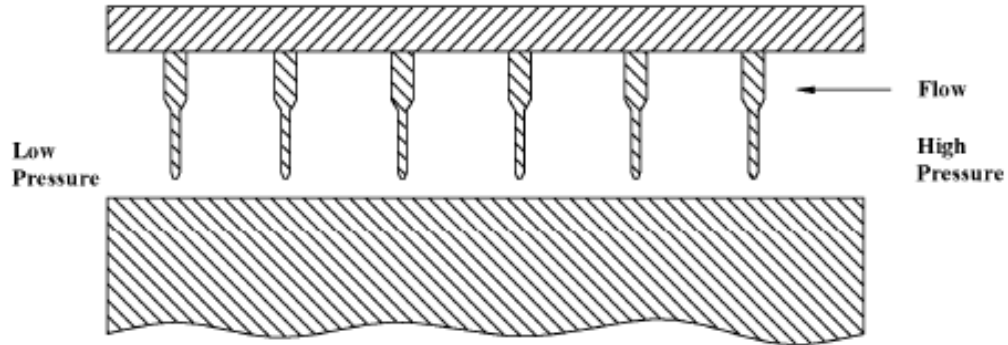


Figure 4.2: Schematic Representation of a Generic Straight-Through Labyrinth Seal, Depicting Two Cycles of a Seal [21]

#### 4.2 Calculation of Leakage Flow

In this study all the calculations are performed using Ebsilon Professional code and excel spread sheet. The following are the equations and theory utilized to calculate the leakage flow in Ebsilon Professional where, calculation of the leakage flow is based on the works of Martin [19] and Egli [20].

The leakage flow can be determined from the following expression,

$$\dot{m} = C \cdot A \cdot \beta \cdot \sqrt{\frac{p_o}{v_o}} \quad (4.1)$$

$$\beta = \sqrt{\frac{1 - \Pi^2}{n - K \cdot \ln(\Pi)}} \quad (4.2)$$

$$\Pi = \frac{p_n}{p_o} \quad (4.3)$$

Where,

$\dot{m}$  ... Mass Flow [ $\frac{kg}{s}$ ]

$C$  .... *Flow Coefficient* [-]

The Flow Coefficient is dependent of the seal geometry and has the order of magnitude of

1. Typical values are in the range of 0.4 to 2.

$A$  .... *Free Cross Sectional Area* [ $m^2$ ]

This area is a function of the shaft diameter and the clearance.

$\beta$  .... *Labyrinth Factor* [-]

$p_o$  .... *Inlet Presssure* [ $Pa$ ]

$p_n$  .... *Outlet Presssure after  $n^{th}$  tooth* [ $Pa$ ]

$v_o$  .... *Specific Volume* [ $\frac{m^3}{kg}$ ]

$n$  .... *Number of Teeth* [-]

$K$  .... *Constant* [-]

$$K = 1 \quad (4.4)$$

$$K = \frac{2}{k} \quad (4.5)$$

Equation 4.4 & 4.5, Reference to Martin Equation [19]

$k$  = *Compressibility* [-]

$$p_n \leq p_o \rightarrow 0 < \Pi \leq 1 \quad (4.6)$$

The above-mentioned formulas are valid for:

$$\Pi \geq \Pi_{crit} \quad (4.7)$$

$$\left(\frac{p_n}{p_o}\right) \geq \left(\frac{p_n}{p_o}\right)_{crit} \quad (4.8)$$

If the pressure ratio is smaller than the critical pressure ratio<sup>2</sup>, the flow remains constant with its flow rate corresponding to the critical pressure ratio, i.e., choked flow.

For the converging nozzle or orifice, the flow is constant for pressure ratio  $\Pi$  being equal or larger the critical pressure ratio (Eqn. 4.7), which corresponds to the choked flow. For the converging-diverging (De Laval) nozzle, the flow continues to accelerate after ‘vena contracta’, and mass flow rate increases with pressure ratio.

The critical pressure ratio is derived as follows:

$$\Pi_{crit} \rightarrow \frac{d\beta}{d\Pi} = 0 \quad (4.9)$$

Solving this equation leads to:

$$\Pi_{crit} = e^{\frac{1}{2} \cdot \frac{k \cdot \text{LambertW}\left(-e^{\frac{2 \cdot n + K}{K}}\right) + 2 \cdot n + K}{K}} \quad (4.10)$$

It is important to use the one branch of the Lambert W() function which has a solution in the interval

$$0 < \Pi_{crit} \leq 1 \quad (4.11)$$

The Figure 4.2 below shows values of  $\beta$  according to Martin’s formulation (Equations 4.2 & 4.4, reference [19])

---

<sup>2</sup> The critical pressure ratio for superheat steam is xxx

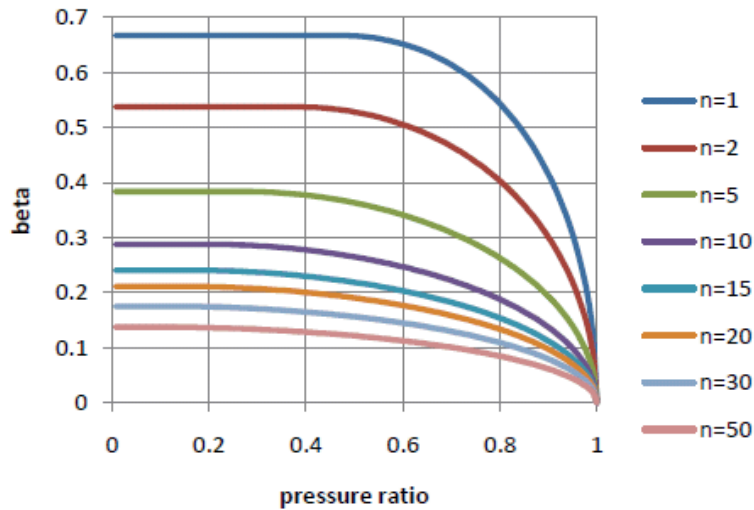


Figure 4.3: Labyrinth Factor according to Equation 4.2 using Martin's Formulation ( $K=1$ ) [1]

Combining Equation 4.1 with Equation 4.2 and replacing  $A$  with Equation 4.12,

$$A = (D + CL) \cdot \pi \cdot CL \text{ for } \gg CL \quad (4.12)$$

$D$  .... Shaft Diameter [m]

$CL$  .... Clearance [m]

$D + CL$  .... Average Clearance Diameter [m]

Leads to:

$$\dot{m} = C \cdot D \cdot \pi \cdot CL \cdot \sqrt{\frac{1 - \Pi^2}{n - K \cdot \ln(\Pi)}} \cdot \sqrt{\frac{p_o}{v_o}} \quad (4.13)$$

Performance Factor (PF) included (Refer Equation 4.14) depends on the seal design. i.e, tooth arrangement and shape to arrest leakages in terms of axial clearance, which has a value of 1 for normal (design condition) performance.

$$\dot{m} = \frac{C \cdot D \cdot \pi \cdot CL}{PF} \cdot \sqrt{\frac{1 - \Pi^2}{n - K \cdot \ln(\Pi)}} \cdot \sqrt{\frac{p_o}{v_o}} \quad (4.14)$$

The Performance Factor is located in the denominator, so that a degradation of performance correlates with  $PF < 1$ . In addition, all geometry data can be simplified to a factor  $C^*A$ ,

$$CA = C \cdot D \cdot \pi \cdot CL \quad (4.15)$$

$$\dot{m} = \frac{CA}{PF} \cdot \sqrt{\frac{1 - \Pi^2}{n - K \cdot \ln(\Pi)}} \cdot \sqrt{\frac{p_o}{v_o}} \quad (4.16)$$

For given geometric dimensions of the labyrinth seal EBSILON Professional calculates  $\dot{m}$  and  $C^*A$ , according to Equations 4.15 & 4.16. The (Performance factor)  $PF = 1$ , for normal performance of the seal.

The number of teeth is an input and is a part of the seal geometric data. If sufficient data are available (several load points), the number of teeth can be estimated from Figure 4.3, since it has significant influence on the shape of the curve. Otherwise, the number of teeth has to be assumed.

#### 4.3 Analysis of the Proposed Improved Labyrinth Seal

**The seal design employed in this study is referenced from various literature [21, 22] to emphasize the significance of utilizing a better seal to enhance the performance of a steam turbine. The results or the leakage percentages of the seal design used in this study are derived from literature and various studies conducted by research organizations [14, 15, 16, 17, 18 24, 25] referenced in this section. Figure 4.4 and table 4.1 are some of the experimental and computation results referenced from**

literature on effective seal design for steam turbine system. Epsilon professional models are created based on these analysis and experimental data. For instance, from Table 4.1 is an EPRI study report published in the year 2005, which shows a 17.3% is the resulted seal leakage flow reduction with respect to the nominal leakage flow for a turbine machine with pressure ratio of 10. Figure 4.4 shows the computation (CFD) analysis results performed on the 60° slant tall knife + 40% high step seal configuration. Part a is result from applying LP turbine section boundary conditions and part b is HP turbine section boundary conditions.

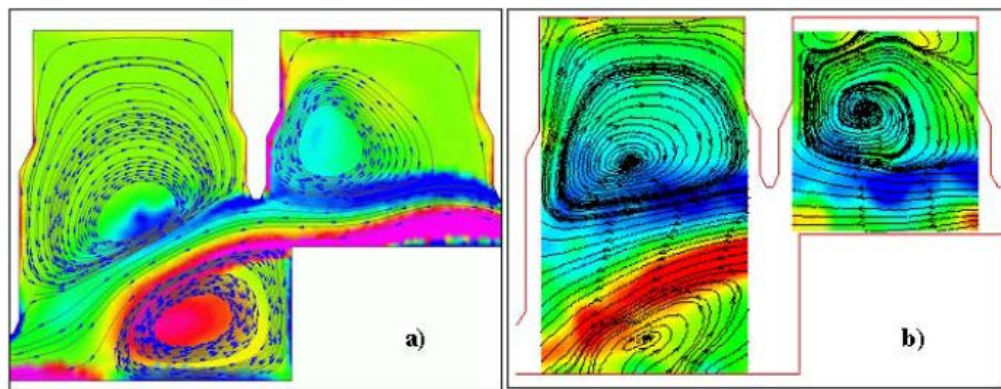


Figure 4.4: Comparisons of Computational and Experimental Results [21]

Table 4.1: Comparison of computational and Experimental Results [21]

Model	Reference	X/L	$P_1/P_{14}$	% Reduction (Experiment)	% Reduction (CFD)
60° slant tall knife + 40% high step	Baseline seal	0.043	10	17.3	17.27

The present study has been mainly concentrated on the analysis of the performance of steam turbine were improved vertical labyrinth inter stage seals (Figure 4.5) are installed. The main objective of this study to quantify performance improvement because

of installation of new designed labyrinth seals using literature data/references and Epsilon Professional modelling. The new labyrinth seals have the following advantages,

- Good dynamic sealing properties
- Higher mechanical strength
- Simple geometry for ease of manufacture and maintenance

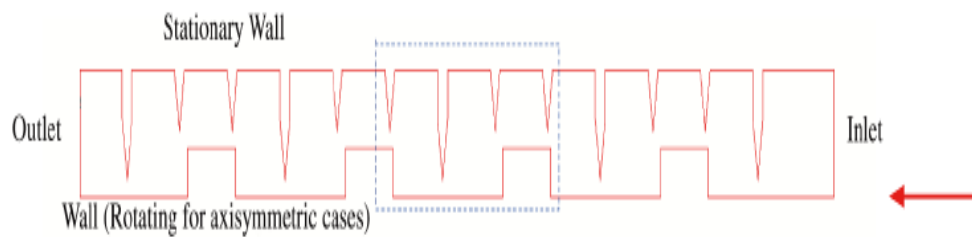


Figure 4.5: Baseline Stepped Labyrinth Vertical Seal Geometry used for Modeling Showing cross-section and teeth's (see Figure 4.1) [21]

Total pressure differential is the overall driver for the flow leakage. Ideally, if the total pressure differential at the last seal and the exit is reduced to a very small value, then the seal leakage will be reduced to a very small amount as well [21]. It is important to note that there is still more than 20% of the total pressure (see Figure 4.6) available in the flow. Reducing the total energy (that is, total pressure) available for the flow at the last throttling point is the objective in reducing leakages for a given clearance [21].

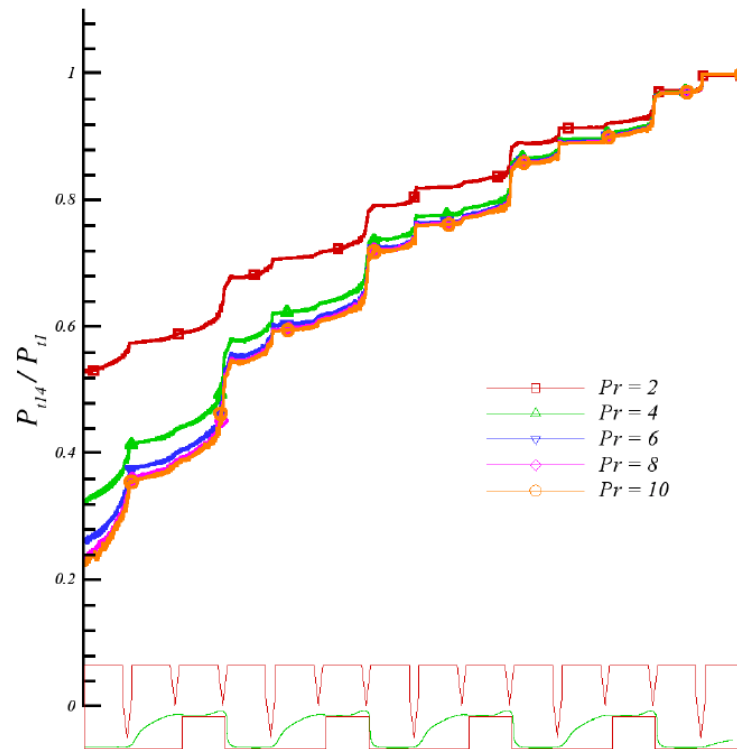


Figure 4.6: Variation of Predicted Total Pressure across the multistage baseline Seal Assembly, flow through the seal being from right to left [21]

The following observations (pressure ratio, Tip clearance gap, step height and axial location of the knife) were derived from the parametric study performed in [37, 38]. Sample results calculated at a pressure ratio of 10 is shown in Table 4.1, where % of reduction in leakage flow is approximately 17%:

- Pressure ratio: Flow parameters  $C$  &  $\beta$  (Flow coefficient and Labyrinth factor) achieve near-constant values at choking conditions (excessive leakage) [37-40].
- Tip clearance gap: Smaller clearances between the rotor and stator are very effective in reducing leakage; this is the case for any type of seal. However, with reduced clearances, wear and damage to shaft and seal are major concerns. The new

improved design (Figure 4.8), described in this study has the potential to achieve smaller operating clearance gaps without damaging the shaft or the seal.

- Step height: Varying step height alone contributes very little (about 2%) to the reduction in a constant rotor diameter seal assembly [37-39].
- Axial location of the knife: Leakage reduces as the short knife-edge moves toward the center of the step as it results in a maximum reduction in leakage. This is also one of the very important parameters that could help reduce leakage, especially when the tall knife between steps could create a significant stagnation of the flow. In practice, however, the knife location in operation varies as a result of relative thermal expansion, and the improved labyrinth design must reduce leakage flow for all relative locations of the short knives and step.

Young's modulus of 200,000 MPa and Poisson's ratio of 0.33 are baseline properties of a vertical seal. The damaged baseline vertical seal with the geometry shown in Figure 4.7 was compared to the improved labyrinth seal with profile/geometry to  $PF = 1$ ,  $C^*A = 0.0526 \text{ m}^2$ , No. of teeth = 30 shown in Figure 4.7.

*Leakage Calculations are performed using Epsilon professional utilizing seal design data and configuration referenced from literature review and historical data reference throughout this chapter. The leakage flow results are presented in Table 4.2, which shows the leakage flow for different pressure ratios ( $p_n/p_o$ ) across the different sections (HP, IP, and LP) of the steam turbine. Figure 4.6 shows the total pressure variation for different pressure ratios ( $P_{inlet}/P_{exit}$ ) across the seal. Total pressure is reduced throughout the length of the seal. There is a sudden drop in total pressure whenever the flow has to*

negotiate the step on the rotor or a knife-edge. Non-isentropic energy conversions (secondary flow and flow separation) take place at different locations across the seal. At each knife-edge, there is a reduction in static pressure and a gain in kinetic energy. Static pressure recovers after the flow passes through the knife, and the gained kinetic energy quickly dissipates.

Table 4.2: Baseline Vertical and Improved Labyrinth Seal Leakage Flows [21, A-1 to 4]

Turbine Section	Pressure Ratio	Main Steam Flow considered for analysis	Leakage w.r.t Main steam flow with Damaged Baseline Vertical Seal [41]	Baseline Seal Leakage Flow (damaged)	Leakage w.r.t Main steam flow with Undamaged Improved seal	Improved Labyrinth, Leakage Flow (Undamaged, Figure 4.6)
		kg/s	%	kg/s	%	kg/s
HP	5.0	505	4.30	21.72	0.0140	7.08
IP	4.5	450	2.20	9.90	0.0074	3.35
LP	38	412	1.10	4.53	0.0035	1.43

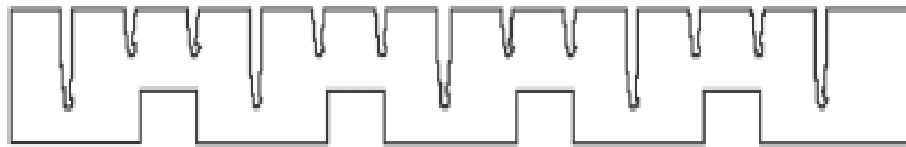


Figure 4.7: Baseline Vertical seal with Bent Knives, Resulting in increased clearance [21]

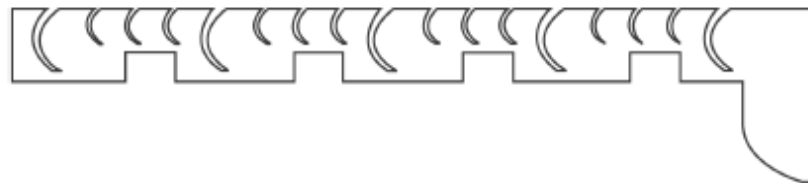


Figure 4.8: Improved Labyrinth Seal - C-Shaped Flat-Edged Knives, One Tall and Three Short Knives (C Flat + CCC) [21]

**For the main steam flow in each section of the turbine for the analyzed base plant configuration, according to literature review and available operational data [3, 4, 41] encountered leakages are stated in Table 4.2.** The new designs (described in the previous section) were analyzed using numerical modeling performed by EPRI [21, 37]. Consider the equation for flow parameter  $C$  &  $\beta$  (Flow coefficient and Labyrinth factor). If the temperature, clearance area, and inlet pressure variables are fixed, it is possible to directly compare the mass flow rates of different configurations. Mass flow rates for all seal configurations were calculated and are tabulated in Tables 4.2 [21, Appendix A]. The percent reduction in leakage is compared to the new baseline seal is as shown.

The results presented in Table 4.2 show that the new improved design employing curved (C) seal with sharp edges (one tall and three short knives) performs best. As discussed earlier, one of the major concerns is the effect of a rub event on the seal and the shaft. The C seal design envisions a flexible knife and therefore able to achieve smaller clearance gaps even after a rub event. It is expected that the performance of vertical seals would worsen once the seal edge was deformed, and a larger clearance gap would thus be permanently created. If the desired design feature (flexibility of the knife) can be accomplished, the new C seal could reduce leakage by about **65% to 68%** compared to the damaged baseline seal for the pressure ratios considered in this study (see Tables 4.2).

#### 4.4 Effect of steam leakage on turbine performance

Performance of the steam turbine cycle was analyzed by using Ebsilon Professional to determine effect of steam leakage and its reduction on turbine power output and steam cycle heat rate, and unit performance (net unit efficiency and net unit heat rate) that would

be achieved by replacing damaged baseline vertical seal with the improved C seal design in the gland sealing system. The results for the baseline design of the labyrinth seal, presented in Table 4.3 were obtained for the Reference plant, described in Chapter 1 and its operating conditions summarized in Table 4.2. The steam leakage flow rates through the gland system calculated by the Epsilon Professional code for the baseline (damaged seal) and improved labyrinth seal (C Seal) and associated steam pressure, temperature, and enthalpy are presented in Figures 4.9 and 4.10, respectively.

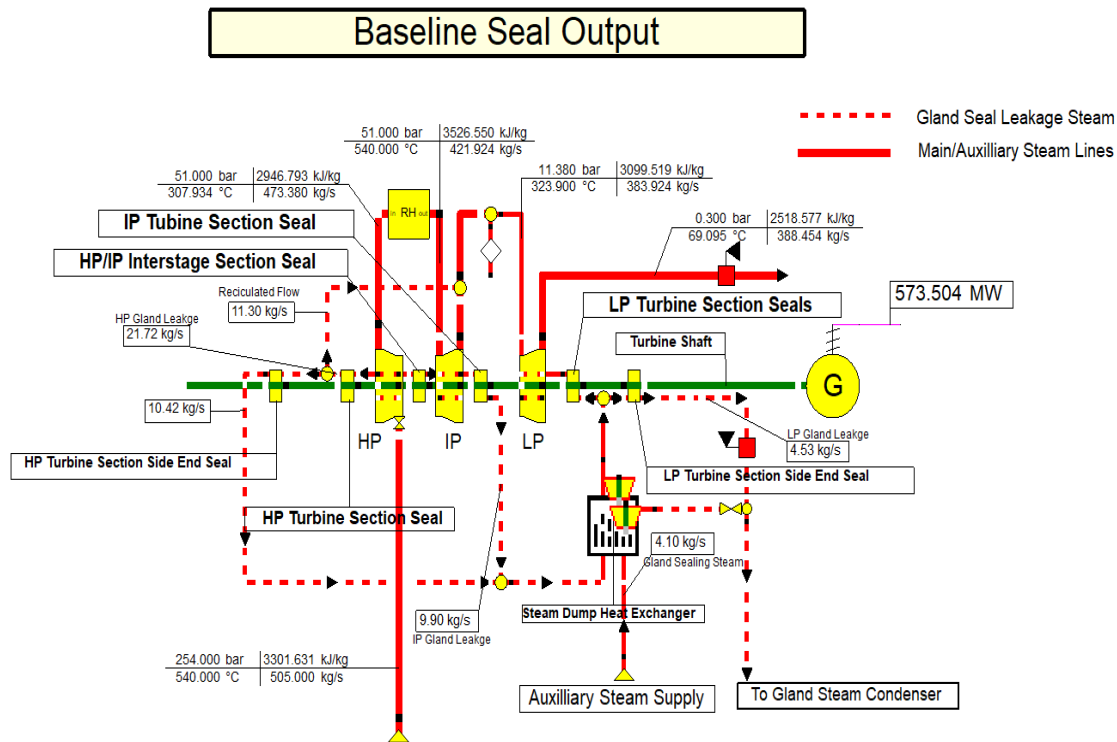


Figure 4.9: Steam Turbine Gland Sealing System with Baseline Labyrinth Seal

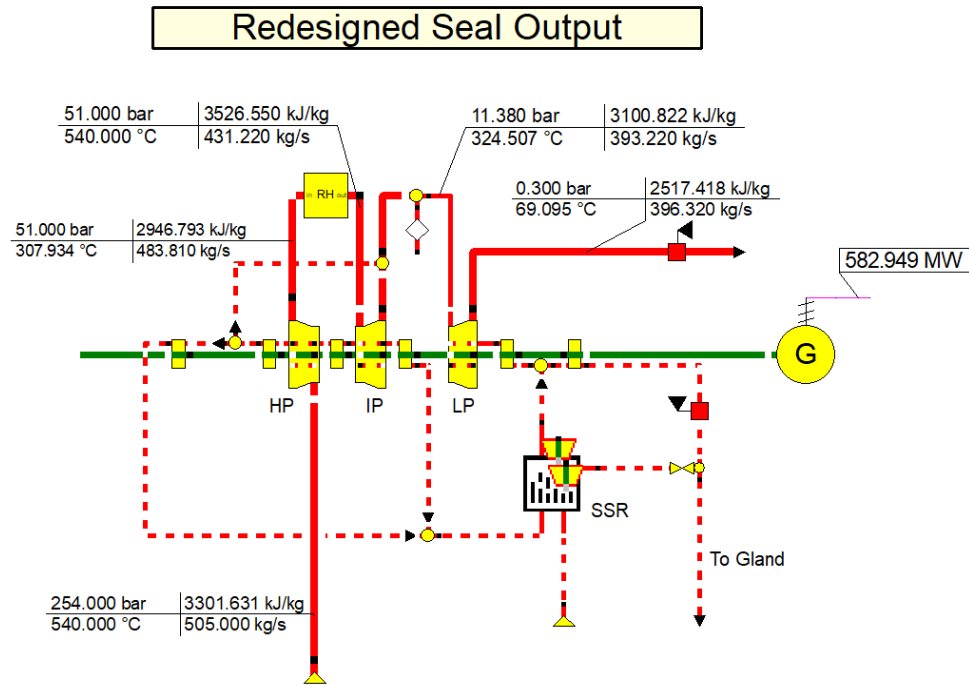


Figure 4.10: Steam Turbine Gland Sealing System with Improved Labyrinth Seal

The results for the baseline design of the labyrinth seal, presented in Table 4.3 were obtained for the Reference plant, described in Chapter 1 and its operating conditions summarized in Table 4.2 (Table 4.2 shows steam leakage flows, not plant operating conditions).

Table 4.3: Power Plant Performance Comparison with Baseline and Improved Labyrinth Seal

Description	$P_G$	$HR_{cycle}$	$\eta_{cycle}$	$P_{SS}$	$P_{net}$	$HR_{net}$	$\eta_{net}$
	MW	BTU/kWh	%	MW	MW	BTU/kWh	%
Baseline	573.50	7,949.50	42.92	44.24	529.26	7,949.50	42.92
Redesigned	582.94	7,755.30	44.00	45.72	546.96	7,695.48	44.34

Locations of the inter stage seals at different pressure sections (HP, IP, and LP) of the steam turbine are shown in the Figure 4.9. The leakage steam flow is arrested with the help of labyrinth seals and auxiliary sealing steam as indicated in Figure 4.9. As per the

schematic in Figure 4.9, the leakage steam from HP & IP is used to preheat the sealing steam in steam dump heat exchanger. The required Auxiliary sealing steam is extracted from steam turbine extraction line to feed water heater (FW3) (not show in Figures 4.9 & 4.10), refer Chapter 2: Figure 2.1 baseline power plant configuration to see the extraction line to FW3. Steam dump heat exchanger is a Kernel script (created using EbScript) component in Ebsilon Professional code. The kernel script in Ebsilon code is used to create user defined components, within the simulation. As Ebsilon code does not have a component which can used as an auxiliary steam dump condenser and perform off-design mode calculations (i.e. constant area based on design condition and varying temperature profile and heat transfer co-efficient). This component decided whether to reuse the sealing steam into the cycle or dump it to the Gland Vent Condenser based on the mass flow, pressure and Enthalpy parameters received as Input. The Gland Vent condenser is not modelled or shown in the circuit in Figure 4.10 as the dump condensate does not affect our heat and mass balance calculation and has very negligible contributions to the fluctuation on the seal overall performance/power improvements.

In the event of no sealing steam required during start-up and low turbine load operations SDHE regulates sealing steam into the labyrinth seal and dump the rest of the steam to gland vent condenser. With the help of a control valve SDHE diverts the excess or all the HP and IP turbine section leakage steam to GCV along with LP section leakage steam. This type of design is known as **self-sealing**, which means that there is an enough supply of steam coming from the leak-off and extraction steam lines into the steam seal system.

The gland sealing system is configured, so that a part of the HP leakage steam is expanded through the LP section of the steam turbine to maximize the heat recovery from leakage steam before condensing it in the Gland Vent Condenser (GVC). The condensate is returned to the condensate cycle (not shown in Figure 4.9 and 4.10).

Performance parameters corresponding to the steam turbine cycle operating with damaged baseline vertical labyrinth seal and improved labyrinth seal are compared in Table 4.3. As the results show, turbine cycle performance is improved as steam leakage flows are reduced. For the analyzed case the improvement in heat rate with respect to the baseline damage seals is 2.44%, the increase in gross power output is 19.2 MW (or 3.34%). Both are significant. Performance improvements are also presented in Figure 4.11. Bituminous coal with TM (Total Moisture) of 8.5% was used in this analysis.

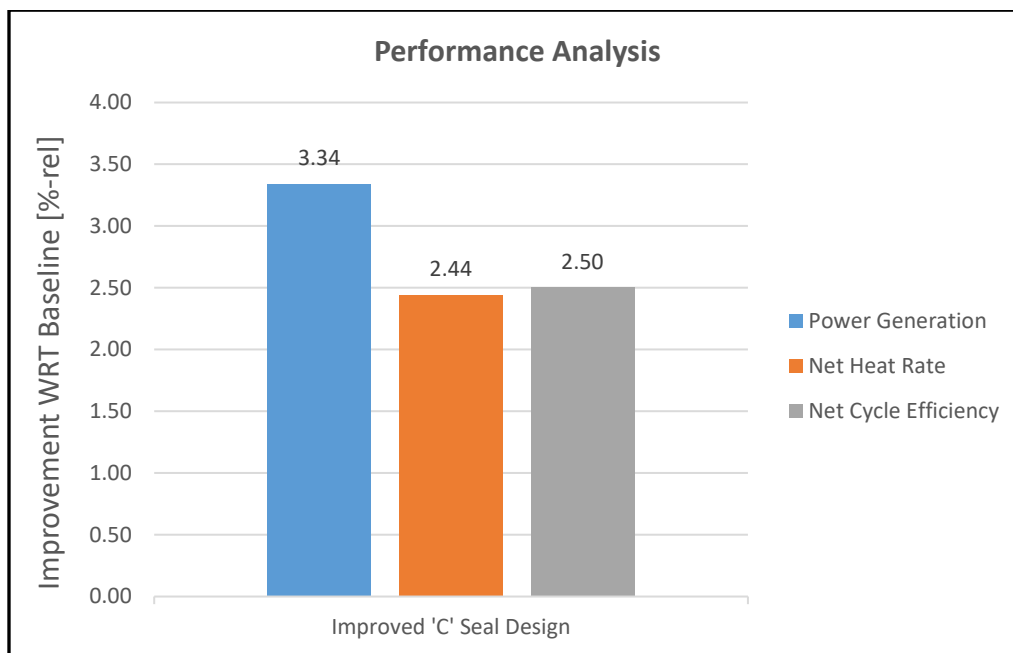


Figure 4.11 Improvement in net plant heat rate and efficiency firing Bituminous Coal

Steam leakage is a significant part of the controllable losses in large commercial steam turbines. In most units, condenser vacuum cannot be maintained without a properly functioning steam seal system. Experience at power-generating utilities has shown that inadequate sealing and valves requiring cycle isolation can cause power loss and contribute to a forced outage. It is estimated that an improvement in the heat rate of up to 5% could be achieved by reducing the steam leakage and upgrading the steam seals in the turbines [43]. Similarly, air leakage into the condenser can also be detrimental to power plant operation. If the steam/gland seal exhauster is not set up properly, steam can flow out from the packing casing along the turbine rotor to the bearings. Steam or water introduced into the turbine bearings may contaminate the turbine lubrication system.

To minimize leakage, an elaborate steam seal system is employed to generate the necessary vacuum and pressure chambers inside gland sealing. It has been demonstrated that isolation valves that do not prevent main steam from flowing into the steam seal system can pass about 1% of the main steam directly back to the condenser. This bypassed steam adversely affects the condenser performance, degrades the seals, and has a significant impact on the plant's heat balance. Test results have documented that main steam leaking into the steam seal system may be responsible for a plant's heat rate loss of the order of 100 Btu/kWh.

In summary, excessive internal leakage of steam within combined HP/IP casings from the HP section to the IP (intermediate pressure) section is a known cause of degradation in performance. Careful performance testing is needed to identify the precise area where steam loss is occurring, but after this, the appropriate combination of seals can

be engineered to address the problem. These are then installed at the next plant outage, when the inner turbine casing is opened. It has been shown that the internal leakage can be reduced by applying means such as restoring correct clearances, replacing attachments and enhancing packing.

Replacing an existing old damaged seal with a new seal of improved design may reduce the steam leakages up to 68%. In this study reduction in steam leakages by upgrading the seals improves the Net power generation by 3.34%, the plant net heat rate by 2.44% and the net cycle efficiency by 2.50%. These are significant improvements and should be considered as a means of improving performance of power plants.

#### 4.5 Improved Seal Configurations

A number of alternate inter stage packing designs is available, such as retractable and brush seals. A configuration incorporating the use of both labyrinth and brush seals has also been studied [23]. Brush seals have special considerations because they can be quite effective in reducing steam leakage [18]. However, these seals do have certain shortcomings. Brush seals work well in reducing leakage if their clearance relative to the shaft is small. They are most effective as contact seals, for which life and wear rate are major concerns. At certain locations along the shaft, the lateral displacement of the shaft at critical speed during startup exceeds the brush seal's limit, and the seal and shaft wear is quite high. In such situations, if the initial clearances for the seals are too small, the seal and the shaft may be damaged. The seal clearances after such a rub event are large, which reduces the seal performance. In addition, bristle loss and debris could lead to maintenance problems [21].

Retractable seals and brush seals ride closer to the shaft than traditional labyrinth seals. The resulting decrease in steam leakage increases the steam turbine output and efficiency. However, tighter clearances can cause rotor vibration instabilities due to higher pressure gradients. Brush seals have lower destabilizing forces than original OEM labyrinth seals [12].

#### 4.2.1 Retractable® Seals

Conventional labyrinth seals are segmented and are positioned using flat radial springs. Retractable seals use a coil spring to increase shaft clearances during startup due to thermal distortion and vibration as the turbine passes through critical speed zones. In addition, the Retractable® seal also reduces the likelihood for seal rub as the unit passes through its critical speed zone(s), usually present below the synchronous speed [24].

Retractable® seals retract from their close clearance position under low-load and no-load conditions. This results in an additional clearance between the stationary seals and the rotating shaft, thereby reducing the likelihood for seal rub during startup and shutdown. This is especially important because excessive rotor vibration can be caused by rotor imbalance present during an initial startup. Such imbalance will be minimized before the unit reaches normal operating condition.

Conventional gland seals are segmented, with each segment held in place by a flat radial spring. Retractable® seals employ coil springs between the seal segments, as shown in Figure 4.12. The coils are oriented in the tangential direction. Based on the manufacturer's input, this results in larger clearance during startup. However, as high-pressure steam enters the gland areas, the seal segments adjust to their design position.

During steady-state operation, the clearance of the Retractable® seal is smaller than the clearance of the conventional labyrinth seal [24].

The Retractable® seals are easier to install compared to conventional labyrinth seals because they have fewer parts. They prolong turbine life by eliminating wear during startup, increase plant turbine efficiency, and lower maintenance costs. At steady-state conditions, steam enters the ring segments to restore design clearances. Retractable seals provide smoother starts and eliminate contact during start-up. Smaller clearances improve unit performance [3,21, 22, 24].



Figure 4.12 : Retractable Seal Segment and Coil Spring  
(Courtesy of Siemens Power Generation)

#### 4.2.2 Abradable Coating Seals

These types of seals use an abradable coating to reduce the clearance between the hard metal rotor and the seal segment base material (Figure 4.13). The abradable coating can be applied to various types of seal segments. It is especially useful in the balance piston and dummy piston sections of high-pressure turbines [3].

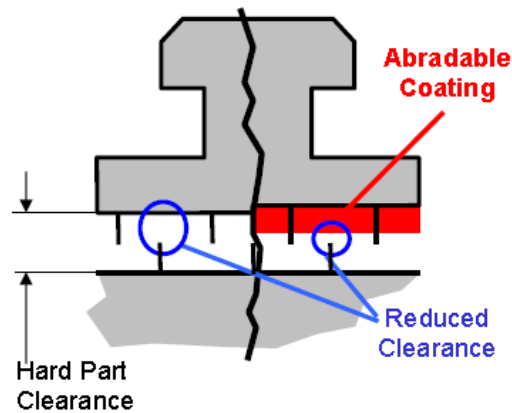


Figure 4.13: Typical Abradable Seal Arrangement [13]

In this approach, an abradable coating is applied by spray between the standard seal segments, as illustrated in Figure 4.13. This reduces seal clearance and thus reduces leakage flow. During rub, the rotor seals, which are harder than the abradable material, will not be damaged.

The operational benefit in the event of a rub is that the sharp edge of the rotor seal, which is harder than the abradable coating material, will cause minimal damage or wear during contact. Based on the specific application, this type of seal provides about 0.1 to 0.2% performance improvements [3].

#### 4.2.3 Brush Seals

Brush seals provide “zero clearance” during operation. Because of their flexible design, brush seals give-way during transient operation (Figure 4.14). Brush seals can be incorporated into retractable seal designs to provide a very effective seal [3, 21, 22].

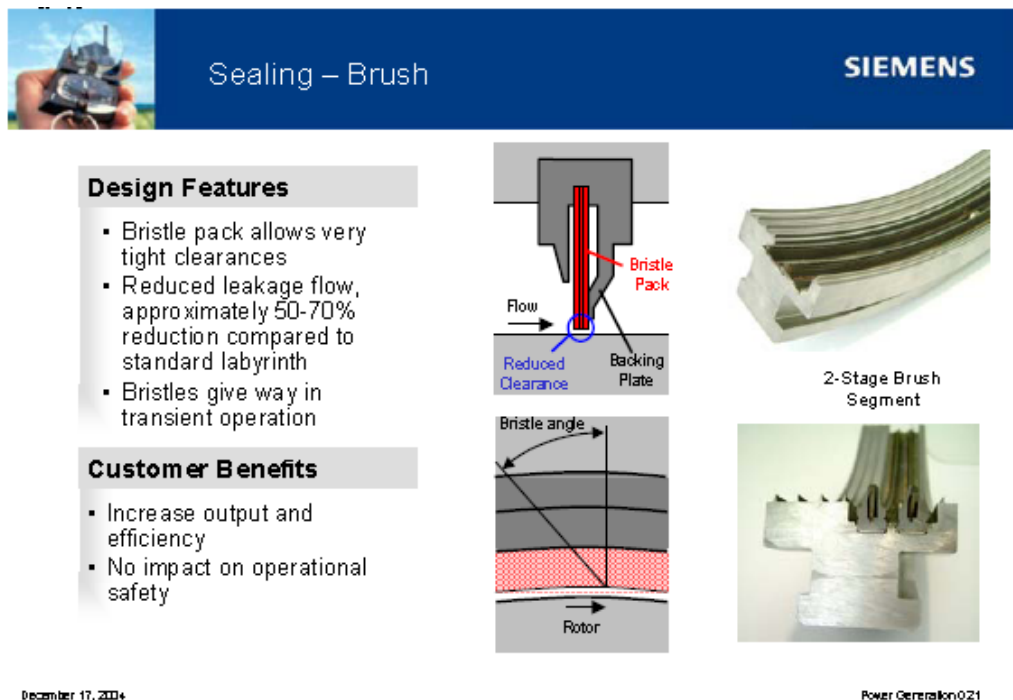


Figure 4.14: Brush Seal Arrangement

#### 4.2.4 Guardian Seal

The geometry of a Guardian® seal is shown in Figure 4.15. In this design, a longer seal strip or post is introduced at the inlet and at the exit of the Guardian® seal segment. These posts are made of a special patented material with a low coefficient of friction. In addition, the subject material is non-galling but erosion resistant. The posts are set at a slightly lower radial clearance than the conventional seal strips. Therefore, during rubs, the Guardian® posts contact the rotor first, preventing damage to the rest of the seals. Furthermore, because of the low coefficient of friction, the Guardian® posts [22], when in contact with the rotor surface, generate substantially less heat than the conventional seals. This reduces galling on the outer surface of the rotor and prevents material damage in the heat-affected zone [22].

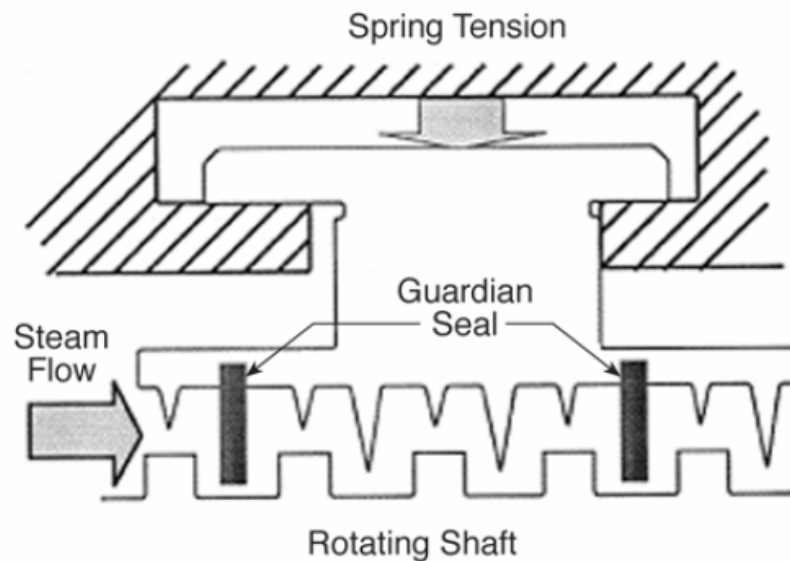


Figure 4.15: Guardian® Seal Geometry

(Courtesy of Turbo Parts, LLC, a division of Mechanical Dynamics & Analysis, Ltd)

The remainder of the seal segment is constructed of 12Cr material, which is known to provide long service life in harsh steam environments.

Guardian® seals maintain tight clearance under a range of operations and extend the efficiency life of the unit. Light coil springs are used to hold the rings in a positive sealing position during startup, turning gear operation, and shutdown. These seals are applicable to both interstage and gland-sealing areas [22, 24].

## CHAPTER 5: FLUE GAS INJECTION INTO COOLING TOWER

### 5.1 Overview

The selection and design of a cooling tower (CT) is based on a number of considerations. They include: ambient conditions, makeup water availability and cost, and the economics of the overall cooling water system. The most common types of cooling towers in use for existing coal-fired power plants are wet natural draft and wet mechanical draft cooling towers. Dry cooling towers are used in arid regions. Wet bulb temperature affects performance of wet cooling towers, while dry bulb temperature is important for dry cooling towers.

In cooling tower systems, the main condenser pressure is limited by the design approach temperature and the ambient wet or dry bulb temperature, depending on the type of cooling tower used. The approach temperature is defined as difference in temperature of the water leaving the cooling tower to that of the ambient wet bulb temperature and the choice of its numerical value used in the main condenser design is an economic decision. The temperature rise across the main condenser is even more important for a cooling tower heat rejection system, because the main condenser cooling water outlet temperature controls the main condenser pressure and sets the cooling tower inlet water design condition, the eventual size of the cooling tower, and the cooling tower basin water temperature (Figure 5.1) [26]. The temperature rise of cooling water across the condenser is called range.

Regardless of the type of cooling tower used for the heat rejection system, two of the most important considerations in the design and operation of a cooling tower are the

materials used for the heat transfer medium (fill) and its design and the water treatment methods used to prevent fouling of the heat transfer medium (water).

Makeup water for the cooling tower can come from a variety of sources that range from fairly good quality river or lake water to low quality brackish wastewater or tidal water from river estuaries. Makeup is needed to replace water evaporated during the cooling process, approximately 1 to 2% of the circulating water flow. Controlling the circulating water quality is the most important aspect of operating a cooling tower [26, 30, 31, 43].

## 5.2 Natural Draft Cooling Towers without Flue Gas Injection

Natural draft cooling towers have a hyperbolic design (Figure 5.1). This design allows air to enter the bottom of the tower where it is heated by the heat transferred from the circulating water system and its humidity is increased by evaporation (1 to 2%) of the circulating water cooled in the cooling tower. The buoyant force of the saturated heated air and difference in ambient pressure between the ground level and CT exhaust causes air flow through the cooling tower [26]. Hot circulating water is pumped into a spray/fill system, which is located just below the center of the tower, where heat transfer between the water and air occurs. The water is sprayed downwards counter-currently to the upward flow of cooling air. To facilitate good contact between air and water a fill is used. The design is quite simple and is trouble-free when properly operated and maintained [58-65]. The natural draft cooling towers may be classified as counterflow evaporative heat exchangers.

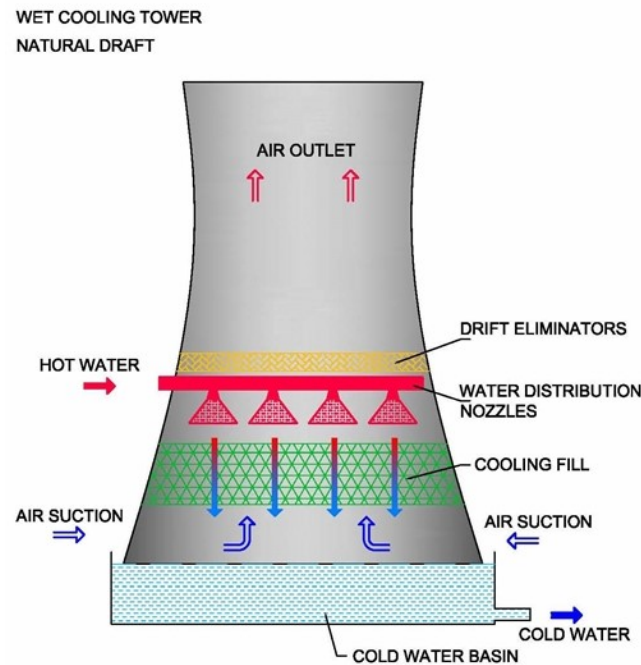


Figure 5.1: Schematic representation of a wet natural draft cooling tower

Due to water shortage in many regions and for environmental reasons, many power plants all around the world rely on natural draft wet cooling towers where hot circulating water (HCW) leaving the main steam condenser is pumped and sprayed inside the cooling tower above the fill to be cooled down by cooling air via heat conduction, convection and evaporation. The cooled circulating water is collected in the CT basin and pumped to the condenser inlet water box as a cold circulating water (CCW). Ambient air is entrained into a CT due to the pressure difference between the top and bottom of the cooling tower, heated and humidified by the HCW sprayed counter-currently (downward) against the upward flow of air, and discharged to atmosphere as saturated air at the top of the tower. Since temperature of the ambient air is lower than temperature of the saturated cooling air

discharged through the tower, moisture in the cooling air condenses creating a white plume – often misinterpreted as pollution.

Ambient conditions, such as temperature and air humidity, have a large effect on cooling tower performance since they affect air density, flow rate, and amount of moisture that could be evaporated from HCW to saturate the cooling air. Cooling air with higher moisture content can hold less evaporated moisture from HCW before it gets saturated, thus reducing evaporative cooling component of heat transfer and resulting in higher temperature of CCW [43, 58, 60]. Higher ambient air temperature has a similar effect; temperature of CCW increases as temperature of the ambient air increases. Thus, performance of a cooling tower is the lowest on hot humid days in the summer and highest on cold dry winter days [26].

### 5.3 Natural Draft Wet Cooling Tower with Flue Gas Injection

To improve the cooling tower performance, it has been proposed to inject flue gas into the cooling tower instead of discharging it through a stack. Injection of the flue gas above the tower fill (above the heat transfer zone) increases temperature of the cooling air, its buoyancy, and thus the air flow through the tower [43].

A natural draft wet cooling tower incorporating the flue gas duct was modeled in this study to determine the effect of flue gas injection on the air flow rate induced through the tower and heat transfer between the HCW and cooling air. The results show from the literature [29, 43] that the flue gas injection helps to improve performance of the cooling tower [58, 64].

Flue gas, as defined in this chapter, constitutes the products of combustion from burning coal. The scrubbing process in a wet FGD significantly lowers the temperature of the flue gas; the scrubbed flue gas leaving the scrubber is saturated or super-saturated with moisture. Traditionally, flue gas has is exhausted into the atmosphere through tall stacks. The stacks lift the pollutants from ground level into the upper atmosphere where they are dispersed greatly reducing their intake fraction (iF) [59, 62, 64, 65]. In order to provide the buoyancy needed for adequate stack flow, the saturated flue gas typically requires reheating through a temperature differential of 70 to 100°C based on data provided by Wark and Warner (1981) [26].

The injection of a scrubbed flue gas into natural draft cooling towers is a relatively new technology, which eliminates the process of reheating the flue gas prior to its discharge through the plant stack. Although natural draft towers are not typically as tall as the stacks, advantage is taken of the upward momentum in the towers, along with the buoyant plume, to achieve the necessary atmospheric rise and dispersion of the flue gas [58, 59].

Another benefit from injection into a cooling tower is that the discharged flue gas gets diluted by as much as a factor of ten before being exhausted to the atmosphere. The flue gas is usually injected a short distance above the fill region in the tower. Figure 5.2 shows a schematic of a natural draft cooling tower with flue gas injection. To overcome pressure (draft) losses, the flue gas may be forced into the tower by means of blowers, although in some applications the negative pressure in the tower is used to pull (induce) the gas from the wet scrubber [59, 64].

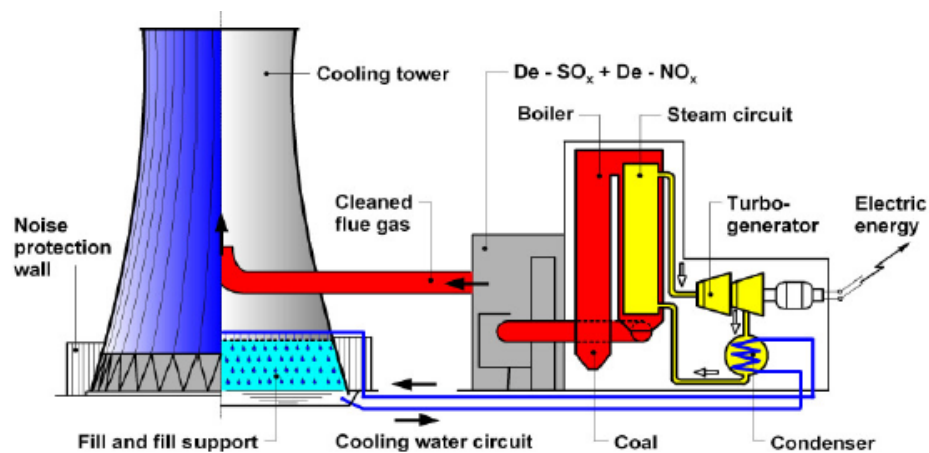


Figure 5.2: Working scheme of a power plant with cleaned flue gas injection [42]



Figure 5.3: Flue gas stack inside a natural draft wet cooling tower [42]

(Courtesy Hamon Thermal GmbH Pvt. Ltd.)

A search of the publicly available literature indicates a need to investigate the effects of flue gas injection on natural draft cooling tower performance [26, 31, 32, 43, 58 to 65]. The results presented in this chapter are based on the Epsilon professional modeling of cooling tower in a super critical coal fired power plant to investigate effects of flue gas

injection on counter-flow natural draft cooling tower performance, and ultimately on plant performance [3]. The independent variables considered in analysis were the flue gas flow rate, flue gas temperature, and the location of injection (Figure 5.3).

In steam power plants, any improvement in thermal performance of the cooling tower will result in lower condenser's temperature and consequently lower condenser pressure, higher power output of the LP turbine section and higher plant efficiency [3].

#### 5.4 Performance Evaluation of a Natural Draft Wet Cooling Tower with flue gas injection

Performance of the cooling tower with flue gas injection was modeled by using the Cooling Tower (CT) model available in the Epsilon Professional. The CT component in the EPV-14 model simulates the boundary conditions considering the characteristics of a natural draft cooling tower with a countercurrent wet cooling zone. This type of cooling tower operates based on evaporation principle. The working fluid and the evaporated fluid (usually water) are one and the same. In a wet cooling tower, the warm water can be cooled to a temperature lower than the ambient air dry-bulb temperature, if the air is relatively dry.

The EPV-14 model of a cooling tower with flue gas injection consists of four zones, as shown schematically in the Figure 5.4. These zones include the wet cooling zone, the dry cooling zone, the cooling tower basin, and the stack. Distribution of the dry to wet cooling duty is set - the air & water flow ratios between the dry and wet zone, size of wet zone and the size of dry cooling zone [1]. The physics of the dry zone is described according to the rules for a general air-water crossflow heat exchanger (see section 5.4.2); while physics of the wet cooling zone may be described by the Merkel's equation [1].

The part-load performance of the wet zone is a characteristic of the Merkel number which is in turn a function of the dry air to water ratio, which is discussed in detail in section 5.4.1. The Epsilon professional code cooling tower model has an empirical; relationship (Section 5.4.3) between stack height, stack inlet section condition (i.e. the air outlet temperature of the cooling zones, Figure 5.4) and air. Injecting flue gas mass flow rate into the tower increases the draft (buoyancy and air flow through the tower).

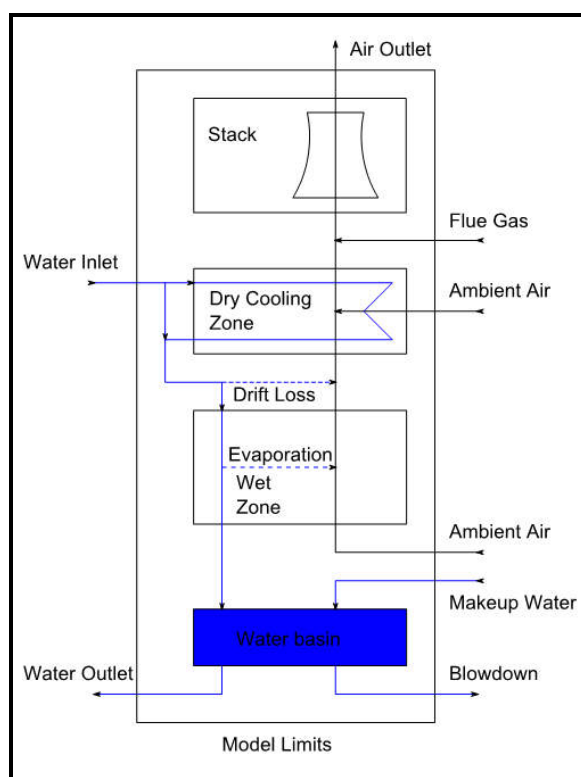


Figure 5.4: Epsilon Professional code different zones inside a cooling tower [1]

The zones in Epsilon Professional code for the cooling tower modeling, governing equations and variables are discussed in detail in section 5.4.1.

#### 5.4.1 Merkel's Equation (Wet Cooling Zone)

Dr. Merkel [28] developed a cooling tower theory for the mass (evaporation of a small portion of water) and sensible heat transfer between the air and water in a counter

flow cooling tower. The theory considers the flow of mass and energy from the bulk water to an interface, and then from the interface to the surrounding air mass. The flow crosses these two boundaries, each offering resistance resulting in gradients in temperature, enthalpy, and humidity ratio. Details of the derivation of Merkel's equation and Merkel's theory are described in [28, 29]. A brief description is provided below.

Merkel demonstrated that the total heat transfer is directly proportional to the difference between enthalpy of the saturated air at the water temperature and enthalpy of air at the point of contact with water.

The analysis of heat transfer process combines both sensible and latent heat transfer into an overall process based on enthalpy potential as the driving force. The process is shown schematically in Figure 5.5 where each particle of the bulk water in the cooling tower is assumed to be surrounded by an interface (film) to which heat is transferred from the water. This heat is then transferred from the film interface to the main air mass by convection and evaporation, i.e., (a) a transfer of sensible heat by and (b) by the latent heat equivalent of the mass transfer resulting from the evaporation of a portion of the bulk water. A graphical representation of heat and mass transfer between the warm water and cooler surrounding air is presented in Figure 5.5.

A typical outdoor thermometer is measuring the "dry bulb temperature" and does not consider the relative humidity in the air. The relative humidity is a measure of the amount of moisture present in the air compared to the maximum amount. The maximum amount of moisture corresponds to the air fully saturated with moisture, i.e., 100% humidity. Any further increase in moisture would result in condensation (formation of

small droplets of water, i.e., fog.) thus preventing evaporation. Psychrometric chart is used to present a relationship between temperature and air humidity together and for calculation of the “wet bulb temperature which is used to describe evaporative cooling in wet cooling towers.

The wet bulb temperature is a function of relative humidity and ambient air temperature (dry bulb temperature) and measures how much water vapor the atmosphere can hold at current weather conditions. A lower wet bulb temperature means the air is drier and can hold more water vapor than at a higher wet bulb temperature. Thus, performance of wet cooling tower decreases as wet bulb temperature is increased.

As mentioned earlier, the cooling tower approach, or approach is the difference between the temperature of the water leaving the tower and the wet bulb temperature of the entering air. For the purpose of tower design, a tower with a smaller approach (small difference between the basin water temperature and wet bulb temperature) is considered superior. Modern towers commonly have approach temperatures as low as 5°F. While it is possible to have a smaller approach, it becomes cost-prohibitive since the size of the tower increases exponentially as approach is decreased [27, 30, 31, 60]. This also leads to more auxiliary power usage and diminishing returns.

The two processes of heat transfer (movement of heat), described by Equations 5.1 and 5.2 can be combined into a single equation known as the Merkel equation [28, 29].

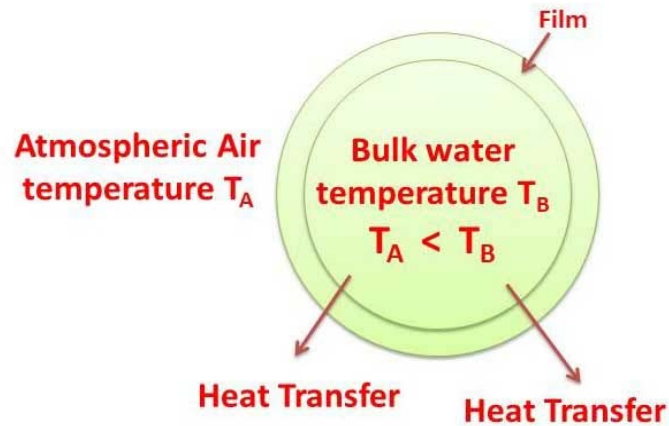


Figure 5.5: Water Drop with Interfacial Film [27]

$$Q = K \cdot S \cdot (h_w - h_a) \quad (5.1)$$

$$S = a \cdot V \quad (5.2)$$

Where,

$Q$  = Total heat transfer, (Btu/hr, J/hr)

$K$  = Mass transfer coefficient (lb /hr ft<sup>2</sup>, kg/hr m<sup>2</sup>)

$S$  = Heat transfer surface (ft<sup>2</sup>, m<sup>2</sup>)

$a$  = Area of heat transfer surface per unit of tower volume. (ft<sup>2</sup>/ft<sup>3</sup>, m<sup>2</sup>/m<sup>3</sup>)

$V$  = Effective tower volume (ft<sup>3</sup>, m<sup>3</sup>).

The water temperature and air enthalpy are changing along the fill and Merkel relation can be applied to a small element of heat transfer surface  $dS$ .

$$dQ = d[K \cdot S \cdot (h_w - h_a)] = K \cdot (h_w - h_a) \cdot dS \quad (5.3)$$

The heat transfer rate from water side is,

$$Q = C_w \cdot L \cdot \text{Cooling Range} \quad (5.4)$$

$$dQ = d[C_w \cdot L \cdot (T_1 - T_2)] = C_w \cdot L \cdot dT \quad (5.5)$$

The cooling Range ( $T_1 - T_2$ ) is the temperature difference between the hot water entering the cooling tower and the cold water leaving the tower.

The heat transfer rate from air side is,

$$Q = G \cdot (h_2 - h_1) \quad (5.6)$$

$$dQ = d[G \cdot (h_2 - h_1)] = G \cdot dh_a \quad (5.7)$$

$$K \cdot (h_w - h_a) \cdot dS = G \cdot dh_a \quad (5.8)$$

$$K \cdot (h_w - h_a) \cdot dS = C_w \cdot L \cdot dT \quad (5.9)$$

Equations from 5.8 & 5.9 can be rewritten as below,

$$K \cdot dS = \frac{G}{(h_w - h_a)} \cdot dh_a \quad (5.10)$$

$$\frac{K}{L} \cdot dS = \frac{C_w}{(h_w - h_a)} \cdot dT \quad (5.11)$$

By integration of Equation for 5.10 and 5.11,

$$\frac{K \cdot S}{L} = \frac{KaV}{L} = \frac{G}{L} \int_{h_1}^{h_2} \frac{dh}{h_w - h_a} \quad (5.12)$$

or

$$\frac{K \cdot S}{L} = \frac{KaV}{L} = C_w \int_{T_2}^{T_1} \frac{dT}{h_w - h_a} = Me \quad (5.13)$$

This basic heat transfer equation is integrated by the four-point numerical integration [27, 32], which uses values of y at predetermined values of x within the interval a to b in numerically evaluating the integral  $\int_a^b y dx$ . The sum of these values of y multiplied by a constant time the interval (b - a) gives the desired value of the integral. In its four-

point form the values of  $y$  so selected are taken at values of  $x$  of 0.102673, 0.406204, 0.593796, and 0.897327 of the intervals  $(b - a)$ . For the determination of  $KaV/L$ , rounding off these values to the nearest tenth is entirely adequate. The approximate formula becomes [32, 66]:

$$\int_a^b y dx = \frac{(b - a) \cdot (y_1 + y_2 + y_3 + y_4)}{4} \quad (5.14)$$

Where,

$$y_1 = \text{Value of } y \text{ at } x = a + 0.1 \cdot (b - a) = T_2 + 0.1 \cdot (T_1 - T_2)$$

$$y_2 = \text{Value of } y \text{ at } x = a + 0.4 \cdot (b - a) = T_2 + 0.4 \cdot (T_1 - T_2)$$

$$y_3 = \text{Value of } y \text{ at } x = b + 0.4 \cdot (b - a) \text{ or } x = a + 0.6 \cdot (b - a) = T_1 + 0.6 \cdot (T_1 - T_2)$$

$$y_4 = \text{Value of } y \text{ at } x = b + 0.1 \cdot (b - a) \text{ or } x = a + 0.9 \cdot (b - a) = T_1 + 0.9 \cdot (T_1 - T_2)$$

Evaluation of  $KaV/L$  using the formula stated in equation 5.14,

$$\frac{KaV}{L} = C_w \int_{T_2}^{T_1} \frac{dT}{h_w - h_a} = \frac{(T_1 - T_2)}{4} \cdot \left( \frac{1}{\Delta h_1} + \frac{1}{\Delta h_2} + \frac{1}{\Delta h_3} + \frac{1}{\Delta h_4} \right) \quad (5.15)$$

$C_w$  = Specific heat of water (Btu/°F/lb, J/°C /kg) = 1

Psychometric chart is used for determining the Enthalpy ( $\Delta h$ ) values for the corresponding temperature, and a sample characteristic curve is shown in figure 5.7.

Where,

$$\Delta h_1 = \text{Value of } h_w - h_a \text{ at a temperature of } T_2 + 0.1 \cdot (T_1 - T_2)$$

$$\Delta h_2 = \text{Value of } h_w - h_a \text{ at a temperature of } T_2 + 0.4 \cdot (T_1 - T_2)$$

$$\Delta h_3 = \text{Value of } h_w - h_a \text{ at a temperature of } T_1 + 0.6 \cdot (T_1 - T_2)$$

$$\Delta h_4 = \text{Value of } h_w - h_a \text{ at a temperature of } T_1 + 0.9 \cdot (T_1 - T_2)$$

$Me$  = Merkel Number

The 1<sup>st</sup> Law of Thermodynamics dictate that the heat removed from the water must be equal to the heat absorbed by the surrounding air,

$$L \cdot (T_1 - T_2) = G \cdot (h_2 - h_1) \quad (5.16)$$

$$\frac{L}{G} = \frac{(h_2 - h_1)}{(T_1 - T_2)} \quad (5.17)$$

Water to air ratio (L/G) is the mass ratio of water (Liquid) flowing through the tower to the air (Gas) flow.

Where,

G = Air (gas) mass flow rate, (lb/hr, kg/hr)

L = Water (liquid) flow rate, (lb/hr, kg/hr)

T<sub>1</sub> = Hot circulating water temperature (°F or °C)

T<sub>2</sub> = Cold circulating water temperature (°F or °C)

T = Bulk water temperature (°F or °C)

h<sub>w</sub> = Enthalpy of air-water vapor mixture at bulk water temperature (J/kg dry air, Btu/lb dry air).

h<sub>a</sub> = Enthalpy of air-water vapor mixture at wet bulb temperature (J/kg dry air, Btu/lb dry air).

h<sub>1</sub> = Enthalpy of air-water vapor mixture at inlet wet-bulb temperature (J/kg dry air, Btu/lb dry air).

h<sub>2</sub> = Enthalpy of air-water vapor mixture at exhaust wet-bulb temperature (J/kg dry air, Btu/lb dry air).

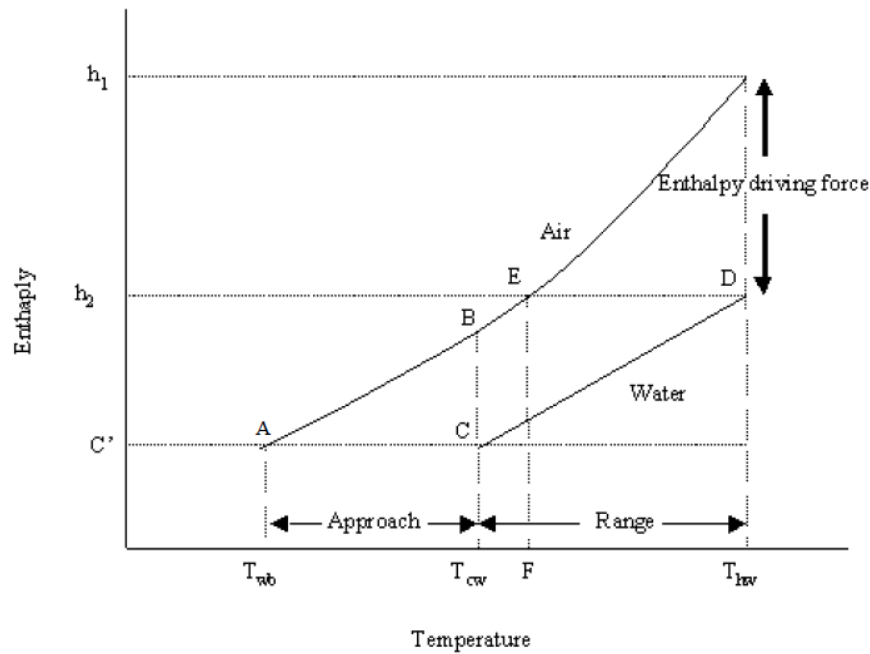


Figure 5.6: Cooling Tower Characteristics [27, 31]

**Range** is the temperature difference between the hot water entering the cooling tower and the cold water leaving.

**Approach** is the difference between the temperature of the water leaving the tower and the wet bulb temperature of the entering air.

**Water/Air Ratio ( $L/G$ )** is the mass ratio of water (Liquid) flowing through the tower to the air (Gas) flow.

Where,

$C'$  = Entering air enthalpy at wet-bulb temperature,  $T_{wb}$ .

$BC$  = Initial enthalpy driving force.

$CD$  = Air operating line with slope  $L/G$ .

$DEF$  = Projecting the exiting air point onto the water operating line and then onto the temperature axis shows the outlet air web-bulb temperature.

As shown by Equation 5.1, by finding the area between ABCD in Figure 5.2, one can find the tower characteristic sometimes called the number of transfer units, NTU. An increase in heat load would have the following effects on the diagram in Figure 5.2:

- a. Increase in the length of line CD, and a CD line shift to the right.
- b. Increases in hot and cold-water temperatures.
- c. Increases in range and approach areas

The increased heat load causes the hot water temperature to increase considerably faster than does the cold-water temperature. Although the area ABCD should remain constant, it decreases about 2% for every 10°F increase in hot water temperature above 100°F. To account for this decrease, an "adjusted hot water temperature" is used in cooling tower design. The area ABCD is expected to change with a change in L/G, this is very key in the design of cooling towers.

The other method to calculate performance of the wet zone is by NTU method [1, 33], Equation 5.18 describes the Net Transfer Units (NTU) in the wet zone. and is similar in concept to the number of transfer units used in the heat exchanger design [27, 30, 31].

$$NTU = Me \cdot \left( \frac{M_{Water\_in}}{M_{Air\_in}} \right) \quad (5.18)$$

Writing the NTU equation in terms of Air Water Ratio (L/G) variables is by substituting the Merkel number from Equation 5.12 or 5.13 in Equation 5.18,

$$NTU = \frac{L}{G} \cdot C_w \cdot \int_{T_2}^{T_1} \frac{dT}{h_w - h_a} \quad (5.19)$$

or

$$NTU = \int_{h_1}^{h_2} \frac{dh}{h_w - h_a} \quad (5.20)$$

The basis of the characteristic diagram in Figure 5.7 is the German industrial standard DIN 1947 [69]. Systems with uncontrolled cooling water pumps, i.e. constant cooling water flow under all operating states, this nomograph can be used to model cooling tower performance throughout the yearly climatic cycle. The characteristic diagram defines the cooling range or cold-water temperature as a function of

- Inlet air dry bulb temperature,
- Inlet air relative humidity,
- Relative water mass flow rate and
- Hot water inlet temperature.

If inputs exceed these limits, the limits can be taken as input parameters. Otherwise, a linear interpolation can be performed. No extrapolation is advisable; all returning values to be kept between the MIN and MAX constraints.

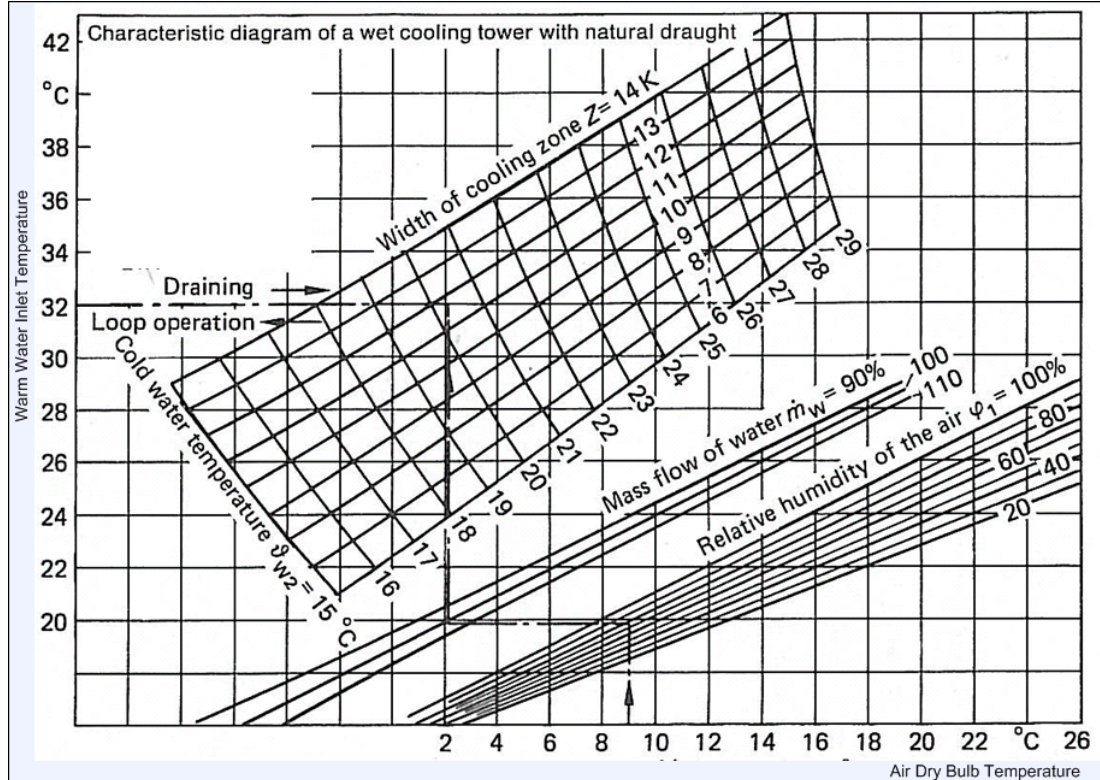


Figure 5.7: Characteristic curves for a natural draft wet cooling tower [69]

Cooling towers are designed according to the highest geographic wet bulb temperatures. This temperature will dictate the minimum performance available by the tower. As the wet bulb temperature decreases, so will the available cooling water temperature.

#### 5.4.2 Dry Zone (Heat Exchanger)

Referring figure 5.4, dry cooling zone in cooling tower design is referred as a normal air to water crossflow heat exchanger and is modeled as a single pass with NTU-Effectiveness Method [33].

In this zone the heat transfer between ambient air to that of the hot water [67, 68],

$$\varepsilon = \frac{q}{q_{max}} = \frac{C_h \cdot (T_{h,i} - T_{h,o})}{C_{min} \cdot (T_{h,i} - T_{c,i})} = \frac{C_c \cdot (T_{c,o} - T_{c,i})}{C_{min} \cdot (T_{h,i} - T_{c,i})} \quad (5.19)$$

Where,

$$q_{max} = C_{min} \cdot (T_{h,i} - T_{c,i}) \quad (5.20)$$

$$NTU = \frac{A \cdot U_{av}}{C_{min}} = \frac{1}{C_{min}} \int_0^A U \cdot dA \quad (5.21)$$

#### 5.4.3 Stack/Tower Height and Air flow

The air flow will be determined by the parameter AWR (Air to Water, Gas to Liquid Ratio; L/G). The relationship between the pressure drop ( $\Delta p$ ) and effective stack height H is given by:

$$\Delta p = (\rho_{ambient\ air} - \rho_{exit\ air}) \cdot g \cdot H \quad (5.21)$$

Where,  $\rho$  = density and  $g$  = gravitational constant

In the Off-Design mode, the pressure drop can be calculated as described below,

The dry and wet zone air flow can be determined from the following equations:

$$\Delta P_{Design} = \frac{\zeta \cdot \rho_{Design}}{2 \cdot (v_{Design})^2} \quad (5.22)$$

$$\Delta P_{Off-Design} = \frac{\zeta \cdot \rho_{Off-Design}}{2 \cdot (v_{Off-Design})^2} \quad (5.23)$$

With A = Cross sectional area, the average air flow velocity can be calculated as

$$v = \frac{\left(\frac{m}{\rho}\right)}{A} \quad (5.24)$$

Eliminating of  $\zeta$  we get the final off-design equation for the off-design air flow:

$$\frac{\Delta P_{Design}}{\Delta P_{Off-Design}} = \frac{(m_{Design})^2}{(m_{Off-Design})^2} \cdot \frac{\rho_{Off-Design}}{(\rho_{Design})^2} \quad (5.25)$$

#### 5.4.4 Cooling Tower Losses

Makeup water is added to the water basin to compensate for the water losses in the circuit. The water losses include evaporation loss (E), drift loss (D), blowdown (B), and other leakage losses (OL) in the system, such as losses from the pump seal, piping leak, wash down water and filter backwash.

**Evaporation Loss (E):** Water evaporated from the circulating water into the air stream in the cooling process.

$$E = 0.00085 \cdot L \cdot (T_1 - T_2) \quad (5.26)$$

**Drift Loss (D):** Circulating water lost from the tower as liquid droplets entrained in the exhausted air stream.

$$D = 0.00085 \cdot M_w \cdot (T_1 - T_2) \quad (5.27)$$

**Blowdown (B):** Water discharged from the system to control concentrations of salts and other impurities in the circulating water.

$$B = \frac{E}{(COC - 1)} \quad (5.28)$$

Where,

COC – Cycles of Concentration (between 4 to 7)

#### 5.5 Illustration of Performance Evaluation using Epsilon Professional Code

The EPV-14 model of a reference plant, 680 MW supercritical coal-fired power plant, presented schematically in Figures 5.4 and 5.5, was used to determine performance improvements (net unit efficiency, net heat rate and other) that would be achieved by

injecting flue gas into the cooling tower. The results are presented in Table 5.1 and Figure 5.7. The plant design parameters are summarized in Table 5.1.

Table 5.1: Reference plant operating parameters

Plant Design Capacity	680 MW
HP Pressure	252 bar
HP Temperature	540°C
HRH Temperature	540°C
CRH Pressure	56.9 bar
CRH Temperature	318°C
RP Pressure	51.9 bar
RH Temperature	540°C
IP Pressure	20.3 bar
IP Temperature	403°C
LP Pressure	6 bar
LP Temperature	255°C

Ambient data:

Wet Bulb Temperature = 22°C; Relative Humidity = 60%

CT Design Parameters:

Inlet Hot water Temperature ( $T_1$ ) = 42.1°C;

Outlet Cold water Temperature ( $T_2$ ) = 33.2°C;

Air Flow rate ( $G$ ) = 32,161.9 kg/s;

Water Flow Rate ( $L$ ) = 22,553.9 kg/s;

Condenser Pressure = 106.8 mbar;

Approach Temperature = 10°C;

COC = 4.

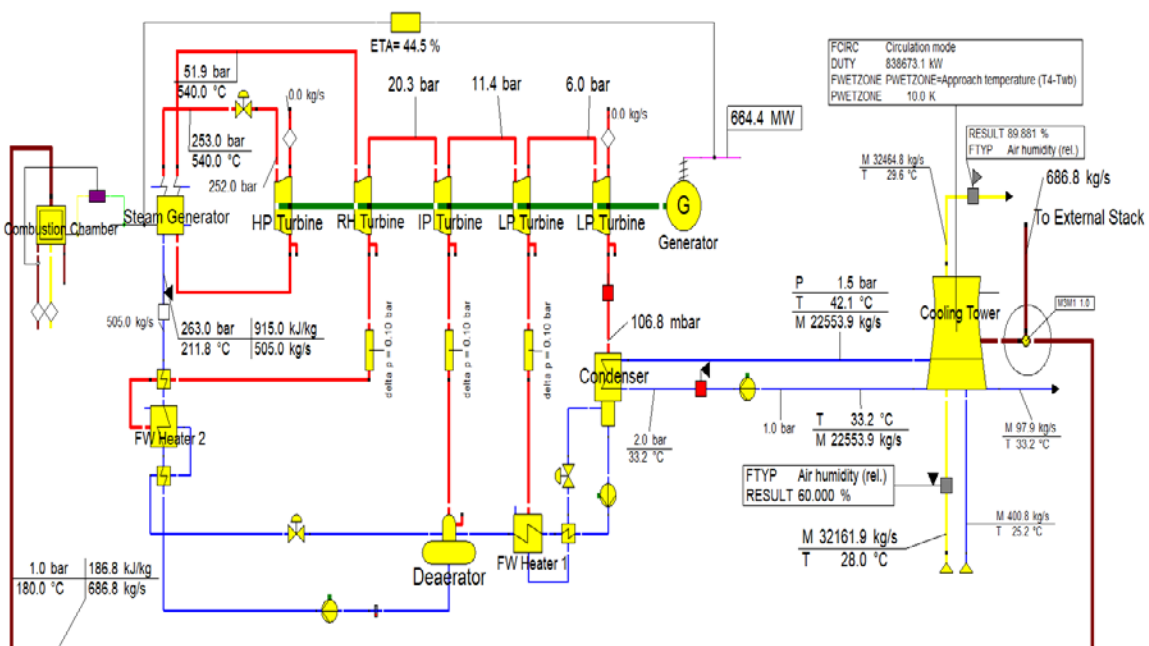


Figure 5.7: Power plant **without** flue gas injection into cooling tower

Table 5.2: Performance comparison between power plants with and without flue gas injection into cooling tower.

Description	$P_G$ MW	$HR_{cycle}$ BTU/kWh	$\eta_{cycle}$ %	$P_{net}$ MW	$HR_{net}$ BTU/kWh	$Q_{condenser}$ MBTU/hr	$\eta_{net}$ %	$\eta_{Boiler}$ %
No Flue Gas Injection	664.00	7,671.31	44.48	612.78	7,671.31	2,828.18	44.48	88.86
Flue Gas Injection	667.40	6,927.12	49.26	615.92	7,506.15	2,345.99	45.46	88.67

As presented in Table 5.2 the plant without flue gas injection into the cooling tower is producing 664 MW gross power output with a condenser pressure of 107.9 mbar (see Figure 5.7). The flue gas (686.8 kg/s) injection into the cooling tower is improving its performance resulting in condenser pressure of 106.9 mbar (see Figure 5.8). The lower

condenser pressure results in 3.7 MW higher power output, higher turbine cycle and unit efficiency, and lower condenser duty as presented in Table 5.2. Performance improvement is also presented in graphical form in Figure 5.9.

### CT Design Parameters:

Inlet Hot water Temperature ( $T_1$ ) = 40.8°C;

Outlet Cold water Temperature ( $T_2$ ) = 31.9°C;

Air Flow rate ( $G$ ) = 38,124.3 kg/s;

Water Flow Rate ( $L$ ) = 22,553.9 kg/s;

Condenser Pressure = 100 mbar;

Approach Temperature = 10°C.

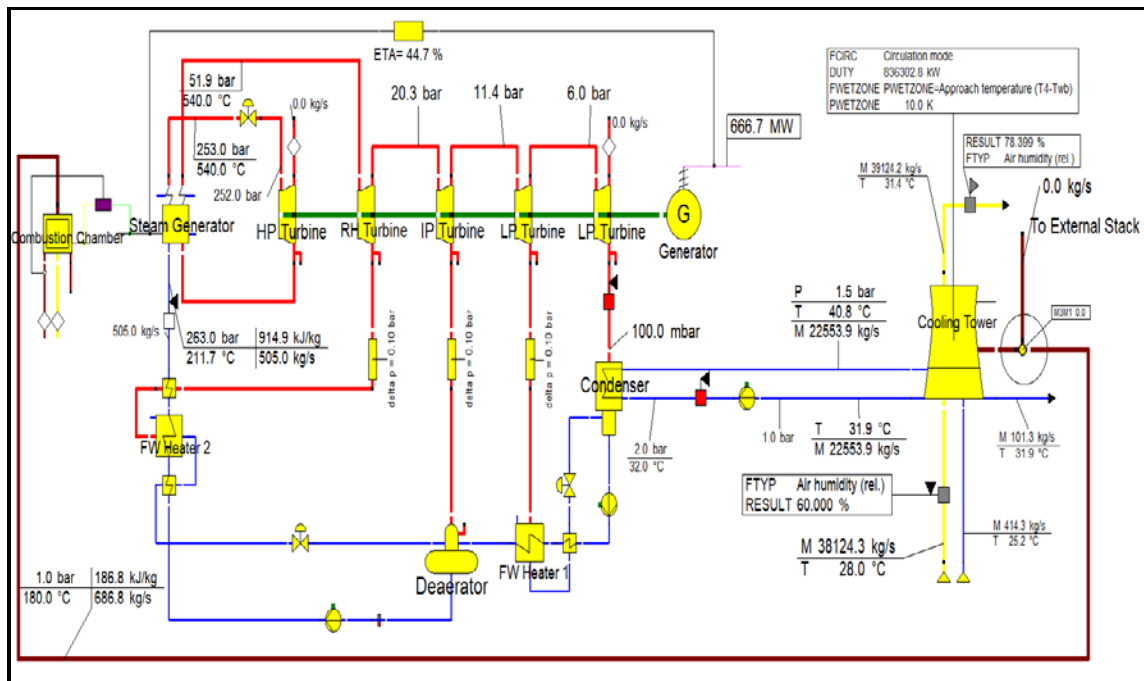


Figure 5.8: Power Plant with Flue gas Injection into Cooling Tower

The saturation line of the air (air enthalpy plotted over the temperature) under the considered ambient atmospheric pressure as well as the change in the inlet and outlet states of the air (enthalpy) and the water (temperature) in the cooling tower with flue gas injection is shown in Figure 5.9.

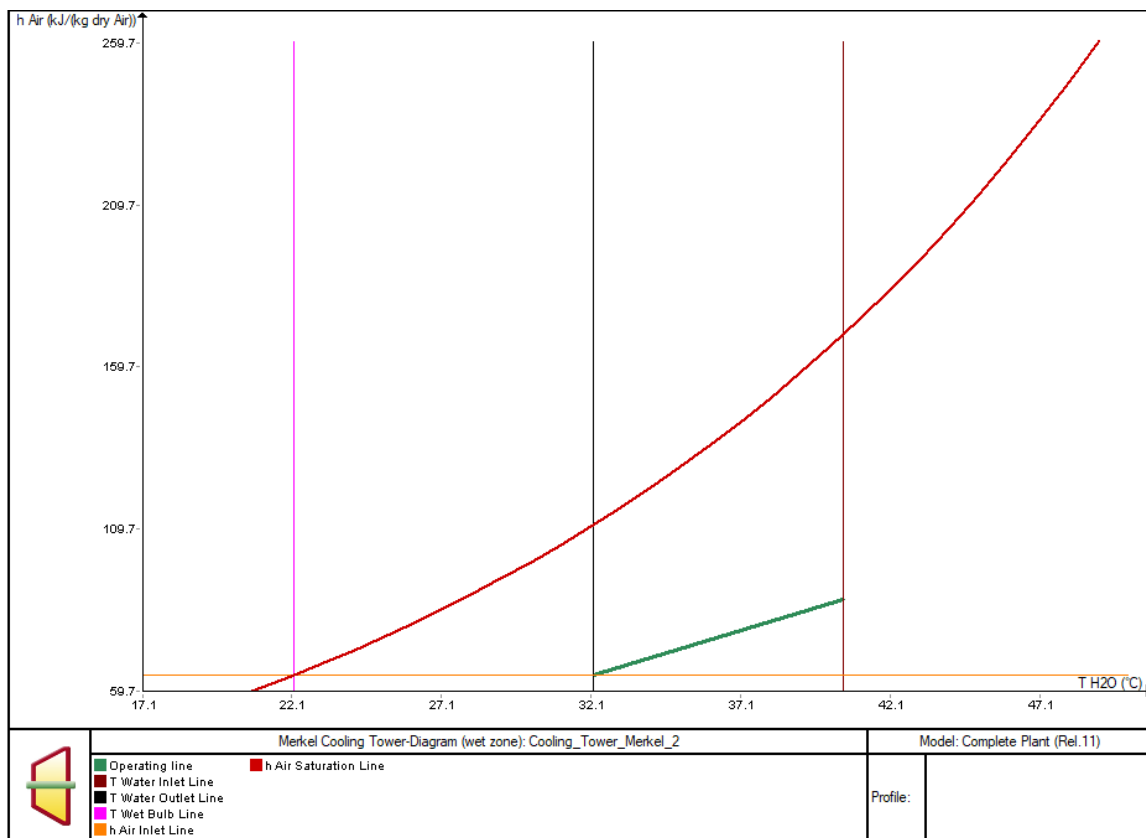


Figure 5.9: Cooling Tower diagram – Wet zone (Merkel)

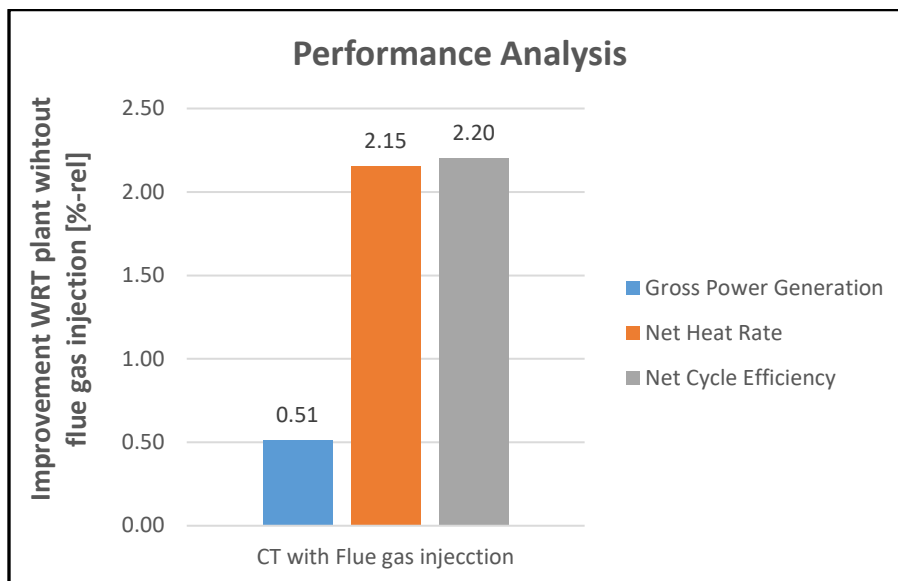


Figure 5.10: Performance Analysis for cooling tower with and without flue gas Injection

In summary, applying flue gas injection to an existing power plant improves its performance. For the Reference plant, the predicted performance improvements include 0.51% (3.40 MW) increase in gross power generation, 2.15% (165 Btu/ kWh) improvement (decrease) in net heat rate, and 2.20% (0.98% point) increase in net cycle efficiency with respect to a plant without flue gas injection. These increments are shown in Figure 5.9.

The flue gas temperature was found to have the most significant effect on tower performance (cold water temperature), because it strongly affects the buoyancy within the tower. The total air flow through a tower is driven by buoyancy forces, and the cooling performance is a strong function of the airflow rate.

By injecting flue gas into the plume of the cooling tower, in addition to performance improvement to the power plant there is also savings from building a separate stack for the power plant since the plume of the cooling tower acts as a stack to vent out the flue gas at a safe height in to the atmosphere.

## CHAPTER 6: CUMMULATIVE PERFORMANCE IMPROVEMENT

### 6.1 Overview

In this chapter we compare the performance of a plant equipped with both flue gas injection into the cooling tower and heat recovery from flue gas by a flue gas cooler (FGC) with respect to a baseline plant as described in Chapter 1 (Refer 1.1). These performance improvement techniques have been discussed in detail in Chapters 2 and 5, respectively. The combined performance improvement is the area of interest, since individual performance improvements may not be additive. To determine cumulative performance improvement, the performance techniques described above were incorporated into the Reference plant model. The plant equipped with both heat recovery using FAC and flue gas injection into a CT is shown in Figure 6.1. The main operating performance parameters for all three cases (Reference plant, Plant with FGC and Plant with FGC and CT flue gas injection) are summarized in Table 6.1. Bituminous coal with a moisture content of 8.5% was considered as fuel in the boiler for this analysis. Also, the feedwater temperature entering the boiler was kept constant for all analyzed cases.

### 6.2 Calculation basis for key performance parameters

To evaluate the performance of each of these existing power plant performance improvement techniques key performance factors are calculated using these equations. These equations form the basis for developing the models in the EPV-14.

$$HR_{cycle} = \frac{[Q_1 \cdot (H_1 - h_2) + Q_2 \cdot (H_3 - H_2)]}{P_G} \quad (6.1)$$

Where,

$HR_{cycle}$  - Turbine Cycle Heat Rate, Btu/kWh

$Q_1$  – Boiler Main steam flow, lb/hr

$H_1$  – Boiler Main steam enthalpy, Btu/lb

$h_2$  - Feed water enthalpy, Btu/lb

$Q_2$  - Hot reheat steam flow, lb/hr

$H_3$  - Hot reheat enthalpy, Btu/lb

$H_2$  - Cold reheat enthalpy, Btu/lb

$P_G$  - gross power output, MW

$$\text{Gross Power Output (} P_G \text{)} = \text{Net power output (} P_{net} \text{)} + \text{Auxiliary power use (} P_{ss} \text{)} \quad (6.2)$$

Over-all plant auxiliary power consumption or the station own use is from the following operating components,

1. Induced draft Fan (ID)
2. Forced draft Fan (FD)
3. Condensate Extraction Pump (CEP)
4. Main Boiler Feed Water Pump (BFP)
5. Feed Water Recirculation Pump (RCP)

Net Power is the power sold to the grid. It is calculated by subtracting auxiliary power from the gross power.

$$\text{Net power output (} P_{net} \text{)} = \text{Gross Power Output (} P_G \text{)} - \text{Auxiliary power use (} P_{ss} \text{)} \quad (6.3)$$

$$HR_{net} = \frac{Q_{fuel}}{P_{net}} = \frac{(M_{coal} \cdot HHV)}{(P_G - P_{ss})} \quad (6.4)$$

$$\eta_B = \frac{P_G \cdot HR_{cycle}}{Q_{fuel}} = \frac{Q_T}{(M_{coal} \cdot HHV)} \quad (6.5)$$

$$HR_{net} = \frac{HR_{cycle}}{\eta_B \cdot \left(1 - \frac{P_{ss}}{P_G}\right)} \quad (6.6)$$

Where,

$Q_T$  – Total Heat input, MBtu/hr

$Q_{fuel}$  - Heat input with fuel, MBtu/hr

$P_{net}$  - Net unit power output, MW

$M_{coal}$  - Flow rate of coal fired to generate gross power output, lb/hr

$P_G$  - Gross power output, MW

HHV - Coal higher heating value, Btu/lb

$P_{ss}$  - Auxiliary power consumed (station service power), MW

$\eta_B$  – Boiler Efficiency, %

$$\eta_{net} = \frac{P_{net}}{Q_{fuel}} = \frac{3412}{HR_{net}} \quad (6.7)$$

Where,

$Q_{fuel}$  - heat input with fuel, MBtu/hr

$P_{net}$  - net unit power output, MW

$HR_{net}$  – Net Unit Heat Rate, MBtu/kWh

$$\eta_{cycle} = \frac{P_G}{Q_{fuel}} = \frac{3412}{HR_{cycle}} \quad (6.8)$$

Where,

$Q_{fuel}$  - heat input with fuel, MBtu/hr

$P_G$  - Gross unit power output, MW

$HR_{cycle}$  – Unit Cycle Heat Rate, MBtu/kWh

$$Q_T = P_G \cdot HHV_{fuel} \quad (6.9)$$

$$Q_{fuel} = \left( \frac{Q_T}{\eta_{boiler}} \right) \quad (6.10)$$

$$M_{coal} = \left( \frac{Q_{coal}}{HR_{cycle}} \right) \quad (6.11)$$

Total Heat Input ( $Q_T$ ), Fuel Heat Input ( $Q_{coal}$ ) and Mass or quantity of coal fired ( $M_{coal}$ )

### 6.3 Illustration of Performance Evaluation using Ebsilon Professional Code

The baseline performance of the Reference plant was determined by using the EPV-14 model of the plant. Calculations were performed by using the condenser back pressure of 0.1 bar corresponding to the summertime operating conditions. This operating condition was used because it better illustrates the benefits of flue gas injection into the cooling tower and waste heat recovery using a FGC, compared to the operation with a variable condenser back pressure, thus allowing more straightforward comparison. Plant configurations modelled by the Ebsilon Professional code considered for this study are presented in Figures 6.1 to 6.4. Figure 6.1 illustrates the base plant configuration with condenser operating pressure set a 0.1 bar (100 mbar).

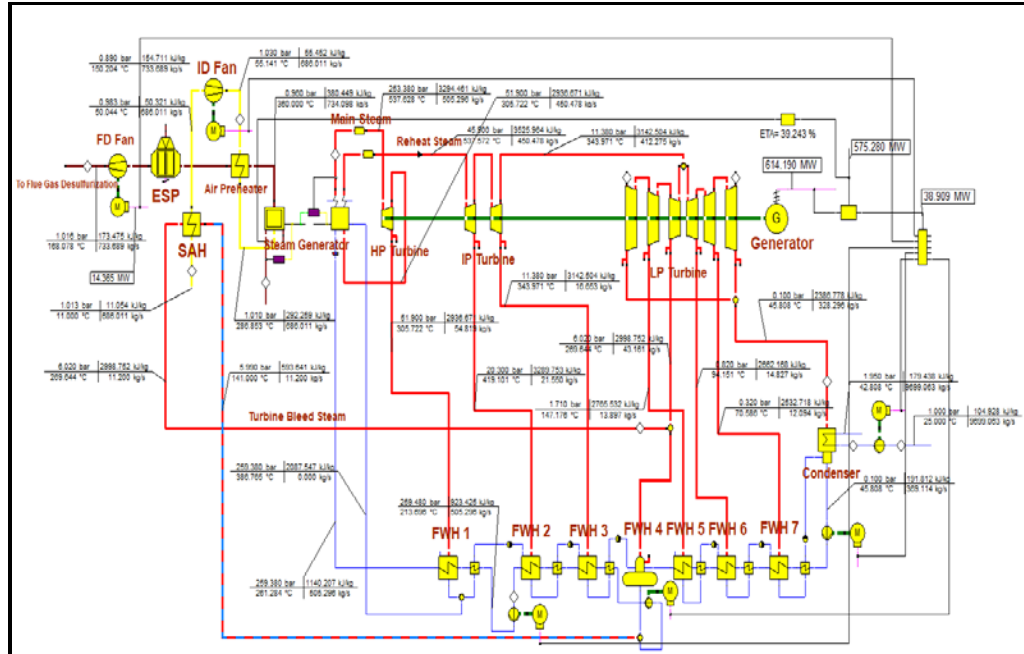


Figure 6.1: Reference power plant with 100 mbar condenser operating pressure

The first investigated configuration is the reference power plant with SAH equipped with a cooling tower with flue gas injection. The exhaust flue gas from the FD fan is injected into the cooling tower to increase buoyancy there by increasing the performance of the plant is shown in Figure 6.2. The idea is to utilize the waste heat from the exhaust flue gas stream to improve the plant performance. The flue gas of 734 kg/s mass at 168°C (334°F) is injected above the dry zone (refer Chapter 5.4 for details) of the cooling tower and exhausted finally into the atmosphere at the exit of cooling tower stack. In this process ~206 Mbtu/hr of waste heat from the flue gas is utilized in improving the plant performance.

#### CT Design Parameters:

Inlet Hot water Temperature ( $T_1$ ) = 42.1°C;

Outlet Cold water Temperature ( $T_2$ ) = 24.7°C;

Air Flow rate ( $G$ ) = 19,227.2 kg/s;

Water Flow Rate ( $L$ ) = 9,696.6 kg/s;

Condenser Pressure = 96.12 mbar;

Approach Temperature = 10°C;

COC = 4.

The flue gas injection into the cooling tower is improving the plant performance resulting in reducing the condenser pressure to 96.12 mbar from 100 mbar. This lowering of condenser pressure results in 1.91 MW higher power output, higher turbine cycle and unit efficiency and lower condenser duty as presented in Table 6.1.

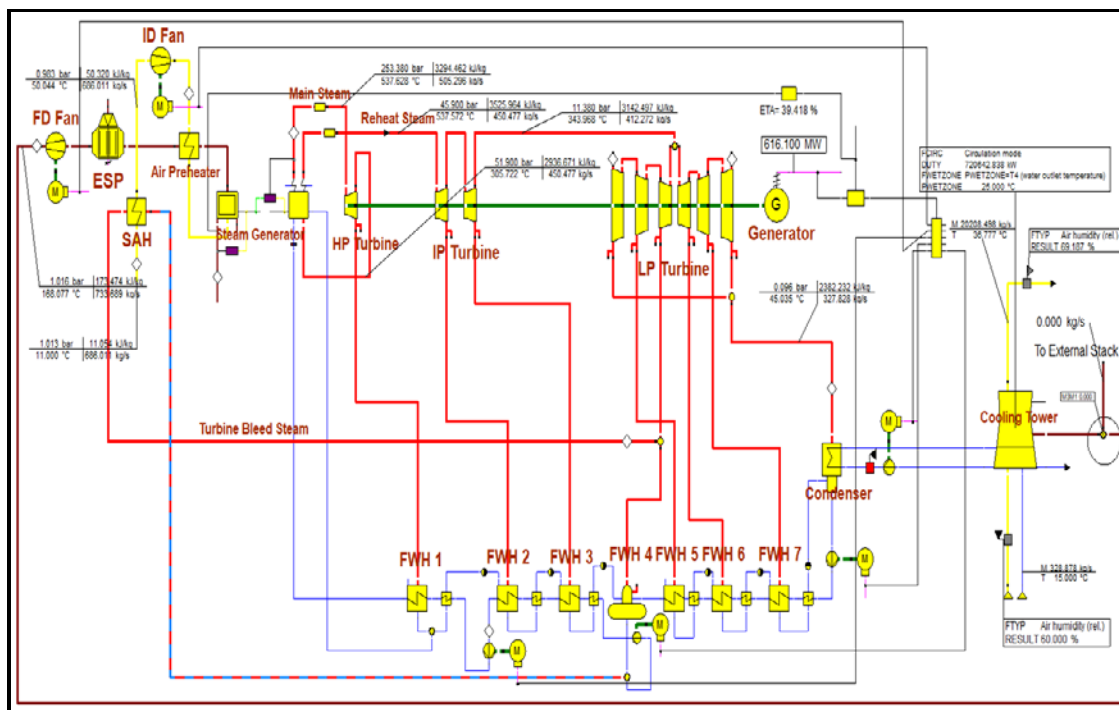


Figure 6.2: Power plant equipped with cooling tower flue gas injection

In the next configuration presented in Figure 6.3, a portion of heat recovered from the flue gas is used for FW heating and another portion of heat is used for the combustion air preheat. Instead of using steam extracted from the steam turbine cycle for the combustion air preheat, combustion air is preheated by the heat recovered from the flue gas stream. This increases steam flow through the low pressure (LP) turbine with resulting increase in the steam turbine power output. Also, since steam extraction for the SAH is eliminated, the heat rejected by the condenser and the condensate flow increase. In the analyzed case the amounts of heat supplied by the extraction steam and recovered from the flue gas were matched  $\sim 97$  MJ/hr ( $\sim 92$  MBtu/hr) to achieve the same level of combustion air preheat. And 100% of the condensate flow leaving the main steam condenser flows through the FGC where it is heated  $\sim 121$  MJ/hr ( $\sim 115$  Mbtu/hr). The heated condensate is circulated back to the steam turbine cycle, eliminating low-pressure (LP) feed water heaters (FWH's) 6 and 7. This arrangement eliminates LP steam extractions and the steam that would normally be used in the FWH6 and FWH7 is expanded in the LP turbine. The result is an increase in the steam turbine power output, increase in steam flow to the condenser and main condensate flow, and increase in heat rejected by the main steam condenser.

For clarity, the FGC is divided into two parts where FGC 1 is used for the FW heating, and FGC 2 is used for combustion air preheat.

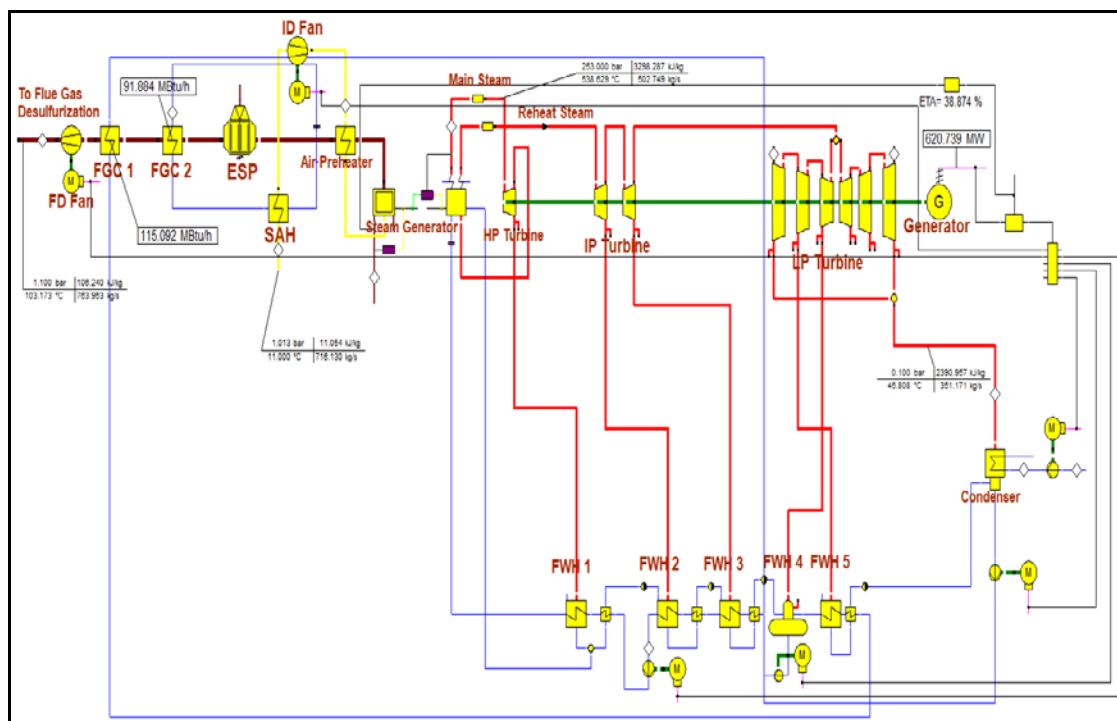


Figure 6.3: Power plant equipped with FGC for waste heat recovery from flue gas

The third Configuration represents combination of the above-mentioned CT injection and FGC configurations, where a portion of heat recovered from the flue gas is used for FW heating  $\sim 121$  MJ/hr ( $\sim 115$  Mbtu/hr) and combustion air preheating  $\sim 97$  MJ/hr ( $\sim 92$  Mbtu/hr), while the another portion of heat is used for improving buoyancy in the cooling tower  $\sim 206$  Mbtu/hr by injecting in to the cooling tower. Schematic of this Configuration is presented in Figure 6.4.

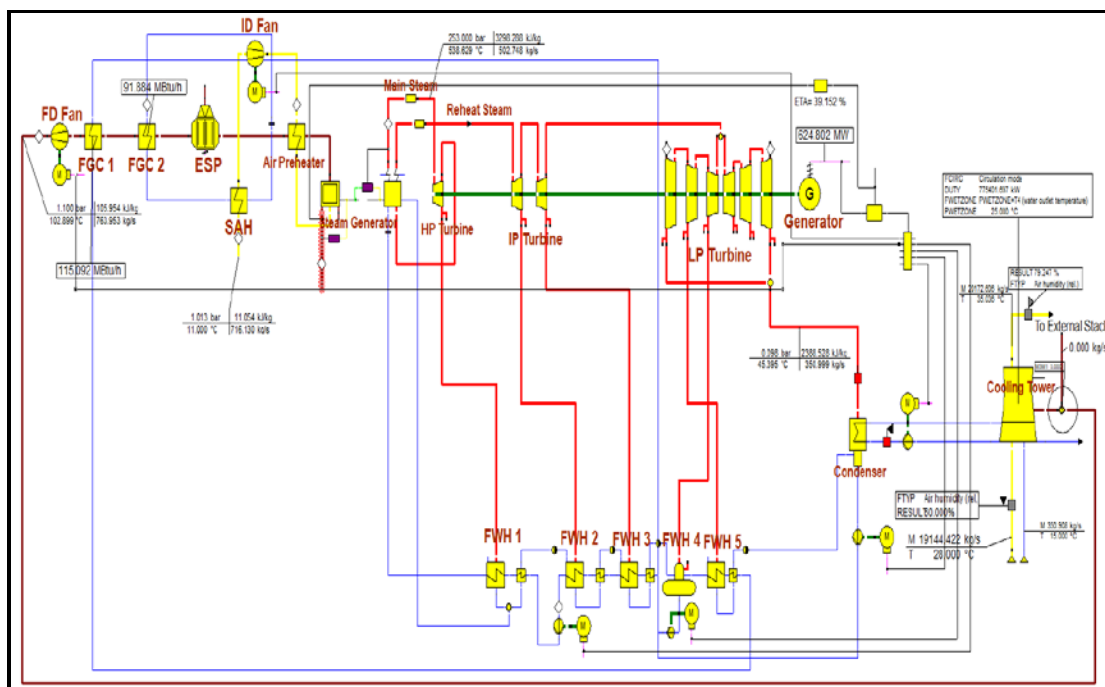


Figure 6.4: Power plant equipped with FGC for waste heat recovery from flue gas and flue gas injection into CT

From the Table 6.1 and Figure 6.5, it is evident that a plant employing both flue gas injection into a CT and having a FGC for heat recovery will have 1.89%, 1.93% and 1.73% improvement (decrease) in net heat rate, net efficiency and gross power output compared to a baseline plant which has not employed both these improvement techniques.

Table 6.1: Performance comparison between power plants with and without Flue gas Injection into Cooling Tower.

Description	$P_G$ MW	$HR_{cycle}$ BTU/kWh	$h_{cycle}$ %	$Q_{condenser}$ MBTU/hr	$P_{net}$ MW	$HR_{net}$ BTU/kWh	$h_{net}$ %
Design with SAH	614.19	7,522.31	45.36	2,432.59	575.28	8,031.09	42.48
Base plant with CT Flue gas Injection	616.10	7,498.84	45.50	2,517.90	580.54	7,958.17	42.87
FGC for air and FW heating	620.74	7,442.80	45.84	2,410.28	581.88	7,939.86	42.97
CT Flue Gas Injection and FGC	624.80	7,394.40	46.14	2,488.20	586.37	7879.02	43.30

Table 6.2: Results – Relative improvements with respect to reference plant in percentage

Description	Gross Power	Net Heat Rate	Net efficiency
	%	%	% point
Base plant with CT Flue gas Injection	0.31	0.91	0.92
FGC for air and FW heating	1.07	1.14	1.15
CT Flue Gas Injection and FGC	1.73	1.89	1.93

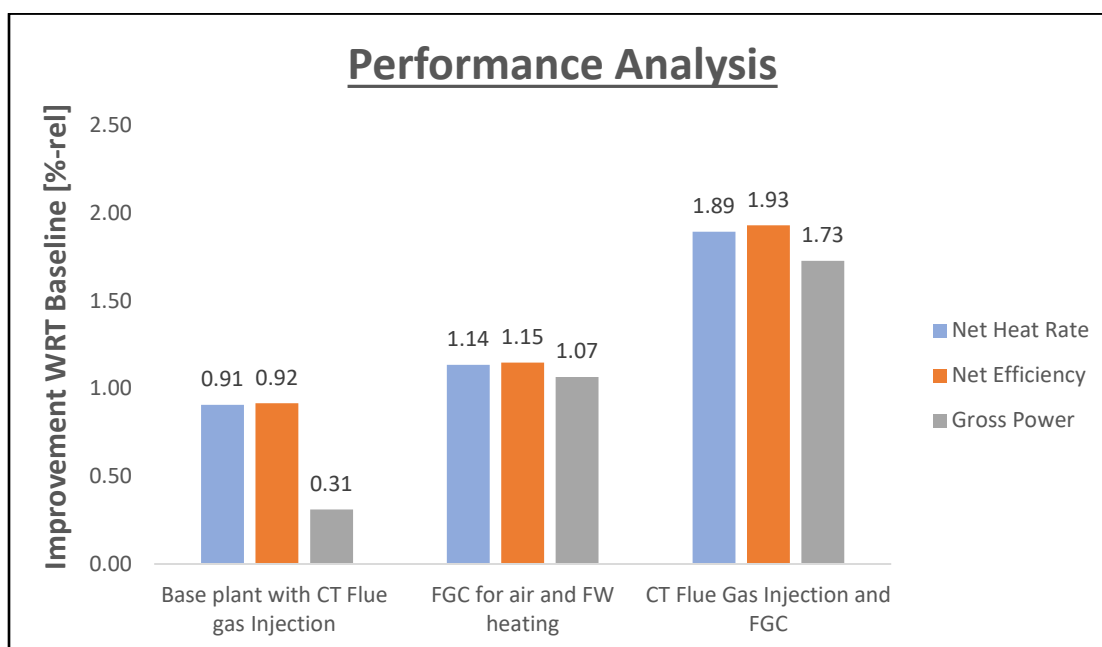


Figure 6.5: Analysis of Cumulative Performance Improvement Technique

Looking at the performance improvements it clearly shows that the individual performance improvements are not additive. The magnitude of change in the performance parameters with respect to are a clear indication of this fact. Even though the amount of waste heat recovered (206 Mbtu/hr) from the exhaust flue gas is kept constant by having a same lower terminal temperature difference for FGC and stack height to accommodate similar area of heater transfer in both the individual performance improvement options and the cumulative

case, the magnitude conversion rate or the heat rate or the net efficiency are not the same.

See below the additive comparison,

$$\text{Gross Power} = 0.31\% + 1.07\% = 1.38\% < 1.73\%$$

$$\text{Net Plant Heat Rate} = 0.91\% + 1.14\% = 2.05\% > 1.89\%$$

$$\text{Net Plant Efficiency} = 0.92\% + 1.15\% = 2.07\% > 1.93\%$$

The losses associated with rate heat extraction for each improvement method (Cooling Tower and FGC) are different, i.e. the conversion rate of net heat absorbed is not the same. From Equation 6.4 and 6.6 it is evident that the heat rate is inversely proportional to net efficiency improvements. The heat input is kept constant (fuel fired in the boiler), however the losses associated with the equipment involved in each method are different. In a Cooling Tower blowdown losses and evaporation losses have a different magnitude compared to the losses due to effectiveness (heat transfer loss) of the heat exchanger associated with the FGC.

Auxiliary power consumption also plays a vital role in determining the magnitude of performance improvement. Both the performance improvement options have different power consumption rate. This difference is observed from the difference between the Net and Gross power generated from each improvement method (Case 2 CT option - 35.56 MW vs Case 3 FGC option 38.86 MW). A detailed parametric analysis provided in table 6.1 on performance parameters calculated using the equation stated in section 6.2 of this chapter has helped us understand the improvement methods are not additive since the system is not linear.

A detailed cost analysis for employing both these techniques will reveal the ROI and required capital to implement these on a brown field plant, unfortunately cost analysis is not in scope of this study. Only fact of having a 10.61 MW increase in net power output should be a compelling reason to employ these improvements in a thermal power plant.

## CHAPTER 7: SUMMARY AND CONCLUSIONS

Efficiency-improving options analyzed in this work included: recovery and utilization of heat from flue gas, improvements to the steam turbine cycle and improvements to the heat rejection system. Descriptions of each option and their effects on plant performance and emissions are summarized in this section. Details are presented in Chapters 1 to 5.

System configurations for using low-temperature heat from the flue gas, analyzed in this work, included a configuration for feedwater (FW) heating and preheating of combustion air presented in Figure 2.3. The low-temperature heat is recovered from the flue gas using a flue gas cooler (FGC) located upstream of the FGD and used for the FW heating and/or air preheating. To quantify benefits of using heat recovered from the flue gas for FW heating and air preheating, an analysis was performed for the system configuration presented in Figure 2.1 to 2.4 and four coals: bituminous, washed Illinois, PRB, and lignite. Results are summarized in Figure 2.5 to 2.7 as a relative improvement in net unit heat rate with respect to the baseline configuration with no heat recovery.

The improvement in net unit heat rate depends on the use of recovered heat and coal type. For the system configuration employing FW heating and air preheating, the relative improvement in net unit heat rate varies from 1.3 to 2.4%, and is largest when recovered heat is used for FW heating and air preheating. The analysis was performed by assuming the same degree of air preheat in all cases. The effect of air preheat temperature on performance is presented in Chapter 2. The performance improvements for system configurations employing condensing heat exchangers for sensible and latent recovery are

higher (up to 3.6%). These configurations and predicted performance improvements are presented in Chapter 2.

In summary, performance improvements achievable by using heat recovered from the flue gas for the FW heating and combustion air preheat can be significant and should be considered as measures for improving performance and reducing emissions for existing and newly constructed power plants. For existing power plants where it is difficult or impossible to raise steam parameters to improve performance, use of heat recovered from the flue gas represents an attractive option.

### 7.1 Flue Gas Cooler

A flue gas cooler (FGC) is an important piece of equipment enabling recovery of heat from the flue gas. Since a significant section of the FGC operates below the acid dewpoint temperature, the heat transfer surface has to be constructed from the corrosion resistant materials, such as corrosion-resistant alloys, carbon steel with corrosion resistant coating, high-temperature corrosion-resistant plastic tubing, or borosilicate glass. Details concerning materials and design are presented in Chapter 2.

Use of corrosion-resistant plastic or alloy tubes increases the cost of an FGC. As a rule of thumb, the cost of an FGC operating below acid dewpoint is about ten times higher compared to the finned tube design employing carbon steels. The cost of an FGC depends on the choice of material and ranges from \$0.06 per Btu/hr of recovered heat for enamel glass lined steel, to \$0.10-0.13 per Btu/hr of recovered heat for corrosion-resistant alloys [3, 4].

## 7.2 Improvements to the Steam Turbine Cycle

Over its lifetime, a steam turbine can lose from 2 to 5% of its efficiency, with the amount of efficiency loss depending on the number of hours of operation, load profile, startups and shutdowns, and the quality of inspection and maintenance. In today's highly competitive electricity generating market, there are both financial and environmental incentives to improve generation efficiencies. The same technology advances that are incorporated into new steam turbines can be used to improve the performance of existing turbines. Upgrading existing turbines can raise efficiencies by as much as 5% in high-pressure (HP) turbines, 4% in intermediate pressure (IP) turbines, and 2-1/2% in low-pressure (LP) turbines [3, 8, 9]. Also, turbine upgrade can result in a significant increase in turbine output. Steam turbine technologies that are available for modernization of existing units and were investigated in this study include: rotors and casings, partial to full-arc admission retrofits, improved inter-stage seals. These improvements can, cumulatively, increase turbine cycle heat rate by 2 to 4.5% (relative) [8, 9], which will improve net unit heat rate.

At full load, there is little efficiency difference between the full-arc and partial-arc admission. However, at partial loads, the full-arc admission has a higher efficiency loss compared to a partial arc admission steam turbine. Most modern controls start with full-arc admission allowing even heat distribution around the circumference of nozzle blocks and uniform warming of control valves. Once the turbine is under load and near rated inlet steam conditions, the control is shifted to partial-arc to avoid unnecessary throttle pressure

losses across turbine control valves. This control mode improves turbine cycle heat rate over a wide range of turbine loads.

One often overlooked performance area in a steam turbine involves improvements in seal design. However, when considering a seal design, the specific operation of the steam turbine needs to be considered. Each application requires an evaluation to determine the best solution. There are four factors that need to be taken into consideration: installation, cost, durability, and performance. For example, replacing straight seals with brush seals in the HP and IP sections of a steam turbine can result in performance gain of about 0.74% as compared to 0.15 and 0.25% increases with dimpled seals and slant tip seals, respectively. On another unit, replacing retractable seals with Turbo seals has resulted in a 1.5% increase in net unit heat rate [8, 9, 22].

### 7.3 Improvements to the Heat Rejection System

The idea of injecting scrubbed flue gas into the stack region of natural draft cooling towers emerged in Europe. Flue gas injection has been put into practice in Europe and appears to be developing into a proven technology. According to McIlvaine (1989), Rheinisch-Westfälisches Elektrizitäts Werke claims to have saved about 300 million German marks on its investment with 14 applications of injecting scrubbed flue gases into cooling towers.

Approximately 50% of the fuel heat input to a subcritical coal-fired power plant is rejected to the ambient (heat sink) by the cooling water system (assuming turbine cycle heat rate of 8,000 Btu/kWh and boiler efficiency in the 85 to 90% range) [3, 9]. However, heat rejected by the coal-fired power plants has low exergy (availability) which

significantly limits its use. The amount of rejected heat decreases as efficiency of the steam turbine cycle increases. The rejected heat represents latent heat from condensing the LP turbine steam exhaust flow in the main steam condenser. This phase change is necessary to increase density of the working fluid and reduce compression work required to increase pressure of the condensate to the boiler inlet pressure. The latent heat of condensation is rejected to the environment by once-through cooling water system where bodies of water are used as a heat sink, or by cooling towers where heat is rejected directly to the atmosphere. Regardless of the approach, condenser pressure has a major effect on performance of the steam turbine cycle.

In cooling tower systems, the main condenser pressure is a function of ambient conditions (relative humidity and temperature of ambient air) and performance of cooling tower heat transfer surfaces (cooling tower fill), which affect heat exchange between cooling air and circulating water and, thus range and cooling water temperature at condenser inlet. It is important to keep the circulating water system clean, through blowdown and chemical treatment of the circulating cooling water, to prevent corrosion and fouling of the heat transfer surfaces both in the condenser and the cooling tower.

Although proper maintenance is a key to good cooling tower performance as it is in main steam condensers, there are opportunities for improving cooling tower performance by upgrading the fill. For example, reducing cooling tower approach (difference between circulating temperature leaving the cooling tower and inlet air wet bulb temperature) from 10 to 5°F on a warm summer day will improve turbine cycle heat rate by 20-40 Btu/kWh. Newer fill materials and designs have improved configurations with

better heat transfer characteristics. Also, variable frequency drives (VFD) applications for circulating water pumps and mechanical draft fans will reduce auxiliary power use and increase net unit power output.

Condenser pressure is also affected by the condenser thermal duty. Thermal duty of a condenser can be reduced through recovery and use of low-temperature heat from the condenser or a circulating water system. Possibilities include: preheating of combustion air (for power plants located in northern climates), building heat, and other low temperature heat uses. Another possibility involves application of the Rankine-Kalina cycle, which can improve cycle efficiency by up to 23% (Korobitsyn, M.A., 1998). However, retrofit to an existing older power station might be difficult, but should be considered as part of a repowering project. In general, despite its thermodynamic advantages compared to the steam cycle, the Kalina cycle was not adopted because ammonia is toxic to humans.

## REFERENCES

1. *Epsilon Professional Program Documentation*. 2017; Available from: [https://www.steag-systemtechnologies.com/epsilon\\_professional+M52087573ab0.html](https://www.steag-systemtechnologies.com/epsilon_professional+M52087573ab0.html).
2. *Proposal: Affordable Clean Energy (ACE) Rule*, August 21, 2018, Available from: <https://www.epa.gov/stationary-sources-air-pollution/proposal-affordable-clean-energy-ace-rule>; <https://www.epa.gov/airmarkets/analysis-proposed-ace-rule>
3. Dr. Nenad Sarunac, Energy Research Center, Lehigh University, Final Technical Report ICCI Project Number: 07-1/5.1A-1 “*Increasing Efficiency and reducing emissions of Existing Pulverized Coal-Fired units*” October 1st 2007, through March 31<sup>st</sup> 2009
4. Sarunac, N., 2009. “*Generation Efficiency Improvement – No Regret Pathway to Immediate Reduction in CO2 Emissions*”, Prepared for the 34th International Technical Conference on Coal Utilization and Fuel Systems, May 31-June 4, 2009, Sheraton Sand Key, Clear water, Florida.
5. *REFPROP version 7.1, NIST standard reference database*. The U.S. Secretary of Commerce.
6. MCLINDEN, M.O., *NIST thermodynamic and transport properties of refrigerants and refrigerant mixtures-REFPROP*. NIST Standard Reference Database, 1998. **23**.
7. Energy Information Administration, February 1995 “*Coal Data: A Reference*” DOE/EIA-0064(93) Distribution Category UC-98. Page 108; Table 53
8. Sarunac, N., “Opportunities for Improving Efficiencies and Reducing Emissions for Existing Fossil-Fired Power Plants – An Update,” Presented at 33<sup>rd</sup> International Conference on Coal Utilization and Fuel Properties,” Clearwater, Florida, June 1-5, 2008.
9. Sarunac, N., “Opportunities for Heat Rate Improvements in Coal-Fired Power Plants,” Annual Fossil Power Plant Technology Meeting, Lehigh University, May 28-29, 2008.
10. Sarunac, N., M. Ness and C. Bullinger, “One Year of Operating Experience with a Prototype Fluidized Bed Coal Dryer at Coal Creek Generating Station,” Third International Conference on Clean Coal Technologies for our Future, May 15-17 2007, Cagliari, Sardinia, Italy.
11. “Sealing off Steam Losses,” Erik M. Sulda, *Energy Tech*, pages 34-35, February 2008.

12. "Balancing Act: Improving Rotordynamic Stability During Steam Turbine Retrofits," Bruce Gans, Energy Tech, pages 24-25, September 2008.
13. "Steam Turbine Modernization Solutions Provide a Wide Spectrum of Options to Improve Performance," Michael W. Smiarowski, Ranier Leo, Christof Scholten and John Blake, Siemens Power Generation, 2005.
14. H.L. Stocker, "Determining and Improving Labyrinth Seal Performance in Current and Advanced High Performance Gas Turbines," AGARD Conference Proceedings no. 237, Seal Technology in Gas Turbine Engines, April 1978.
15. G.L. Morrison and D. Chi, "Incompressible Flow in Stepped Labyrinth Seals," ASME Paper 85-FE-4, Joint ASME/ACSE Applied Mechanics, Bio-Engineering, and Fluids Engineering. Conference, Albuquerque, NM, June 1985.
16. J.S. Wyler, "Design and Testing of a New Double Labyrinth Seal," ASME Paper 81-Lub-58, ASME Winter Annual Meeting, Washington, D.C., November 1981.
17. H.L. Stocker, "Advanced Labyrinth Seal Design Performance for High Pressure Ratio Gas Turbines," ASME Paper 75-WA/GT-22, ASME Winter Annual Meeting, Houston, TX, November/December 1975.
18. R.C. Hendricks, T.A. Griffin, T.R. Kline, K.R. Csavina, A. Pancholi, and D. Sood, "Relative Comparison between Baseline Labyrinth and Dual-Brush Compressor Discharge Seals in a T-700 Engine Test," NASA Technical Memorandum 106360, 39<sup>th</sup> International Gas Turbine and Aeroengine Congress and Exposition by ASME, Hague, The Netherlands, June 1994.
19. Martin, H. M., & "Steam Turbines", The Engineer, London, 1913, p. 1610.
20. A. Egli, & "The Leakage of Steam Through Labyrinth Seals", Transactions American Society of Mechanical Engineers, Paper FSP-57-5, 1935.
21. EPRI Report, "*Advanced Steam Labyrinth Seal Design: Phase 1 Initial Concept Evaluation*". EPRI, Palo Alto, CA: 2005. 1011932.

22. EPRI Report, "*Turbine-Generator Auxiliary Systems, Volume 2: Turbine Steam Seal System Maintenance Guide*". EPRI, Palo Alto, CA: 2006. 1013462.
23. U.S. Patents: 4,420,161; 5,224,713; 5,244,216; 5,639,095; 6,394,459; 6,644,667; 6,435,513; 6,257,586; 6,131,911; 6,131,910; 6,105,967; 6,045,134; 6,027,121; and 5,749,584.
24. G.L. Morrison et al., "Labyrinth Seals for Incompressible Flow – Final Report," NASA Contract Report CR-170938, November 1983.
25. W.J. Kearton and T.H. Keh, "Leakage of Air Through Labyrinth Glands of Staggered Type," IME Proceedings, vol. 166, no. 2, 1952.
26. Air pollution: its origin and control by Kenneth Wark, Cecil Francis Warner; Harper and Row, 1981.
27. Cooling Towers: Design and Operation Considerations; Chemical Engineering Tools and Information, 2010.
28. F. Merkel, "Verdunstungskuehlung," VDI Forschungsarbeiten No. 275, Berlin, 1925.
29. H. B. Nottage, "Merkel's Cooling Diagram as a Performance Correlation for Air-Water Evaporative Cooling Systems," ASHVE Transactions, vol. 47, 1941, p. 429.
30. The Standard Handbook of Plant Engineering, 2nd Edition, Rosaler, Robert C., McGraw-Hill, New York, 1995.
31. Perry's Chemical Engineers' Handbook, 6th Edition, Green, Don W. et al, McGraw-Hill, New York, 1984.
32. An Implementation of algorithm 699 from TOMS; TRANSACTIONS ON MATHEMATICAL SOFTWARE, VOL. 17, NO. 4, DECEMBER, 1991, PP. 457-461
33. VDI Wärmeatlas, Section Ca; Compact Heat Exchangers; by W.M. Kays and A.L. London
34. Air-Preheater (RAPH) product information brochure from Howden (OEM).  
<https://www.howden.com/Brochures/Air%20Pre%20Heater%20Brochure.pdf>

35. Air-Preheater (RAPH) case study at AES Itabo I power plant Dominican Republic from Howden (OEM). [https://www.howden.com/Brochures/CASE17\\_ItaboI.pdf](https://www.howden.com/Brochures/CASE17_ItaboI.pdf)
36. Copen, J. H., T. B. Sullivan and B. C. Folkedhal, "Principles of Flue Gas Recovery System," Presented at POWER-GEN International 2005, Las Vegas, Nevada, December 6-8, 2005.
37. A.D. Vakili, A.J. Meganathan, M.A. Michaud, and S. Radhakrishnan, "An Experimental and Numerical Study of Labyrinth Seal Flow," Paper No. 2005-68224, Proceedings of ASME Turbo Expo 2005, Reno, NV, June 6–9, 2005.
38. M. Michaud, A.D. Vakili, A.J. Meganathan, R. Zielke, L. Shuster, and J. Terrell, "An Experimental Study of Labyrinth Seal Flow," Paper No. 2003-40097, Proceedings of ASME IJPGC, 2003 International Joint Power Conference, Atlanta, GA, June 16–19, 2003.
39. M. Michaud, "An Experimental Study of Labyrinth Seal Flow," MS Thesis, University of Tennessee, August 2002.
40. D.L. Rhode and M.J. Guidry, "Importance of Labyrinth Seal Through-flow Deflection for Enlarging Clearance without Increasing Leakage," *Tribology Trans.*, vol. 36, part 3, 1993, p. 477–483.
41. Steam Leakage through Labyrinth - Steam Turbine (OEM and operators discussion thread). <https://www.eng-tips.com/viewthread.cfm?qid=178922>
42. Wilfried B. Krätzig, Reinhard HARTE, Ulrich MONTAG, Ralf WOERMANN, "Giga-Shells for Energy Generation: Natural Draft Cooling Towers and Solar Updraft Chimneys," 6<sup>th</sup> International Symposium on Cooling Towers, Cologne, June 20-23, 2012.
43. Leak Detection Services, Inc. "Cycle Isolation Opportunities." Presented to EPRI Turbine-Generator Users Group: San Antonio, TX (January 22, 2002).
44. Steam power and Co Generation 4 (Steam Turbine Operation and Control); 360training.com: [https://www.youtube.com/watch?v=\\_oGwq-10cIo](https://www.youtube.com/watch?v=_oGwq-10cIo)
45. Professor Q.H. Nagpurwala: Steam Turbines, PEMP PMD 2501, "M.S. Ramaiah School of Advanced Studies"
46. Van Wylen, G.J. and Sonntag, R.E. (1976) Fundamentals of Classical Thermodynamics, section 14.1 (SI Version 2e), John Wiley & Sons, Inc., New York

47. Van Wylen, G.J., and Sonntag, R.E. (1965), *Fundamentals of Classical Thermodynamics*, John Wiley & Sons, Inc., New York
48. L. J. Clancy (1975), *Aerodynamics*, Pitman Publishing Limited, London. ISBN 0-273-01120-0
49. Cengel, Boles, "Thermodynamics, an engineering approach, McGraw Hill, ISBN 0-07-254904-1.
50. Van Wylen and Sonntag, *Fundamentals of Classical Thermodynamics*, section 14.1.
51. Van Wylen and Sonntag, *Fundamentals of Classical Thermodynamics*, equation 5.50.
52. Contribution from David Charlton, PE (david.charlton@tgadvisers.com), senior consultant for TG Advisers Inc. <https://www.powermag.com/managing-minimum-load/>
53. TG Advisers Article posted on June 13 2018, <https://tgadvisers.com/steam-turbine-and-generator-reduced-minimum-load-considerations/>
54. THERMAL POWER PLANTS – Vol. III - Steam Turbine Operational Aspects - R.A. Chaplin - Department of Chemical Engineering, University of New Brunswick, Canada.
55. Admission conversion improves part load performance by Simon Hogg Alstom Power, Rugby, UK on November 1<sup>st</sup>, 2005; With the method for calculating valve points by *J.A. Hesketh of Alstom Power, Rugby, UK*
56. “Experimental Investigation of Performance, Flow Interactions and Rotor Forcing in Axial Partial Admission Turbines” by *Jens Fridh*; Doctoral Thesis 2012; Division of Heat and Power Technology - Department of Energy Technology; Royal Institute of Technology, Stockholm, Sweden.
57. “Steam Turbine Thermal Evaluation and Assessment” by *Paul Albert*, GE Power Systems, Schenectady, NY.
58. An Investigation of the Effects of Flue Gas Injection on Natural Draft Cooling Tower Performance by T. V. Eldredge, D. J. Benton, J. W. Hodgson - *Journal of Engineering for Gas Turbines and Power* · April 1997.
59. Feasibility Study of the Thermal Performance Improvement of Natural Draft Dry Cooling Towers Due to Flue Gas Injection by Ali Jahangiri and Aliakbar Golneshan - Faculty of Mechanical Engineering, Semnan University, Semnan, Iran. *World Applied Sciences Journal* 12 (4): 568-575, 2011; ISSN 1818-4952.

60. The Energy-saving Benefit and Economic Evaluation Analysis of Cooling Tower with Flue Gas Injection by Q. Han, D. Y. Liu, F. S. Chen, Z. Yang.
61. "WET COOLING TOWERS: 'RULE-OF-THUMB' DESIGN AND SIMULATION" by Stephen A. Leeper, July 1981; U.S. Department of Energy - Idaho Operations Office Idaho National Engineering Laboratory.
62. DESIGN OF COOLING TOWER by B. Bhavani Sai, I. Swathi, K S L Prasanna, K Srinivasa Rao; International Journal of Scientific & Engineering Research, Volume 4, Issue 5, May-2013; ISSN 2229-5518.
63. Air Cooled Heat exchanger and Cooling Towers thermal-flow performance Evaluation and design. Volume II by Detlev G. Kroger; ISBN 1-59370-019-9.
64. "Experimental Study of the Flue Gas Injection to Improve the Natural Draft Cooling Tower Performance under Crosswind" by Mohammad Hassan Kayhani, Ali Abbas Nejad, Mojtaba Khaksar; Presented at International Conference on Mechanical, Automobile and Robotics Engineering (ICMAR'2012) Penang. Malaysia.
65. Flue gas diffusion for integrated dry-cooling tower and stack system in power plants by Lei Chen, Lijun Yang, Xiaoze Du, Yongping Yang; International Journal of Thermal Sciences.
66. Algorithm 699: A New Representation of Patterson's Quadrature Formulae by FRED T. KROGH and W. VAN SNYDER; Jet Propulsion Laboratory, California Institute of Technology.
67. F. P. Incropera & D. P. DeWitt 1990 Fundamentals of Heat and Mass Transfer, 3rd edition, pp. 658–660. Wiley, New York
68. F. P. Incropera, D. P. DeWitt, T. L. Bergman & A. S. Lavine 2006 Fundamentals of Heat and Mass Transfer ,6th edition, pp 686–688. John Wiley & Sons US.
69. Cooling Tower Acceptance Testing and Cooling Tower Characteristics - DIN 1947 (version of May 1989); page 11.